Geochemistry of Groundwater and Naturally Occurring Pyrite in the Holocene Fluvial Aquifers in Uphapee Watershed, Macon County, Alabama

by

Md Mahfujur Rahman

A thesis submitted to the Graduate Faculty of
Auburn University
In partial fulfillment of the
Requirements for the Degree of
Master of Science

Auburn, Alabama
December 14th, 2019

Keywords: arsenic, pyrite, groundwater, geochemistry, bioremediation

Journal Style: Geology

Approved by

Dr. Ming-Kuo Lee, Co-Chair, Robert B. Cook Professor of Geology
Dr. Ashraf Uddin, Co-Chair, Professor of Geology
Dr. Martin Medina, Associate Professor of Geology

Abstract

Naturally occurring biogenic pyrite has been found in Holocene fluvial aquifers in Uphapee watershed, Macon County, Alabama. The electron microprobe (EMP) analysis showed that the pyrite grains contain 0.20-0.92 weight% of arsenic (As). The scanning electron microscope and energy dispersive spectroscopy (SEM-EDS) analysis confirmed a similar level of As concentration in pyrite that was consistent with the EMP analysis. The SEM analysis also confirmed the presence of additional trace elements such as cobalt (0.19 wt.%), and nickel (0.15 wt.%), indicative of pyrite's capacity to sequester arsenic and other metals. Pyrite grains were naturally formed and developed as large (20-200 μm) euhedral (i.e. cubes, truncated octahedron) crystals and none-framboid aggregates. The XRF analysis of the collected lignitic wood (from the wells) also showed the presence of As. However, the ICP-MS analysis showed that As level in the groundwater was not high and it was within the EPA drinking water standards (<10 ppb). These results indicate that dissolved arsenic is sequestered in naturally formed pyrite found in the fluvial sediments.

The groundwater was moderately reducing to slightly oxidizing (Eh= 46 to173 mV), and nearly neutral to slightly acidic (pH = 5.53 to 6.51). Groundwater geochemistry data indicate a redox sequence of oxidation, Mn(IV) reduction, Fe(III) reduction, and sulfate reduction along the flow path in fluvial aquifers. The down-gradient increases in dissolved Mn and then Fe concentrations reflect increased Mn(II) and Fe(II) production via microbial competition as the aquifer becomes progressively more reduced. Bacterial sulfate reduction seems to dominate near the end of the groundwater flow path as the availability of Mn- and Fe-oxyhydroxides becomes

limited in sediments rich in lignitic wood where increased sulfate-reducing activities, leading to the formation of biogenic pyrite. The groundwater is a Ca-SO_4 type, is not SO_4-limited, as compared to most Holocene groundwater systems in Bangladesh, thus sulfate may serve as an electron acceptor for the bacterial sulfate-reducing reactions that sequester As into pyrite, which in turn results in very low groundwater As concentration (≈1-2 ppb). This result implies that groundwater in Holocene alluvial aquifers in Bangladesh (a sulfate-limited system) must be amended with an electron acceptor (e.g., iron sulfate) and labile organic carbon to stimulate the metabolism of indigenous sulfate-reducing bacteria (SRB).

This study compared the size and morphology of biogenic pyrite precipitated naturally in the Uphapee fluvial sediments with those formed via biostimulation at a Florida industrial site, where groundwater was severely contaminated with an elevated level of As (300-500 ppb). Arsenian-pyrite grains formed via a biostimulation process appear either as well-defined euhedral nano-crystals or as spherical aggregates (framboids) of 1-50 μm in diameter, smaller than those formed naturally in the Uphapee watershed. The biogenic pyrites formed at the Florida site contained between 0.05-0.40 wt.% of As, indicating similar As adsorbing capability.

Acknowledgements

This research project was funded by the National Science Foundation (NSF). I would like to acknowledge the additional funding sources that came from the Geological Society of America (GSA), the Alabama Geological Society (AGS), the Gulf Coast Association of Geological Societies (GCAGS), and Department of Geosciences, Auburn University.

I would like to thank the advisor and co-chair of the thesis committee Dr. Ashraf Uddin for his enthusiastic support in this research work. He was actively involved in my research and brought the best out of me. I also acknowledge his efforts for supporting my application for admission in Auburn University. Dr. Uddin inspired and supported to get many awards throughout the period I have been at Auburn University.

I would like to thank the other advisor and co-chair of the thesis committee Dr. Ming-Kuo Lee who spent his valuable time to supervise the thesis. Dr. Lee provided me with invaluable guidance and mentorship during the research. He always had an open door and was more than willing to help with any problem or question I encountered during this research.

I would like to thank Dr. Martin Medina for his guidance and support. He was always ready to help in any issue related to my thesis.

I would like to thank Dr. James Saunders for finding the problem in Macon County that initiated this project in Alabama. I also appreciate his thoughtful comments on some of my dataset on geochemistry.

I would like to acknowledge the support of Dr. Billor, another member of the Auburn Geosciences Department. He provided me with strong support during the laboratory analysis portion of my thesis and taught me many lessons on laboratory procedure. I would also like to thank Dr. Hames for helping with electron microprobe analysis and Dr. Miller from the Department of Biological Sciences for training and helping me during the use of scanning electron microscope.

Finally, I would like to thank all of my friends whom I met at Auburn Geosciences department. I want to express special thanks to Alicia Fischer, Collin Sutton, Connor Cain, Neeraja Chinchalkar, and Ozan Turkes who helped in the fieldwork. I want to thank a former graduate student of this department Mohammad Rezaul Huq for his assistance in the fieldwork.

Table of Contents

List of Tables

List of Figures

List of Abbreviations

As	Arsenic
COD	Crystallography Open Database
DOC	Dissolved Organic Carbon
Eh	Redox potential
EPA	Environmental Protection Agency
EMP	Electron microprobe
Fe	Iron
GWB	Geochemist's Workbench
GIS	Geographic Information System
H_2S	Hydrogen Sulfide
ICP-MS	Inductively Coupled Plasma Mass Spectroscopy
Mn	Manganese
ORP	Oxidation-Reduction Potential
Ppm	Parts per million
Ppb	Parts per billion
Ppm	Parts per million
SEM	Scanning Electron Microscope
SO_4	Sulfate
SRB	Sulfate Reducing Bacteria
XRD	X-Ray Diffraction
XRF	X-Ray Fluorescence

Introduction

Sources of Arsenic

Arsenic (As) is one of the most common metalloid contaminants found in groundwater; and the mode of occurrence and mobility of arsenic in sedimentary aquifers are mainly influenced by local geology, geomorphology, hydrogeology, and geochemistry of sediments and water, as well as anthropogenic activities (Bhattacharya et al., 1997, Welch et al., 2000; Harvey et al., 2002; Smedley and Kinniburgh, 2002; van Geen et al., 2003; Shamsudduha, 2007). Naturally-occurring arsenic contamination is a widespread problem in Holocene aquifers worldwide (Figure 1) (Turner, 2006), and it is relatively abundant in crustal rocks, with an average concentration of 10 parts per million (ppm) (Smedley and Kinniburgh, 2002). It can be found as different types of ore deposits with a higher concentration (Kruger et al., 2013). The most abundant arsenic ore mineral is arsenopyrite (FeAsS), commonly associated with igneous rocks (Shamsudduha, 2007). Arsenic can occur as a major constituent in more than 200 minerals, including elemental arsenic, sulfides, oxides, arsenates, and arsenites (Smedley and Kinniburgh, 2002). Arsenic-bearing pyrite is considered the major solid arsenic phase formed under sulfate-reducing conditions in natural systems (Saunders et al., 1997; 2005a; 2008). Certain geological, microbiological, and geochemical conditions exist in shallow aquifers that cause unusually high levels of As, Sr, Ba, Mn, and Fe in groundwater (Dowling et al., 2002; Akai et al., 2004). Alluvial aquifers, black shales and hydrothermal systems have been shown to contain more elevated levels of arsenic than other natural environments (Nordstrom, 2002).

Anthropogenic sources of arsenic are three times more common worldwide than natural sources (Wilson, 2018). The most common anthropogenic sources of arsenic in groundwater are mining, burning of fossil fuels, wood treatment, and the use of arsenical herbicides and insecticides (Mondal et al., 2013). Many industrialized countries such as the USA used excessive agricultural products such as insecticides and herbicides, wood preservatives as well as the high arsenic concentrations in mine tailings in the mid-twenty century that resulted in significant increase in arsenic concentration in both sediment and groundwater (USEPA, 1997; Mandal and Suzuki, 2002).

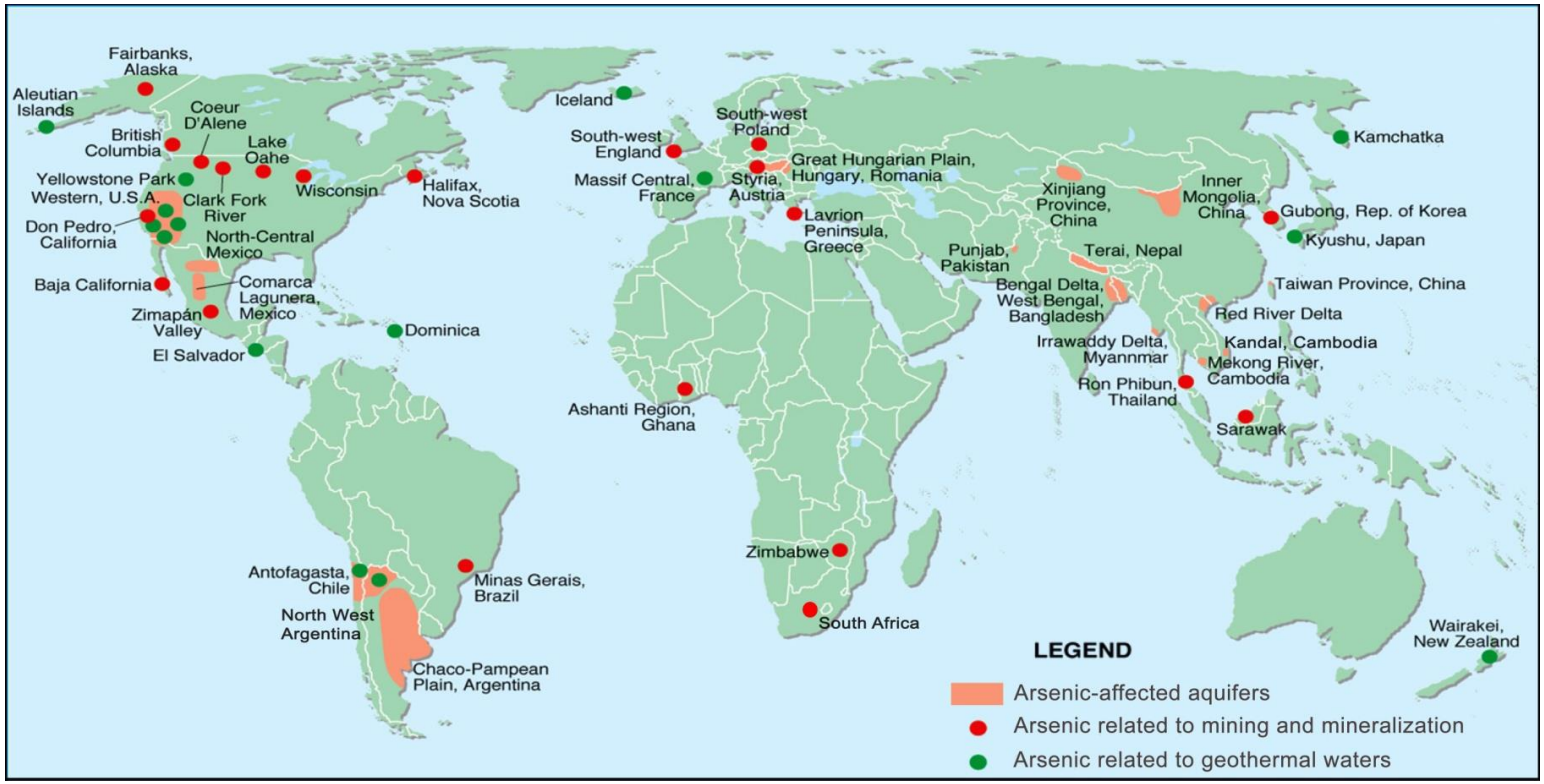

Figure 1. Distribution of arsenic-contaminated groundwater from both natural and anthropogenic sources in major aquifers of the world (Smedley and Kinniburgh, 2002). The map shows that the northern side of the United States is affected due to anthropogenic (mining) activity; and the western side is affected by both anthropogenic and natural activity.

Global Arsenic Scenario

Natural origin of arsenic in groundwater has been reported in many countries including Argentina, Australia, Bangladesh, China, Chile, India (West Bengal), Pakistan, Taiwan, Thailand, Mexico, Vietnam, and many parts of the United States (Figure 1) (Smedley and Kinniburgh, 2002; Nickson et al., 2005; Liu et al., 2006, Shamsudduha, 2007). The list of arsenic-affected countries is getting longer as recent groundwater quality reports were issued also in Nepal, Myanmar, and Cambodia. Arsenic associated with mining and geothermal waters including hot springs has been reported in Argentina, Chile, France, Ghana, Greece, Iceland, Japan, New Zealand, Thailand and the USA (Smedley and Kinniburgh, 2002).

Quaternary alluvial aquifers are contaminated with elevated levels of arsenic worldwide. These include aquifers in parts of Argentina, Bangladesh, Chile, China, Hungary, India, Mexico, Myanmar, Nepal, Romania, southwest United States, and Vietnam. These areas have similarities in geology and hydrogeology. The majority of the high-arsenic groundwater provinces are in young unconsolidated sediments mostly of Holocene (<12,000 years) age (Ravenscroft et al., 2005). These aquifers are usually large inland closed basins in arid or semiarid settings (e.g., Argentina, Mexico, and the southwest United States) or large alluvial and deltaic plains (e.g., Bengal delta, Yellow River plain, Irrawaddy delta, Red River delta) (Smedley and Kinniburgh, 2002).

Arsenic scenario in Bangladesh

Alluvial aquifers of South Asian countries, such as Bangladesh, are most affected by natural arsenic contamination (Kinniburgh and Smedley, 2001; Mandal and Suzuki, 2002; Nordstrom, 2002) and thus are ideal to study arsenic enrichment in relation to their local geology. In Bangladesh part of the Bengal Basin arsenic enrichment is mainly restricted to the Holocene alluvial aquifers at shallow and intermediate depths (Ahmed et al., 2001; McArthur et al., 2001; Mukherjee and Bhattacharya, 2001; Bhattacharya et al., 2002a,b). Arsenic concentrations as high as 250-300 μg/L occur in these aquifers at shallow depths (Rahman, 2015, Rahman et al., 2018). Holocene alluvial sediments are rich in organic matter and reactive minerals, and groundwater is mostly of Ca–Mg–HCO_3 and Ca– Na–HCO_3 types (Figure 10) (Bhattacharya et al., 2002b). Low SO_4^{2-} and NO_3^- and high dissolved organic carbon (DOC) and NH_4^- concentrations are typical chemical characteristics of groundwater in Bangladesh (Ahmed et al. 2004). Groundwater is moderate to strongly reducing in nature. Saunders et al., (2008) had a similar observation in the Ganges–Brahmaputra floodplain in central Bangladesh.

In Bangladesh, the occurrence of arsenic and its mobilization is associated with geochemically reducing subsurface environment (Shamsudduha, 2007). Several hypotheses invoke pyrite (FeS_2) or arsenopyrite (FeAsS) oxidation resulting from a lowering of the water table as a mechanism for arsenic mobilization (Mandal et al., 1996; Mallik and Rajagopal, 1996). But several recent studies agreed that microbial reduction dissolution of Fe-oxyhydroxides and the limited amount of dissolved SO_4^{2-} that limits biogenic precipitation of sulfide minerals are the primary release mechanism of arsenic mobilization in the groundwaters of the alluvial aquifers in

Bangladesh (Ahmed et al., 1998b; Bhattacharya et al., 1997; Nickson et al., 1998, 2000; Routh et al., 2000; McArthur et al., 2001; Dowling et al, 2002, Zheng et al., 2004). Harvey et al. (2002) suggested that arsenic mobilization is associated with recent inputs of carbon (C) due to large scale irrigation pumping in central Bangladesh. Routh et al. (2000) noticed microbial processes influence the arsenic mobilizing when the sediments in the aquifer are rich in organic matter. The authors suggest that microbial activity creates a reducing environment that favors the transformations of Fe(III) to Fe(II) as well as As(V) to As(III), and helps mobilizing arsenic.

Saunders et al. (2005) attempted to link the elevated arsenic occurrences in groundwater with the retreat of continental glaciation at the end of Pleistocene, which led to the rise of sea level during the Early to Middle Holocene and deposition of alluvium and extensive marsh and peat and finer sediments in Bengal lowlands. During the Pleistocene time the mechanical weathering of rocks in source areas (e.g., Himalayas, Indian Shield, and Indo-Burman mountains) was enhanced due to mountain building activities and glaciation. The aquifer sands in the Bengal Basin were largely derived from physical weathering and erosion at a time of extended glaciation in the Himalayas, but the intensity of chemical weathering was limited by the low temperatures during erosion (McArthur et al., 2004).

Arsenic Scenario in the United States

The United States has a different arsenic situation compared to South Asia. Though arsenic is considered as the second most common contaminant of groundwater in the United States (USEPA, 2002), arsenic concentrations in groundwater vary regionally due to a combination of climate and geology. Higher arsenic concentrations (>10 μg/L) are particularly observed in western United States (Welch, 2000). Higher arsenic concentrations are reported in many states such as Michigan, Minnesota, South Dakota, Oklahoma, and Wisconsin. Arsenic concentrations in groundwater of the Appalachian Highlands and the Atlantic Plain are generally very low (≤1 μg/L) and relatively higher in the Interior Plains and the Rocky Mountain System (Welch, 2000). In contrast with the younger Holocene sediments of the Bangladesh coastal plain, the sediments of the study area in Alabama are much older and usually their arsenic content is low (Starnes, 2015).

Objectives of the Study

(i) To determine the geochemistry of groundwater and naturally occurring biogenic pyrite in a natural fluvial aquifer along groundwater flow path near Uphapee Creek at Macon County, Alabama.

(ii) To understand the biogeochemical reactions controlling the fate and transport of arsenic and other trace metals under changing redox condition.

(iii) To compare groundwater geochemistry in similar fluvial system at natural sites (Alabama and Bangladesh) and an industrial site (Florida)

(iv) To compare arsenic sequestering capability of pyrite that formed naturally in Alabama natural site with biogenic pyrite formed due to a bioremediation experiment at an industrial site in Florida.

Background

Location of the Study Area at Macon County, Alabama

The study area is located inside the Tuskegee National Forest at Macon County, Alabama, approximately 17 miles south-west from Auburn University campus (Figure 2). More specifically it is located along the bank of Uphapee Creek.

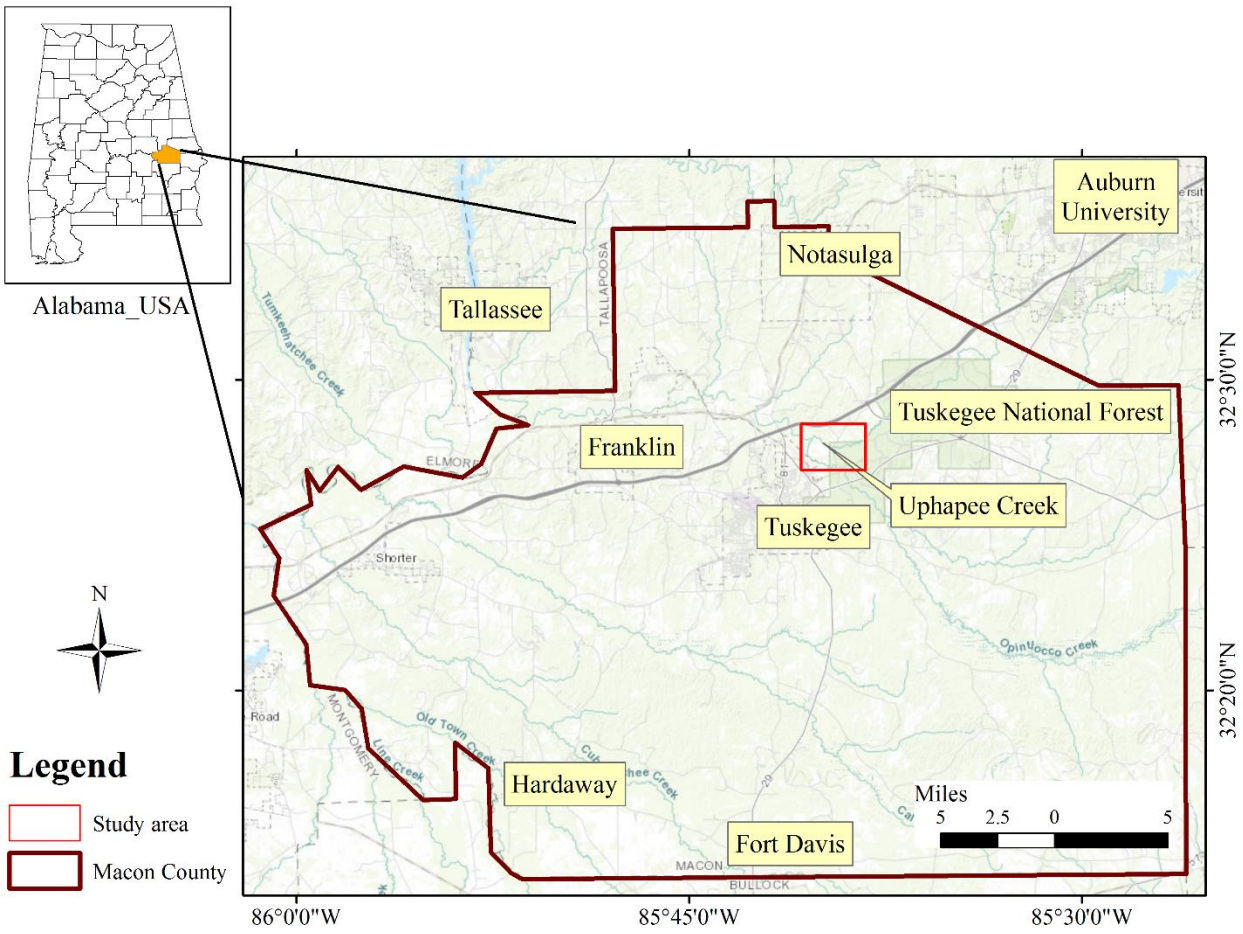

Figure 2. A map showing the location of the study area at Macon County, Alabama.

Geology and Geomorphology of the Study Area at Macon County, Alabama

The Uphapee Creek is a relatively large fourth-order stream; a tributary of the lower Tallapoosa River. In the northern side of the drainage basin, Appalachian Piedmont is present which consists of Precambrian-Paleozoic crystalline rocks (Figure 3). The creek flows through the Coastal Plain province of the Southeastern United States, more specifically east-central Alabama (northern Macon County) (Markewich and Christopher, 1982b, Saunders et al 1997). Tallapoosa River and Uphapee Creek drain both Piedmont and Coastal Plain terranes, but Uphapee Creek is predominantly a Coastal Plain drainage, incised into the non-marine Upper Cretaceous Tuscaloosa Group (Markewich and Christopher, 1982b). Coastal Plain aquifer materials and associated sediments consist of non-marine alluvial deposits (Penny et al., 2003). The sediments are characterized by petrified and lignitic wood fragments, which are commonly associated with crystalline pyrite with no signs of visible organic matter (Markewich and Christopher, 1982b). These undifferentiated sediments consisting of gravel, sand, silt, and lignitic wood, which were derived from the weathering and erosion of the Appalachians and were deposited in a Holocene floodplain (Saunders et al., 2008). Weathering of a variety of crystalline rock types may lead to release of arsenic and other metals/metalloids to the hydrosphere. Groundwater in Alabama and Florida coastal plain sediments however do not normally have high concentrations of arsenic (Welch et al., 2000). Arsenic (if present) has been largely flushed out by gravity-driven regional flow over a longer geologic period of time (Starnes, 2015). By contrast, high arsenic level has been sustained in the Ganges–Brahmaputra–Meghna Delta where low hydrologic gradients hinder groundwater flow and cause slow flushing

of aquifers (Shamsudduha et al., 2008). The arsenic concentration fluctuates regionally, due to a combined influence from geology and climate (Welch et al., 2000).

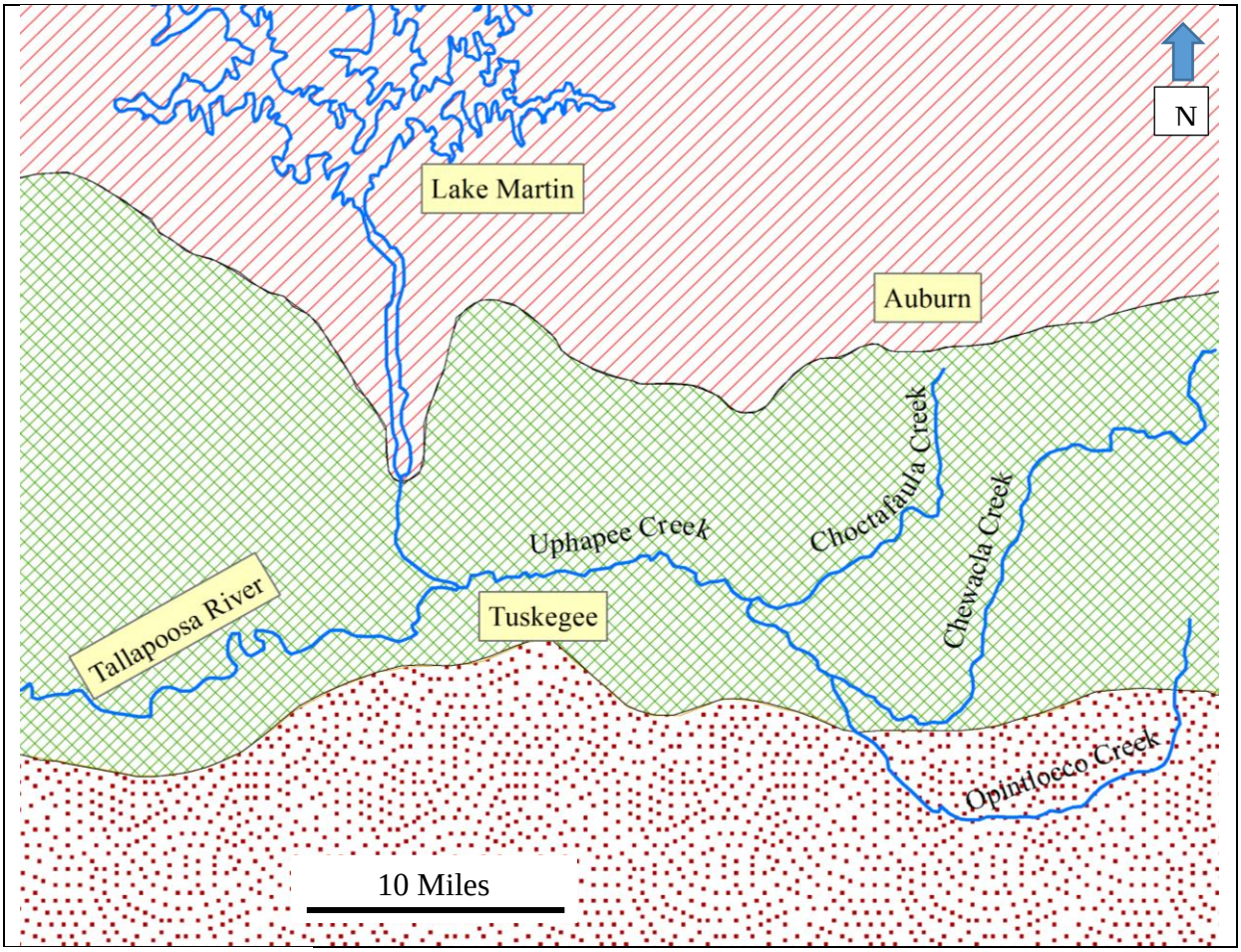

Figure 3. Geologic map of the study area at Macon County, Alabama showing the major rivers and streams and approximate outcrop patterns of the Piedmont crystalline rocks and the sediments of Late Cretaceous age (modified after Markewich and Christopher, 1982b).

Geologic Setting of the Industrial Site, Florida

The industrial site is located in Bay County, Florida. The specific name and location are not mentioned in this thesis as the site is located in a private property and it was requested not to disclose detail information. In the geologic context, the study area is located in the western part of the Apalachicola Embayment which is a shallow basin between the Ocala and Chattahoochee uplifts (Ghandehari, 2016). The hydrogeologic units of the area are categorized into four major groups: the surficial aquifer system, the intermediate confining unit, the Floridian aquifer system, and the sub-Floridian confining unit. Three of these hydrogeological units occur in the shallow subsurface, from top to bottom as follows: surficial aquifer, the Jackson Bluff confining bed, and the Intracoastal Formation aquifer (Schmidt and Clarke, 1980). The top unconfined Surficial Aquifer mainly composed of quartz sand and gravel. This aquifer extends from the surface to a depth of approximately 6-7.6 meters (Levitt, 2017) and the water table at the study site is very close to the surface (4-7 ft.) (Wilson, 2018). The Surficial Aquifer is underlain by the Jackson Bluff Formation, which consists of three clayey, sandy shell beds (Schmidt and Clark, 1980). This formation acts as a barrier, restricting flow from the Surficial Aquifer downward to the other hydro-stratigraphic units. The groundwater of the Surficial Aquifer became severely contaminated with an elevated level of arsenic by the use of herbicides. The average arsenic level observed at this site was around 150 ppb, with levels reaching as high as 577 ppb (Starnes, 2015).

Previous Research

Arsenic speciation, mobilization, and remediation became one of the major interests of research in the last several decades. Hounslow (1980), Smedley and Kinniburg (2002) identified redox potential (Eh) and pH as the two main driving factors that determining arsenic speciation and whether arsenic will mobilize in subsurface aquifers. An Eh-pH diagram is showing different species and stability field of arsenic (Figures 12). Mobilized arsenic is most commonly observed in two oxidation states arsenate [As(V)], which has an oxidation state of +5; and arsenite [As(III)], which has an oxidation state of +3 (Saunders et al., 2018). In oxidizing environments, arsenate species (H_3AsO_4, $H_2AsO_4^-$, $HAsO_4^{2-}$, and AsO_4^{3-}) are dominant, and more toxic arsenite is found under moderately reducing conditions (Farquhar et al., 2002; Wolthers et al., 2005). The arsenate tends to be mobile under oxidizing conditions and its speciation is highly pH-dependent, however, arsenate can heavily sorb onto iron and manganese oxy-hydroxide (FeOOH and MnOOH) coatings if present in the environment (Saunders et al., 1997). Arsenite can exist as neutral aqueous complexes such as $As(OH)_3$ and which makes it is highly mobile.

Korte (1991) first proposed that the arsenic enrichment of alluvial aquifer groundwater is caused by the co-deposition of hydrous ferric oxides (HFO) containing sorbed arsenic and natural organic matter in river floodplain alluvium; and the organic matter caused a reductive dissolution of HFO, releasing both Fe(II) and As to groundwater. Saunders et al. (1997), Penny et al. (2003) and Lee et al. (2007) explaining the releasing Fe, As and other trace elements such as Mn, Co, Ni, Ba, V, etc. in alluvial aquifers in the USA, extended the geochemical model developed by Korte (1991) to include the metabolic effects of Fe-reducing bacteria (FeRB) and Mn-reducing bacteria (MnRB). The contribution of Fe-reducing bacteria and Mn-reducing bacteria for releasing arsenic and other metal contaminants was also reported by Dowling et al. (2002). Saunders et al. (1997, 2005) and Lee et al. (2005) proposed that arsenic is mobile under iron-reducing conditions and immobile under sulfate-reducing conditions, given ample supplies of necessary electron donors and acceptors. Similarly, Keimowitz et al. (2007) demonstrated based on laboratory experiments that arsenic is released under Fe-reducing conditions and immobilized during biogenic sulfate-reduction.

Saunders et al (1997) studied a portion of the drainage basin of Uphapee Creek, in east-central Alabama. They found that groundwater in the alluvial aquifer of Holocene floodplain deposits contain 0.10-4 mg/L of Fe, 1-10 μg/L of As and other trace elements such as Co, Ni, Zn, La, and Ce, and 40-175 μ/L of Ba. The study indicated that the groundwater chemistry is largely controlled by the reduction and dissolution of ferromanganese coatings mediated by Fe- and Mn-reducing bacteria. Lignitic macro wood fragments were replaced by the authigenic euhedral pyrite crystals and from sulfur isotope data it was evident that pyrite crystals were precipitated as a consequence of bacterial sulfate reduction. The authigenic pyrite contains several hundred ppm of As, Co, and Ni, indicating that these trace elements were coprecipitated in pyrite during bacterial sulfate reduction.

Starnes (2015) studied the geochemistry and hydrogeology of arsenic contaminated shallow alluvial aquifers in Alabama (Macon County) and Florida. The study found biogenic pyrite naturally forming at the Macon County site, and had removed arsenic, presumably by co-precipitation and sorption. Starnes (2015) also studied groundwater of a contaminated industrial site in Florida. That was contaminated with an elevated level of arsenic (up to 0.57 ppm). This research suggested a high degree of mixing of meteoric and carbonate groundwater in the surficial aquifer. The main hydro-chemical facies of groundwater in the surficial aquifer is characterized as a Ca-HCO_3-Na-Cl type. Groundwater is enriched in Ca, Mg, and HCO_3- relative to the conservative mixing line of seawater. The groundwater is sulfate-limited (sulfate concentration <9 mg/L).

Saunders et al. (2008) presented data from field bioremediation experiments and geochemical modeling to illustrate the principal geochemical behavior of arsenic in anaerobic groundwater. Two field bioremediation experiments were carried out, one in Bangladesh and the other one is in the USA. Three former graduate students of Auburn University worked on thesis projects (Turner, 2006; Shamsudduha, 2007; and Dhakal, 2010) related to groundwater contamination in Bangladesh. In central Bangladesh at Manikganj district groundwater in Holocene alluvial aquifers was amended with labile, water-soluble organic carbon (molasses) and magnesium sulfate ($MgSO_4$) to stimulate the metabolism of indigenous sulfate-reducing bacteria (SRB). In the United States, groundwater was amended with similar ingredients such as sucrose and methanol to stimulate sulfate-reducing bacteria. These studies showed that arsenic is mobile and released under iron-reducing conditions and becomes immobile under sulfate-reducing conditions (Figure 4). The studies showed that if sulfate reduction can be engineered and maintained, it is possible to reduce the arsenic concentration at the field scale.

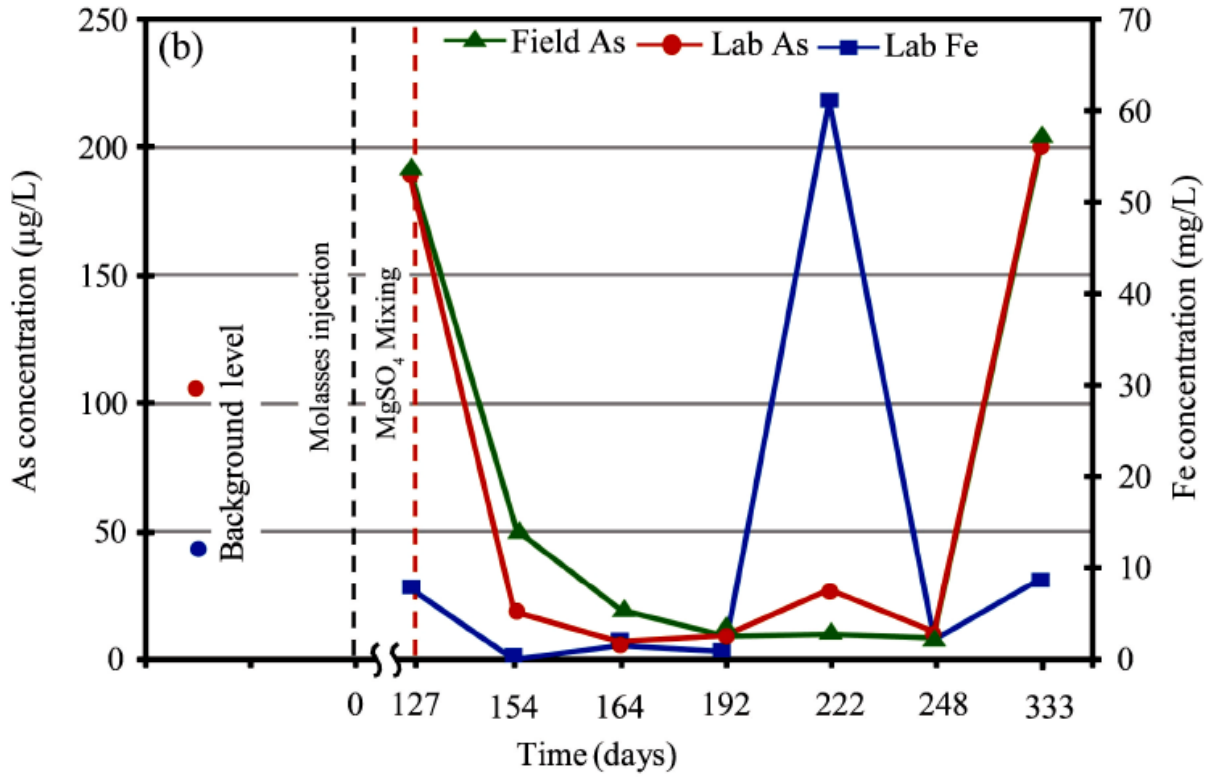

Figure 4. The plot showing As and Fe concentration versus time for an bioremediation experiment in Bangladesh. Initially groundwater was controlled by FeRB and injection of molasses increased As concentration. As decreased significantly in 4 weeks after adding a source of sulfate (Epsom's salt or $MgSO_4$) (Saunders et al., 2008).

Ghandehari (2016), Levitt (2017) and Wilson (2018) conducted a bioremediation experiment using sulfate-reducing bacteria at field-scale in an arsenic-contaminated industrial site, in Florida. These researches demonstrated that the stimulation of natural sulfate-reducing bacteria in groundwater can precipitate biogenic pyrite nanoparticles that can play an active role in sequestering dissolved arsenic from contaminated groundwater. To introduce an artificial sulfate-reducing condition the aquifer was amended with a nutrient rich solution. Eh-pH diagrams (Figure 5) from Levitt (2017) showing the arsenic species under various redox conditions and formation of stable arsenian-pyrite solid phase under strongly reducing condition. These studies confirmed the formation of bio-mineralized pyrite and it sequestered appreciable amount of arsenic. The dissolved arsenic concentration in the groundwater decreased to below the site regulatory limit of 50 ppb in a few weeks after injection. Lee et al. (2018) compiled all the field observations made by Ghandehari (2016), Levitt (2017), and Wilson (2018). This presented additional sulfur isotope data to support the idea bacterial metabolism is responsible for the biogenic pyrite formation. Enrichment of heavy ^{34}S (range from 2.02 to 4.00 ‰) was observed in treated groundwater with most active bacterial sulfate reduction compared to unaffected well water (0.40–0.61 ‰). More detail of these studies is described in the result section.

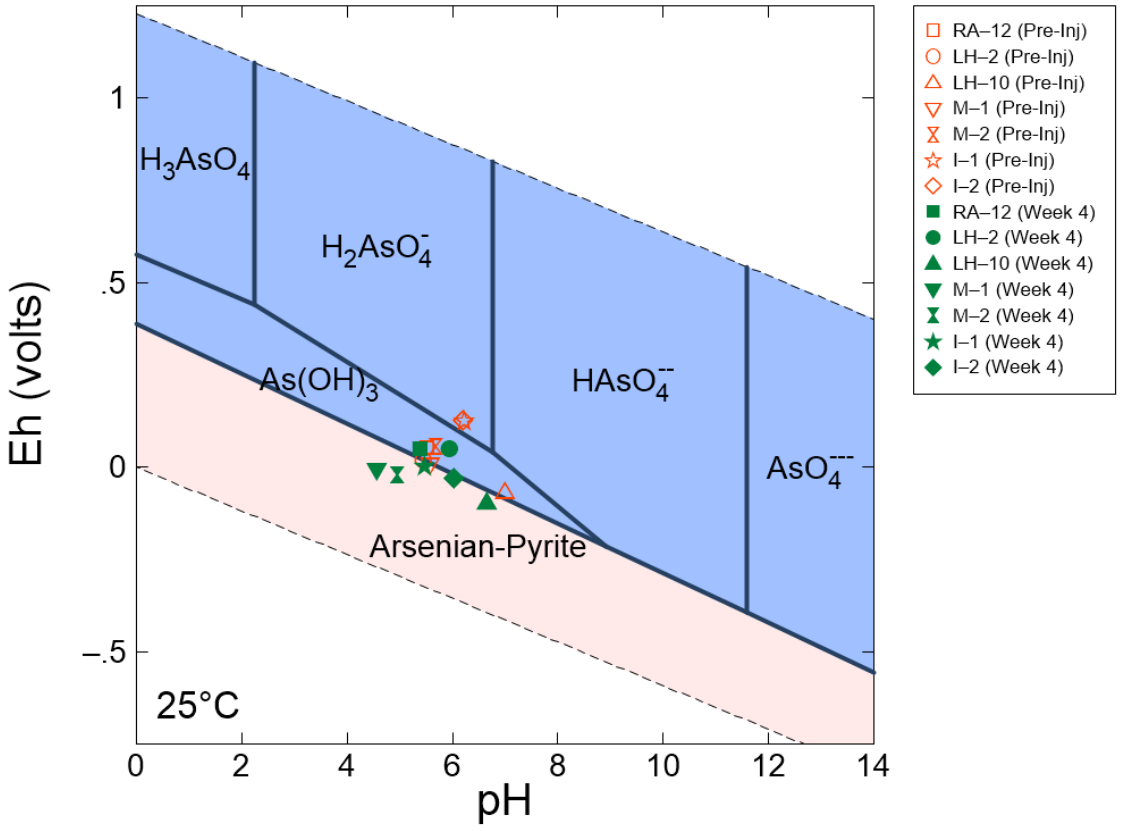

Figure 5. Eh-pH diagram showing stable As species under various redox conditions. The groundwater Eh-pH diagram showing a clear shift of the groundwater condition and formation of stable arsenian-pyrite solid phase after 4 weeks of injection. (Levitt, 2017).

Methodology

Well Drilling

An appropriate location for drilling new wells was identified through preliminary fieldwork. We followed the Uphapee Creek towards downstream to find the location where authigenic pyrites were forming naturally and Fe- and Mn-oxidizing surfaces were exposed (Figures 6, 8A). Four wells have been drilled on the bank of Uphapee Creek using a hand-held auger. On 17th July, 2018 graduate students Md Mahfujur Rahman, Collins Sutton and Professor Dr. Ming-Kuo Lee and Dr. Ashraf Uddin of Auburn University Geosciences Department visited the site and drilled the first well. Subsequent field works were conducted in October, 2018 to complete the first well; and to drill another three wells in the same location. The well diameter was 3.5 inches and the casing material was PVC. The study area and well locations are showed in Figures 6 and 7, respectively. A newly installed well is shown in Figure 8B. In January 17th, 18th and 24th, 2019, all four wells were developed, purged and representative groundwater samples were collected. Wells were named based on the sequence of drilling, such as well-1, well-2, well-3, and well-4. Well-1 and well-4 are 5ft apart from each other; and well-2 and well-3 further downgradient toward the creek are 3.5 ft apart from each other. The ground surface elevation for well-1 and well-4 was 266.5 ft; and well-2 and 3 was 255 ft.

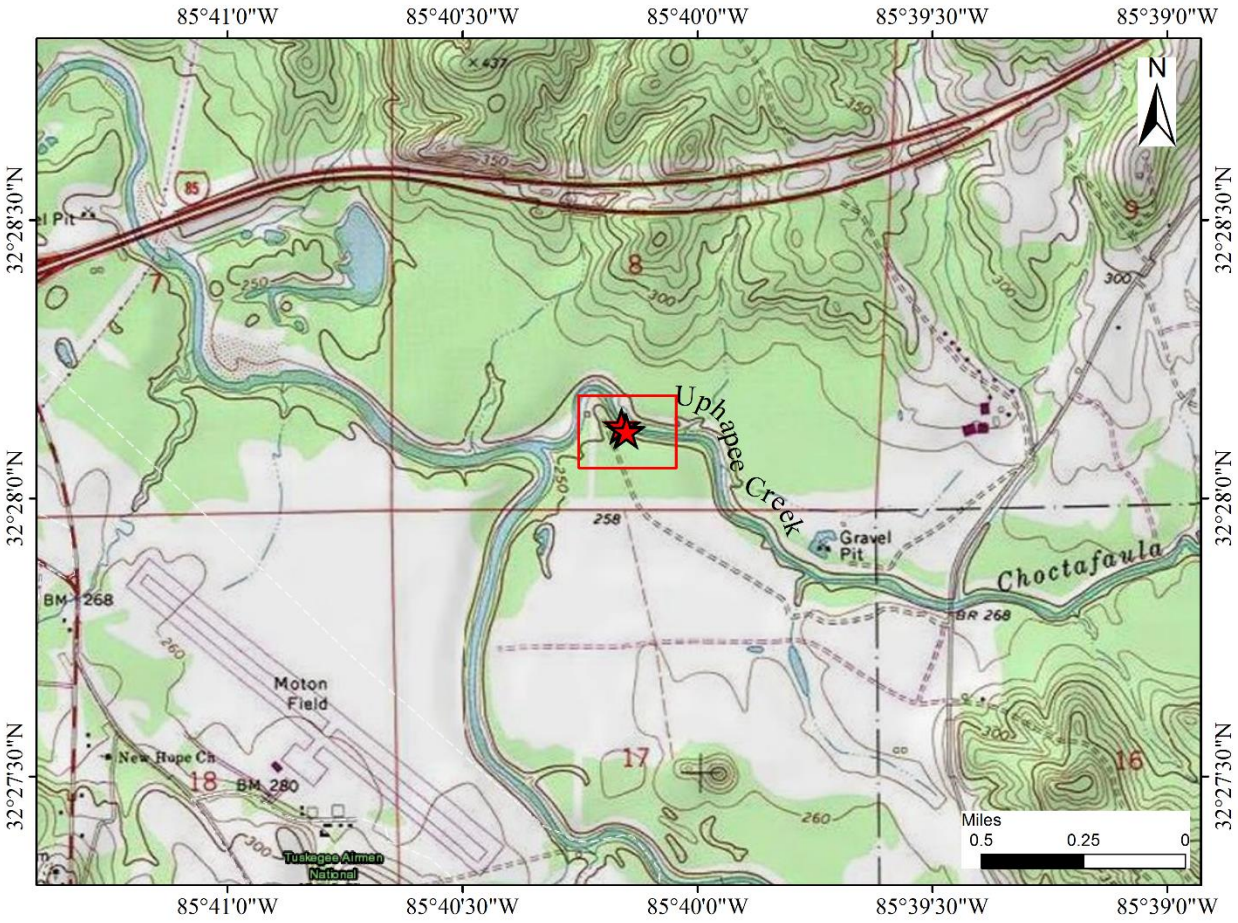

Figure 6. Map showing the locations of wells marked with red star inside the square box, in the bank of Uphapee Creek at Macon County, Alabama.

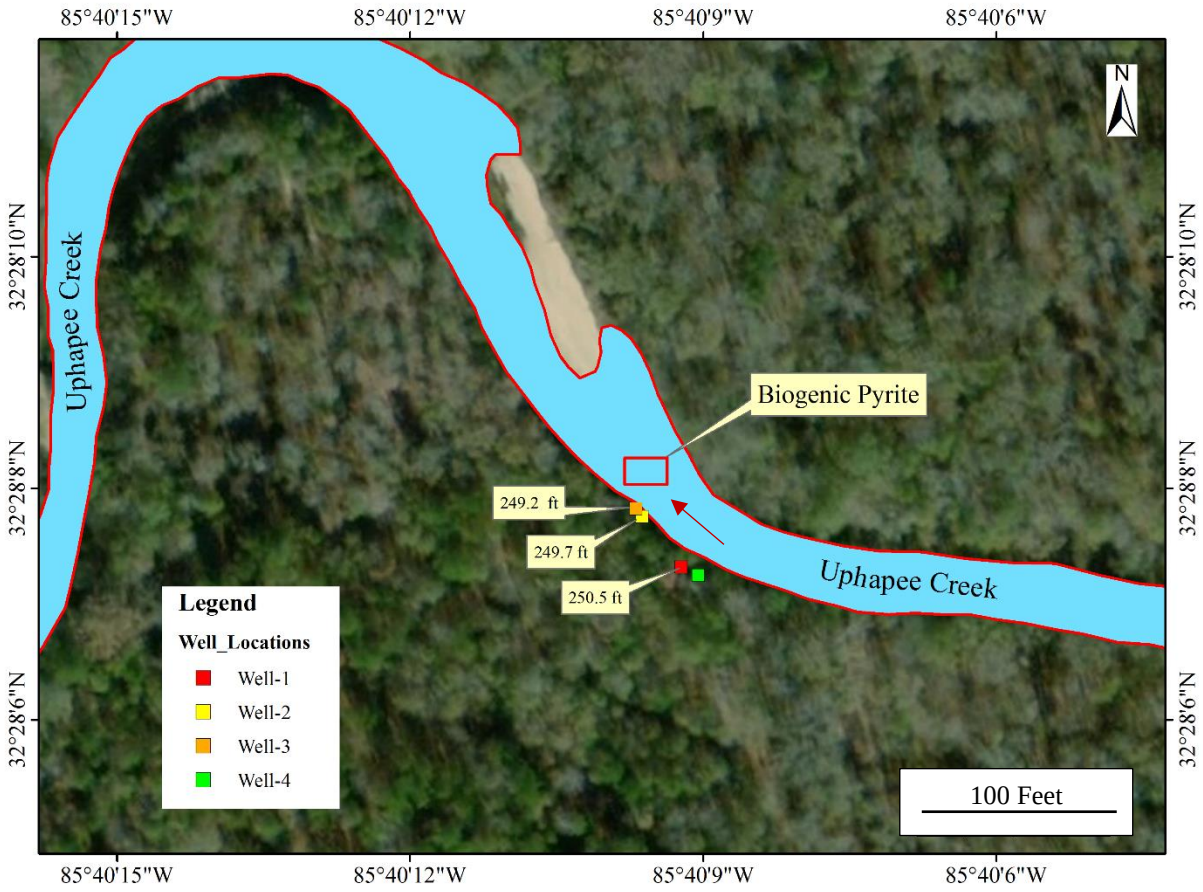

Figure 7. Map showing the relative position of the wells and the location where arsenic-rich biogenic pyrite found in the middle of the creek replaces wood fragments in the Uphapee Creek watershed at Macon County, Alabama. The numbers (yellow rectangular boxes) representing groundwater table elevations relative to sea level on 20th November, 2018 and the arrow is indicating both surface water and groundwater flow direction.

Figure 8. (A) An outcrop of Fe- and Mn- oxidized zone formed from spring discharge; (B) A newly installed well in the study area, (C) A bucket of aquifer material including large gravels that were recovered from the upper aquifer.

Injection at Industrial Site, Florida

Ghandehari (2016), Levitt (2017), and Wilson (2018) described the detail of the injection process conducted at the arsenic-contaminated industrial site in Florida. Here just a brief description of the injection process is described. The injection was conducted in February, 2016 by former graduate students Eric Levitt, Shahrzad Saffari; and Professor Dr. Ming-Kuo Lee, Dr. James Saunders of Geosciences Department, Auburn University. Two injection wells (I-1 & I-2) were used where I-1 was injected with 2,000 gallons of a "weak" solution and I-2 was injected with 1,000 gallons of a "strong" solution. The solution injected into well I-1 had the following mixture ratio per 1000 gallons of water: 2.5 kilograms of ferrous sulfate, 2 pounds (0.9 kg) of 10/10/10 All-purpose fertilizer, and 60 pounds (27.2 kg) of molasses. The mixture ratio for the I-2 injection solution per 1000 gallons had 5 kilograms of ferrous sulfate, 2 pounds (0.9 kg) of 10/10/10 All-purpose fertilizer, and 60 pounds (27.2 kg) of molasses. In the strong solution, the amount of $FeSO_4$ was doubled relative to the weak solution per 1000 gallons of water. Two monitoring wells (M-1 & M-2) were installed 1 meter downgradient to monitor the changes in arsenic level and groundwater geochemistry during different stages of the bioremediation experiment.

Field Sampling and Measurements

Pyrite samples along with lignitic wood were found along the Uphapee Creek fluvial system during the preliminary fieldworks. Four monitoring wells were installed adjacent to this location to study the fluvial sediments and groundwater geochemistry slightly up-gradient from where pyrite minerals were formed. While drilling the wells, a lignitic wood layer was encountered in well-1 and well-3. Samples were collected and preserved for mineralogical and geochemical analysis.

To collect groundwater samples from the aquifer, a peristaltic pump was used to purge the wells by removing about three well volumes of water for at least two hours. The purpose of purging the wells is to make sure that all of the stagnant water residing inside the well casing is flushed out and fresh groundwater percolates through the well screen. This process allows us to get representative groundwater samples and analyze actual geochemistry of the aquifer.

An YSI 556 hand-held multiparameter probes connected to a flow cell was used in the field to measure the water quality parameters including temperature, pH, dissolved oxygen (DO), oxidation-reduction potential (ORP), and electrical conductivity (EC) etc. Measured ORP values are often normalized to a standard hydrogen electrode (SHE), depending on the type of ORP electrode (e.g., Ag/AgCl) used. Since pH and ORP electrodes are built together as a single probe for YSI 556, ORP is read relative to the standard SHE, so no conversion of ORP measurements to Eh values is needed. When the readings for these parameters became stable the numbers were written down. To measure the dissolved sulfide concentration, a HACH DR2700

spectrophotometer was used in the field, via the standard Methyl Blue Method (USEPA Method 8131). A HACH DR820 colorimeter was used to measure the ferrous iron concentration via 1.10 phenan-throline Method (USEPA Method 8146) in the field. The HACH digital titrator test kit was used to measure the alkalinity in the field using titration method (USEPA Method 8203) was used.

Groundwater samples were filtered through a 45-micron filter using a syringe and purged into four 30mL vials. One of the filtered water was also filtered through disposable arsenic speciation cartridges (Meng, 1998) to determine arsenic speciation. The vials were used for different geochemical analyses, including arsenic speciation, ICP-MS (the Inductively Coupled Plasma Mass Spectrometry), IC (Ion Chromatography), and DOC (dissolved organic carbon). The samples for ICP-MS analysis were acidified and preserved using 70% nitric acid for trace metal and cation analysis.

The first 5 mL of the filtrate that passed through the arsenic speciation cartridge was discarded before collecting the samples. As speciation cartridges contain an adsorbent that adsorbs the negatively charged As ions [such as As(V), $H_2AsO_4^-$] while allows the neutral arsenic complexes [such as As(III), H_3AsO_3] to pass through. The ICP-MS analysis of these two sets of samples will indicate the amount of total As and As(III) concentration in the water. After collecting the water samples they were kept with dry ice but remained unfrozen, until they were delivered to the refrigerator in the laboratory before ICP-MS analysis.

Laboratory Groundwater Chemistry Analyses

The groundwater samples were analyzed in different labs for water chemistry. An Agilent 7900 Quadrupole Inductively Coupled Plasma Mass Spectrometry (ICP-MS) at Auburn University was used to determine major cation and trace element concentrations in groundwater samples. Un-acidified groundwater samples were packed with dry ice and shipped overnight to Activation Laboratories located in Ontario, Canada. A DIONEX DX-120 Ion Chromatography was used to determine anion concentrations. Dissolved organic carbon (DOC) analyses were performed to quantify the level of organic matter contents in groundwater. To analyze DOC, groundwater samples were sent to the Stable Isotope Ecology Laboratory, University of Georgia.

Geochemical Analysis

X-ray Fluorescence (XRF) Spectrometer provides fast, nondestructive semi-quantitative analysis of powdered samples on their overall bulk chemical composition (Fitton, 1997). XRF measures the emission of characteristic fluorescent X-rays released from a material that has been excited by being bombarded with high-energy X-rays. Pieces of the black lignitic woody material were separated from the associated fluvial sediments along the creek bank and wells using a petrographic microscope. The lignitic woody material that was associated with the pyrite was powdered before analysis to get better results. The results were used to characterize the bulk elemental composition of the samples including the presence of iron, sulfur, arsenic and other trace elements in a semi-quantitative manner. The analysis was conducted using a portable Bruker Elemental Tracer IV-ED XRF in the Department of Geosciences, Auburn University.

X-Ray Diffractometer (XRD) can be used to identify unknown crystalline materials (Bish and Post, 1989). XRD analysis provides peaks corresponding to different minerals present in selected lignitized wood collected from the creek and wells during drilling. XRD analysis was conducted using a Bruker D2 Phaser X-ray Diffractometer. When the volume of the sample was not enough to fill a standard Bruker powdered sample holder the sample was mounted on a zero background glass sample holder. Samples were run from 2-theta values of 5 degrees to 75 degrees with a 0.02-degree step interval which is considered as standard for a geologic sample. The mineral composition of the samples was determined by a peak search and match with the resultant XRD spectra using DIFFRAC.EVA software. This software, using Bragg's Law, converts the dominant peaks detected on the spectra to d-spacings, which can be searched and matched to the unique d-spacings of known minerals thus identifying the mineral composition of the sediments. This analysis was conducted at the Department of Geosciences, Auburn University.

Electron Microprobe (EMP) Analysis

To better quantify the chemical composition and arsenic content of the pyrite grains collected from the Uphapee Creek, three samples were selected for analysis using the JEO – JXA 8600 Superprobe Electron Microprobe (EMP) and accompanying Geller System automation in the Department of Geosciences, Auburn University. The pyrite samples recovered from the creek were sent to National Petrographic Service, Texas to prepare polished (uncovered) thin sections. Theses thin sections were named as MC-1, MC-2, and MC-3; where MC stands for Macon County. Unlike the XRF, EMP can analyze spots on mineral grains as small as 1-2 microns in diameter in a quantitative manner (Reed, 2005). Thus this allows assessing and mapping compositional changes across a single pyrite grain and more importantly to quantify the amount of arsenic per unit mass. As pyrite is not naturally conductive, the thin sections were carbon coated to increase conductivity for EMP analysis. The AU microprobe is equipped with BSE and SEM imaging along with EDS and WDS detectors, which were instrumental in understanding the size, morphology, and composition of the pyrite grains. BSE and elemental map images were obtained at a current of ~ 50 mA and an accelerating voltage of 15KeV. The standards for Fe, S, Si and As were used to obtain the element contents as weight % and the elemental maps in the grains within certain areas of the thin section. The software programs used for the analyses include: (1) Geller System dPict: BSE and Elemental Mapping; (2) Geller System dQuant and dSpec: Spot and line analyses for major oxide wt%; and (3) National Institute of Health Image J: Image processing.

Scanning Electron Microscope Analysis

A scanning electron microscope (SEM) analysis was conducted to determine the size and texture of the pyrite grains using a Zeiss EVO 50VP SEM at the Auburn University Instrumentation Facility. Pyrite samples as well as the same carbon coated thin sections that were used for EMP analysis was used in SEM studies. The scanning electron microscope produces images by scanning the sample with a high-energy beam of electrons. As the electrons interact with the sample, they produce secondary electrons, backscattered electrons, and characteristic X-rays. These signals are collected by one or more detectors to form images. An INCA EDS system was connected with the SEM that was used to study the quantitative elemental composition of the samples. The software programs used for the analyses include: (1) Zeiss SmartSEM; (2) RemCon32, and (3) EDS INCA.

Geochemical Modeling

Geochemist's Workbench (GWB) was used to model the speciation of arsenic, iron, manganese under various Eh-pH conditions and to calculate saturation index SI (logQ/K) of various Fe- and Mn-minerals. The thermodynamic database presented by (*Saunders et al., 2008*) were used to prepare Eh-pH diagram for arsenian-pyrite-

$$FeS_{1.99}As_{0.01} + 1.02\ H_2O + 3.5\ O_2(aq) = Fe^{2+} + 1.995\ SO_4^{2-} + 0.01\ As(OH)^{4-} + 2\ H^+,$$

$$\log K_{25} = 199.78$$

Results

Hydrostratigraphy at the Natural Fluvial Site in Macon County, Alabama

The wells were logged based on visual inspection of samples brought to the surface during drilling (Figure 9). Well logs showed a consistent lithology among the wells. Two fining upward sequence were identified, though the second sequence was not completely observed as we did not drill that deep. Two aquifer systems were observed (upper unconfined and lower confined). The lower aquifer was of interest in this study where groundwater occurs under confined aquifer condition.

Total depth for well-1 and well-4 was about19ft. First 6 – 6.5ft below the land surface was very fine sand, followed by 1ft of pebbly sand. At depth 7.5ft – 12ft a gravel layer with coarse sand was observed underlain by 6 inches of clay layer. Fine to medium sand was found at a depth of 12.5ft – 16ft and 16ft – 19ft was coarse sand. A lignitic wood layer was encountered at 17.5ft depth from the surface. During July 17th, 2018 the water table was at 13.5ft below the ground surface in well-1 but in October 9th, 2018 during the completion of the wells water level went down to 17ft in the same well-1 indicating 3.5ft water level drop. Ground surface elevations of well-1 and well-4 are 10 – 12ft higher than those of well-2 and well-3. Groundwater table elevations measured at well-1, well-2, well-3 on 20th November, 2018 were 250.5ft, 249.7ft and 249.2ft respectively relative to sea level, indicating well-1 is an upgradient well. Water table data was not available for well-4 on the same day as this well was drilled after 20th November. The water table elevations and calculated gradient (0.016) suggested

groundwater is moving in a general direction from south-east to north-west (Figure 7) and eventually discharges into the Uphapee Creek.

Total depth of well-2 was about 9ft and well-3 was 17ft. For these two wells, the lithology consists of 2ft of clay from the top underlain by fine to medium sand that extends 2ft – 4.5ft of depth. A 6-inch clay layer was found at depth of 4.5ft. A medium to coarse sand layer was encountered at a depth of 5ft that extended down to 11ft depth. The same lignitic wood layer was found at a depth of 5.5ft. To know more about the subsurface lithology we continued to drill well-3 down to 17ft. A clay layer (reddish color) was found at depth of 11 ft – 17 ft, suggesting that the aquifer is confined from above and below by the low permeability clay layers.

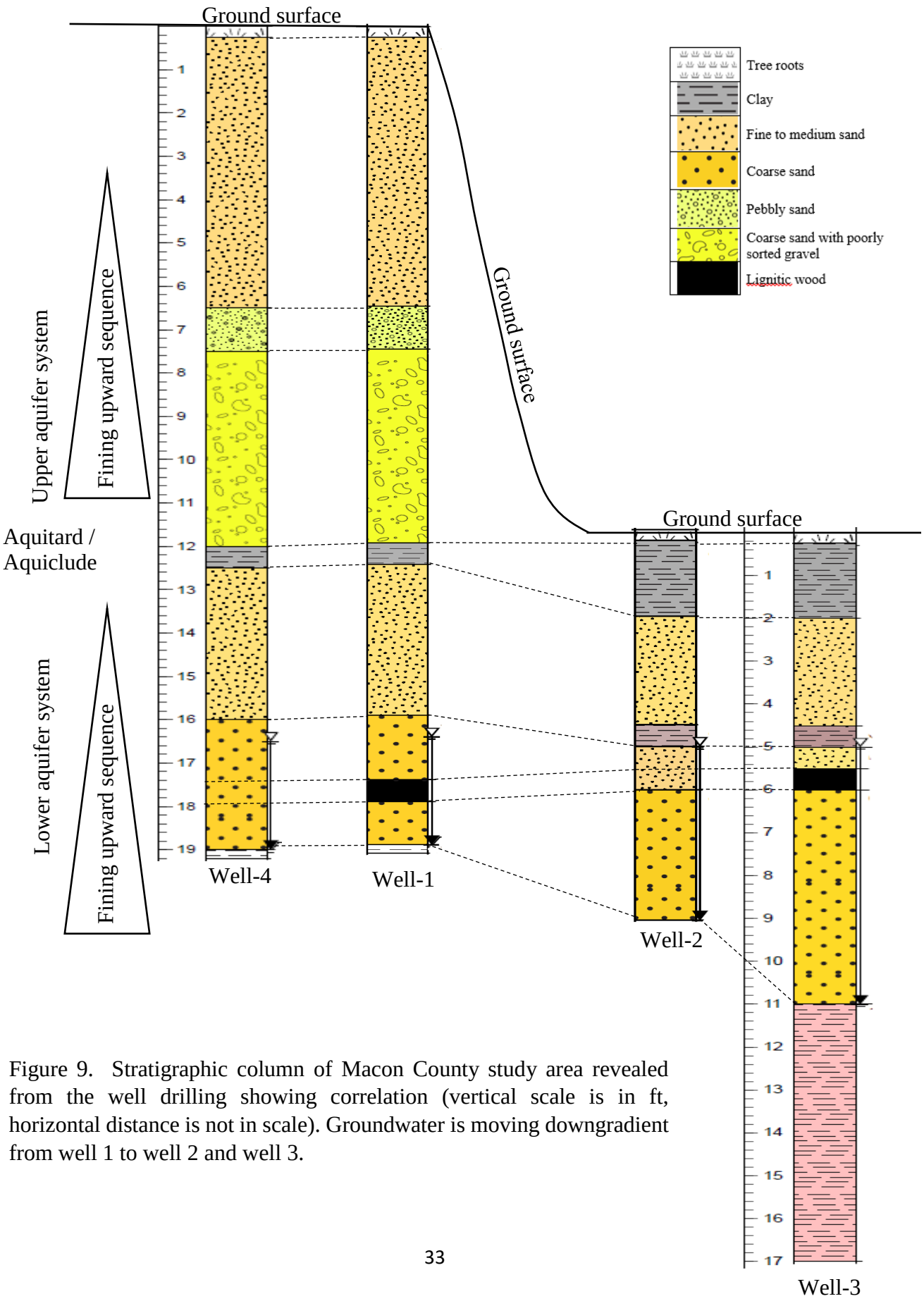

Figure 9. Stratigraphic column of Macon County study area revealed from the well drilling showing correlation (vertical scale is in ft, horizontal distance is not in scale). Groundwater is moving downgradient from well 1 to well 2 and well 3.

Groundwater Chemistry

Field measurements: Table 1 shows water quality parameters and concentrations of ferrous iron, hydrogen sulfide and alkalinity of well water measured in the field. ORP values indicate that groundwater in the fluvial aquifer occurs under slightly oxidizing to moderately reducing conditions (Eh= 46 to173 mV), and nearly neutral to slightly acidic (pH =5.53 to 6.51). Concentration of ferrous iron is much higher in well-3 (3.30 mg/L) than those in well-1 and well-4 (0.08 mg/L and 0.32 mg/L, respectively). By contrast, ORP values are significantly lower in well-2 and well-3 (68.5 and 46 mV, respectively) than those in well-1 and well-4 (121 and 173 mV respectively). Sulfide concentration in these wells ranges from 16 to 39 µg/L. Iron and sulfide measurements were not taken in well-2 as the water coming from the well had too much sediments.

Laboratory measurements: Results of IC analysis of anions in well water are shown in Table 1. Results of ICP-MS analysis of cation and trace elements are showed in Table 2. Piper diagram was prepared based on the major ion concentrations. The diagram shows that the groundwater from the Uphapee Creek wells is a Ca-SO_4 type (Figure 10), which typical As-rich groundwater in Bangladesh Holocene aquifers is a Ca-Mg-HCO_3 type. Dissolved total iron and arsenic concentrations are much higher in well-2 and well-3 than those in well-1 and well-4. Figure 11A shows that As is positively correlated to Fe and inversely correlated to ORP. Low dissolved Fe, Mn, and As concentrations and relatively high ORP values in well-4 reflect an oxidized condition. Nitrate level decreases downgradient from well 1 and well 4 (0.02-0.03 mg/L) to well 2 and well 3 (<0.01 mg/L), indicating nitrate reduction reactions. Elevated Mn concentration (318 µg/l) and moderately high Fe level (239 µg/L) in well-1 suggests that the

groundwater is predominantly under Mn reduction condition (Figure 11B). The combination of very high total Fe (1.3 to 4.2 mg/L), ferrous Fe, and lower ORP values indicate an Fe(III) reduction condition further downgradient in well-2 and well-3. Fe- and Mn-rich groundwater oxidizes to form black (Mn-rich) and orange (Fe-rich) solids as it discharges into the creek as springs (Figure 8A). Arsenic level is slightly higher in well-2 and well-3, suggesting that some As adsorbed by Mn- and Fe- oxyhydroxides may be released under Mn(IV) and Fe(III) reduction condition. Arsenic mobilized in groundwater is subsequently adsorbed by biogenic pyrite formed under sulfate reduction condition further downgradient (see next section) near where groundwater discharges into the creek. Sulfate level in groundwater (Table 1) is relative high (up to 53 mg/L) in downgradient well-2 and well-3, providing ample electron acceptors for bacterial sulfate reduction. Overall the fluvial aquifer groundwater is not limited in SO_4, Fe, and organic carbon (supplied by the lignite wood), which facilitates bacterial sulfate reduction, precipitation of biogenic pyrite, and sequestration of arsenic in pyrite formed (see next section).

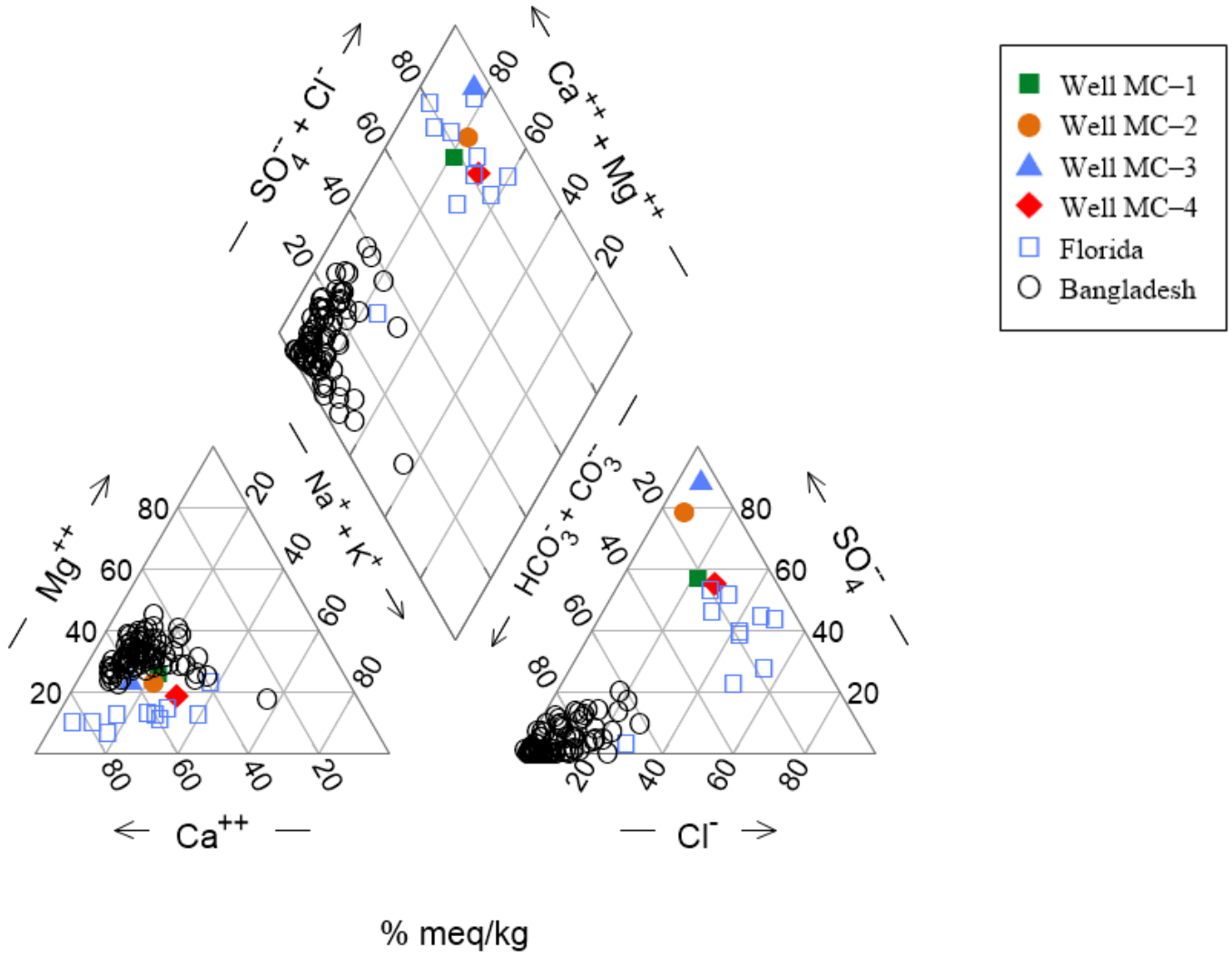

Figure 10. A Piper diagram representation of groundwater samples from Alabama (Macon County), Florida, and Bangladesh fluvial aquifer system.

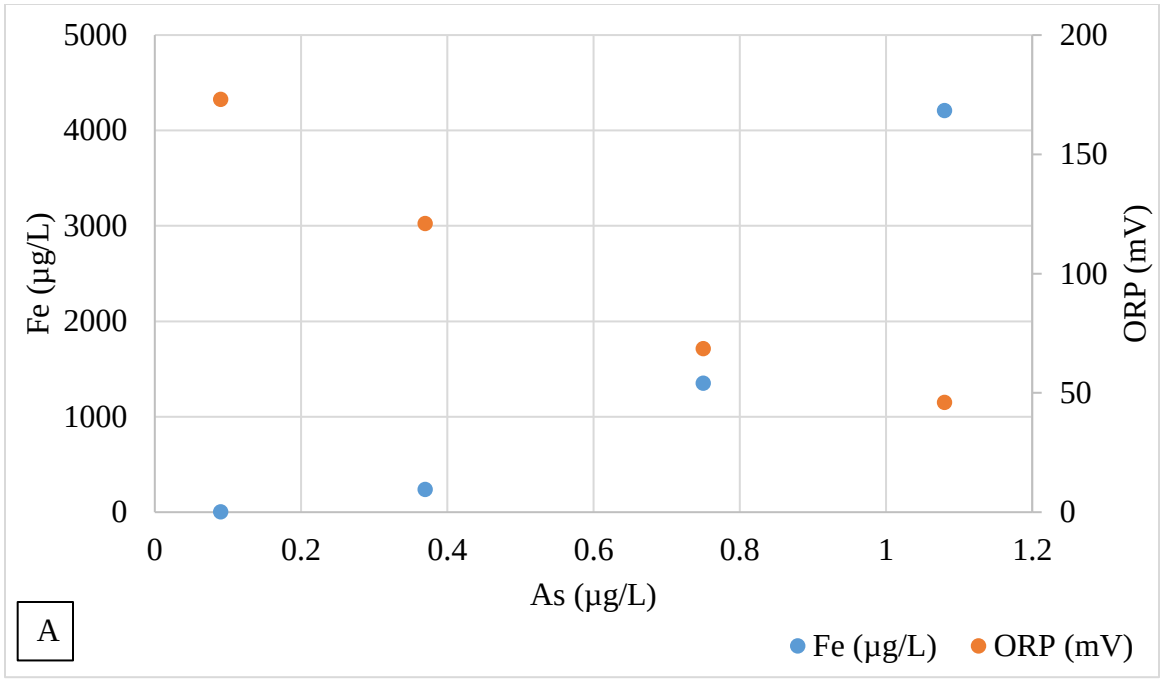

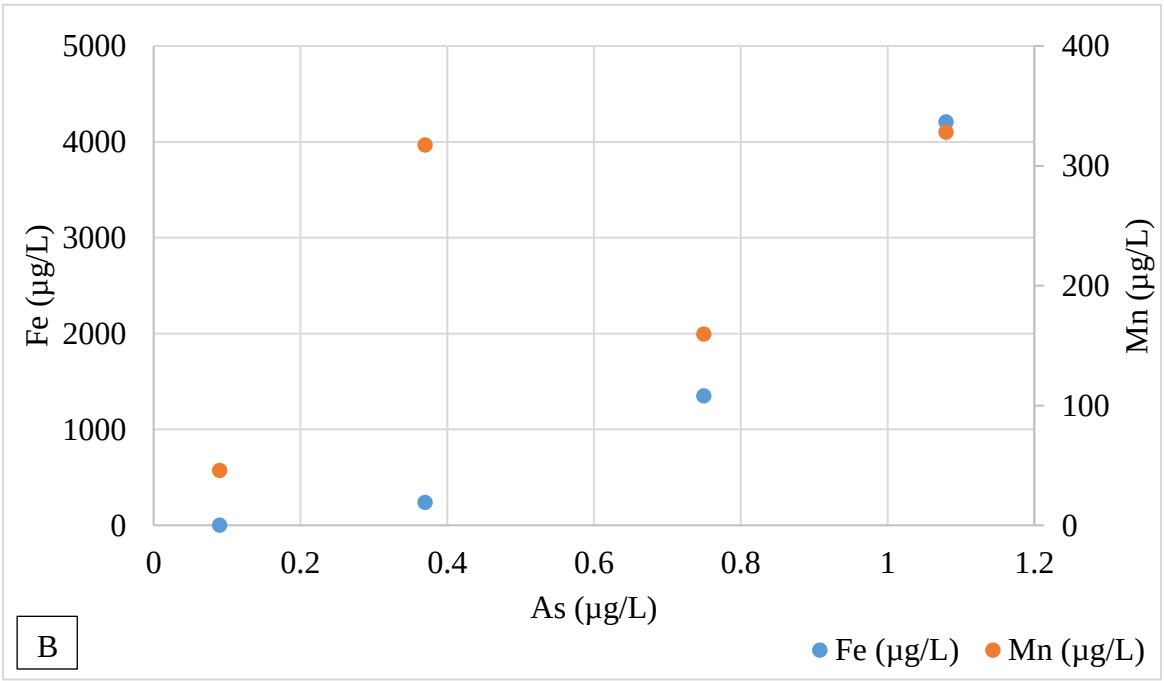

Figure 11. X-Y plot showing (A) a relation of arsenic concentration with iron concentration and ORP, and (B) a relation of arsenic concentration with iron and manganese concentration.

Table 1. IC analysis and field parameters of the groundwater samples at natural site, Macon Co. AL. Units are in mg/L (except as noted)

	Well-4	Well-1	Well-2	Well-3
F	0.02	0.02	0.01	0.06
Cl	2.51	2.15	2.21	2.93
Br	< 0.03	< 0.03	< 0.03	< 0.03
NO_2	< 0.01	< 0.01	< 0.01	< 0.01
NO_3	0.02	0.03	0.01	< 0.01
PO_4	< 0.02	< 0.02	0.09	< 0.02
SO_4	6.75	7.48	30.6	53.1
DOC	2.741	3.706	7.382	3.714
Alkalinity	6.50	12.10	-	27
Ferrous Iron	0.08	0.32	-	3.30
pH	6.51	5.53	6.07	6.08
Sulfide (µg/L)	17	39	-	16
ORP (mV)	173	121	68.5	46
Temp (^oC)	16	17.12	15.60	15.50

Table 2. ICP-MS analysis (cation and trace elements) of the groundwater samples at natural site, Macon Co. AL. Units are in µg/L.

	Well-4	Well-1	Well-2	Well-3
Na	1872.35	1361.62	8800.18	5492.71
K	1685.58	3774.89	4295.06	4952.12
Ca	4060.79	7471.53	24177.84	28853.27
Mg	889.75	2178.08	5863.65	6651.73
Mn	45.92	317.62	159.58	328.32
Fe	2.42	239	1350.60	4210.04
As (total)	0.09	0.37	0.75	1.08
As (III)	0.06	0.27	0.66	1.01
Co	1.44	2.12	0.60	0.55
Ni	3.97	2.71	1.56	0.066
Zn	5.74	9.74	4.70	7.34

The ICP-MS laboratory analysis showed that highest arsenic concentration (1.08 µg/L) occurs in well-3 and lowest concentration (0.09 µg/L) in well-1. The analysis of groundwater from all the wells showed that both total As and As(III) has similar concentration indicating As(III) is consistently higher in concentration than that of As(V). As(III) is the dominating species of arsenic in the groundwater. These analytical results were consistent with the geochemical models. Field Eh-pH data of wells 1, 2, and 3 (Figure 12) showed that dominant arsenic aqueous species were found in the form of As(III) (or $As(OH)_3$) under moderately reducing conditions. . As(V) is the dominant species in well 4 under oxidized condition.

Iron exists in water as either ferrous (Fe^{2+}) or ferric iron (Fe^{3+}). Field measurement of ferrous iron and lab measurement of total iron it indicates that ferrous iron is the dominant species in wells 1, 2, and 3 under Fe(III) reducing conditions (Figure 13). Fe(III) oxyhydroxides represent the stable phase in well 4 under oxidized condition. Table 3 shows calculated saturation index (SI = log Q/K) of various Fe and Mn oxides in groundwater. The results indicate that the dominant amorphous Fe-oxyhydroxides in fluvial sediments are highly under-saturated in well 1, well 2, and well 3, the bacterial-mediated reduction reaction will lead to high-Fe water. Amorphous Fe-oxyhydroxides may convert to more thermodynamic stable phases such as Hematite, Goethite and Magnetite over geologic time. Saturation index for arsenian-pyrite and arseno-pyrite is too negative in all wells under oxidized condition in well 4 and iron reducing condition in well 2, well 3, and well 4. It can be predicted that probably further downgradient, in the sulfate reducing zone saturation index becomes positive for arsenian-pyrite as it is precipitating there. Saturation indices for Mn solid phases (i.e. Pyrolusite, Bixbyite,

Hausmannite) are also strongly negative indicating under saturation. Field Eh-pH data indicate that aqueous Mn(II) (Figure 14) is the dominated Mn species in the wells. Lower Mn concentration is observed in well 4, where Mn oxyhydroxides likely form under oxidized condition.

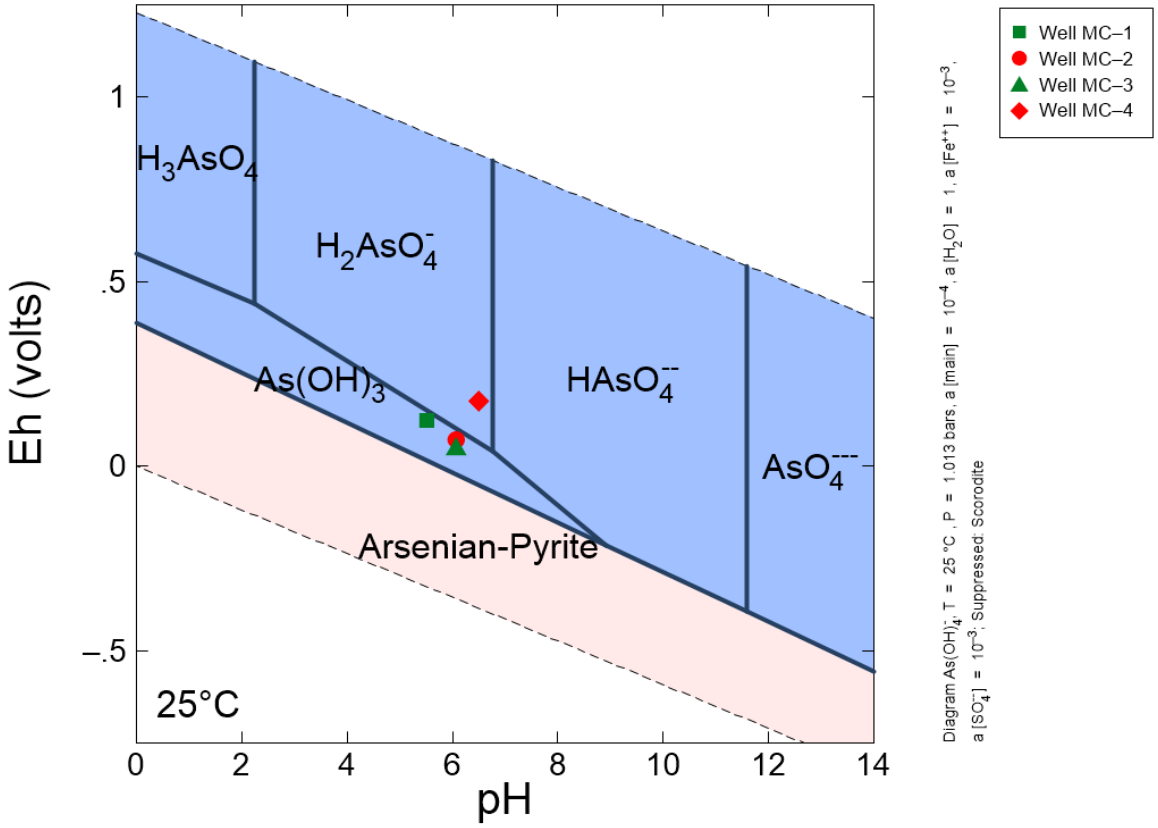

Figure 12. Eh-pH diagram showing As species under various redox conditions with plotted groundwater samples from the wells, where As log activity is -4, for both Fe and SO_4^{2-} log activity is -3, Scorodite (As oxides) is suppressed. Blue fields are aqueous phase and pink fields are solid phases.

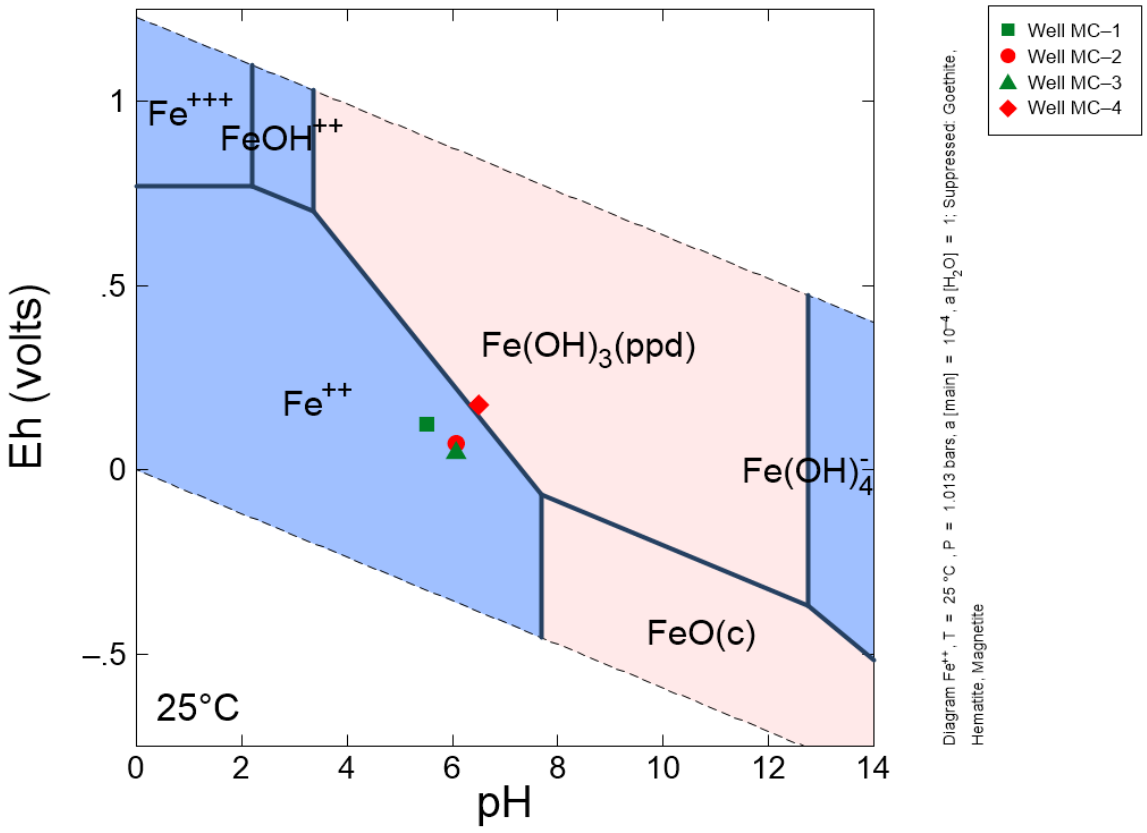

Figure13. An Eh-pH diagram showing stable Fe species under various redox conditions, where Fe log activity is -4, Goethite, Hematite, Magnetite are suppressed. Plotted on the diagram are the redox conditions for each groundwater sample from the wells. Blue fields are aqueous phase and pink fields are solid phases.

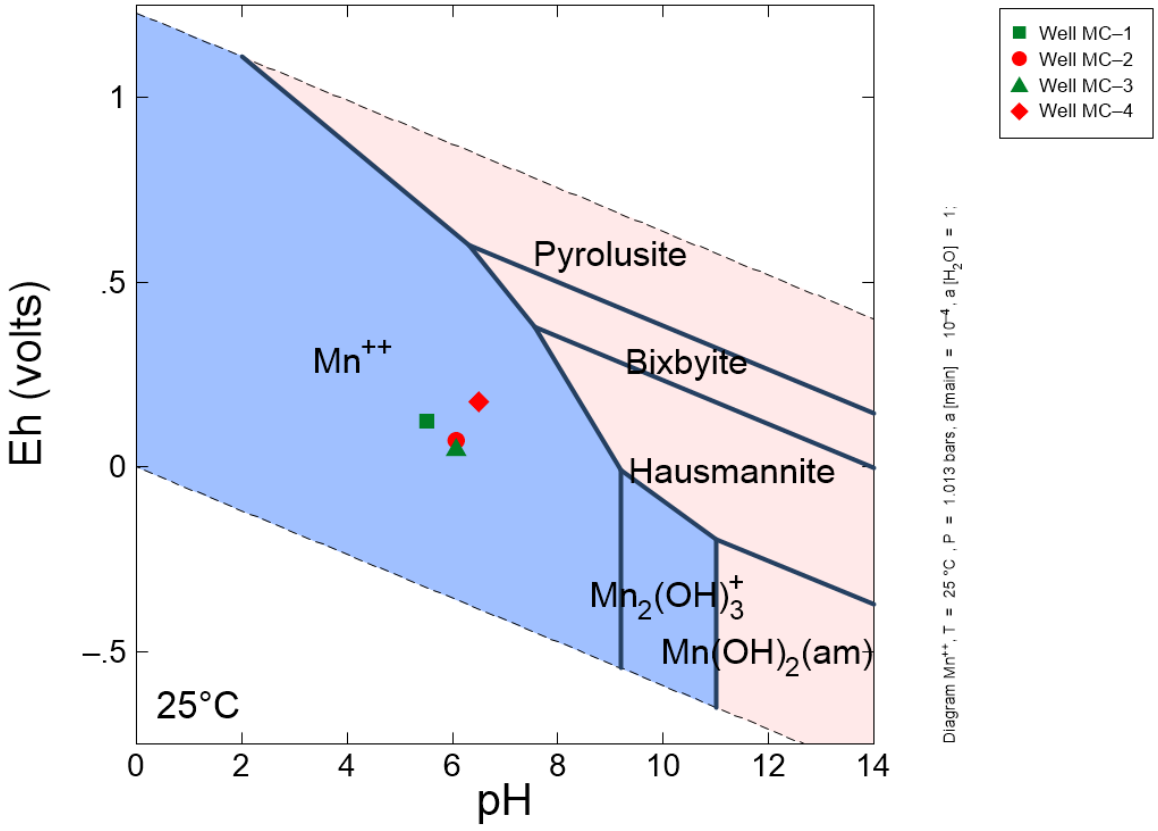

Figure 14. An Eh-pH diagram showing stable Mn species under various redox conditions, where Mn log activity is -4. Pyrolusite, Bixbyite and Hausmannite are the major solid phases. Blue fields are aqueous phase and pink fields are solid phases.

Table 3. Calculated saturation index (SI) for the groundwater sample from the wells

Saturation Index	Log Q/K			
	Well-4	Well-1	Well-2	Well-3
Hematite	7.03	0.57	3.08	3.23
Goethite	3.03	-0.19	1.06	1.14
Magnetite	3.90	-3.93	0.18	0.78
Fe(OH)3(ppd)	-1.35	-4.58	-3.33	-3.25
Pyrolusite	-15.81	-20.66	-20.63	-21.05
Bixbyite	-17.56	-23.55	-22.78	-22.89
Hausmannite	-21.79	-28.92	-27.43	-27.22
Arsenian-pyrite	-58.3501	-29.6983	-24.2970	-18.2552
Arseno-pyrite	-85.8697	-60.3395	-55.1280	-50.2149

Oxidation-reduction sequences

A sequence of redox reactions occur in natural groundwater in confined aquifers as the groundwater migrates from recharge zones to areas of discharge. As the reactions proceed towards downgradient, usually the potential (Eh) of the groundwater decreases and alkalinity increases (Champ et al., 1978). This variations in Eh and variations in concentrations of elements with variable oxidation states (e.g., oxidized, nitrate reduction, manganese reduction, iron reduction, sulfate reduction, and methanogenesis) can be accounted for by a sequence of oxidation-reduction reactions occurring in groundwater flow systems (Champ et al., 1978). The oxidized species reduced in the sequence- O_2, NO_3^-, Mn(lV), Fe(III), and SO_4^{2-}. Oxygen levels remain high in higher Eh value but is decrease as the redox potential decreases. Nitrate is also stable in the presence of oxygen, but rapid denitrification occurs at the redox boundary. In the

iron reducing section of the aquifer a zone (+100 to 0 mV) appears to be controlled by Fe^{2+}. Sulfide, together with Fe^{2+}, affects the Eh value to drop below 0 mV in sulfate reduction zone.

A similar oxidation-reduction sequence has been observed in the fluvial confined aquifer system of the Uphapee Creeck watershed (Figure 15). Oxidized condition has been observed in well-4 (ORP = 173 mV) where natural organic matter is being decomposed and oxygen is the dominant terminal electron acceptor. The measured alkalinity was 6.50 mg/L. Well-4 groundwater, under oxidized condition (ORP = 173 mV), contains notable concentration of NO_3 (0.02 mg/L) and very low level of Fe (2.42 µg/L) and Mn (45.92 µg/L). As the groundwater move down-gradient and the denitrification reactions remove nitrate (<0.01 mg/L) as the aquifer becomes more reducing. A significant increase in Mn (317 µg/L) concentration, and alkalinity (12.10 mg/L) were observed in well-1. Well-1 is probably located in an overlapping zone of NO_3^- and Mn(IV) reduction.

Fe(III) reducing conditions in well-2 and well-3 are evident from very high iron concentrations (1350.60 µg/L and 4210.04 µg/L, respectively), high alkalinity (up to 27 mg/L), and relatively low ORP (68 mV and 46 mV, respectively). Fe(III) oxyhdroxides were reduced and ferrous iron as well as sorbed arsenic is released into groundwater by bacterial iron reduction. Further downgradient from the iron-rich zone, ferrous iron reacts with H_2S generated by bacterial sulfate reduction to form pyrite in sulfate reduction zone.

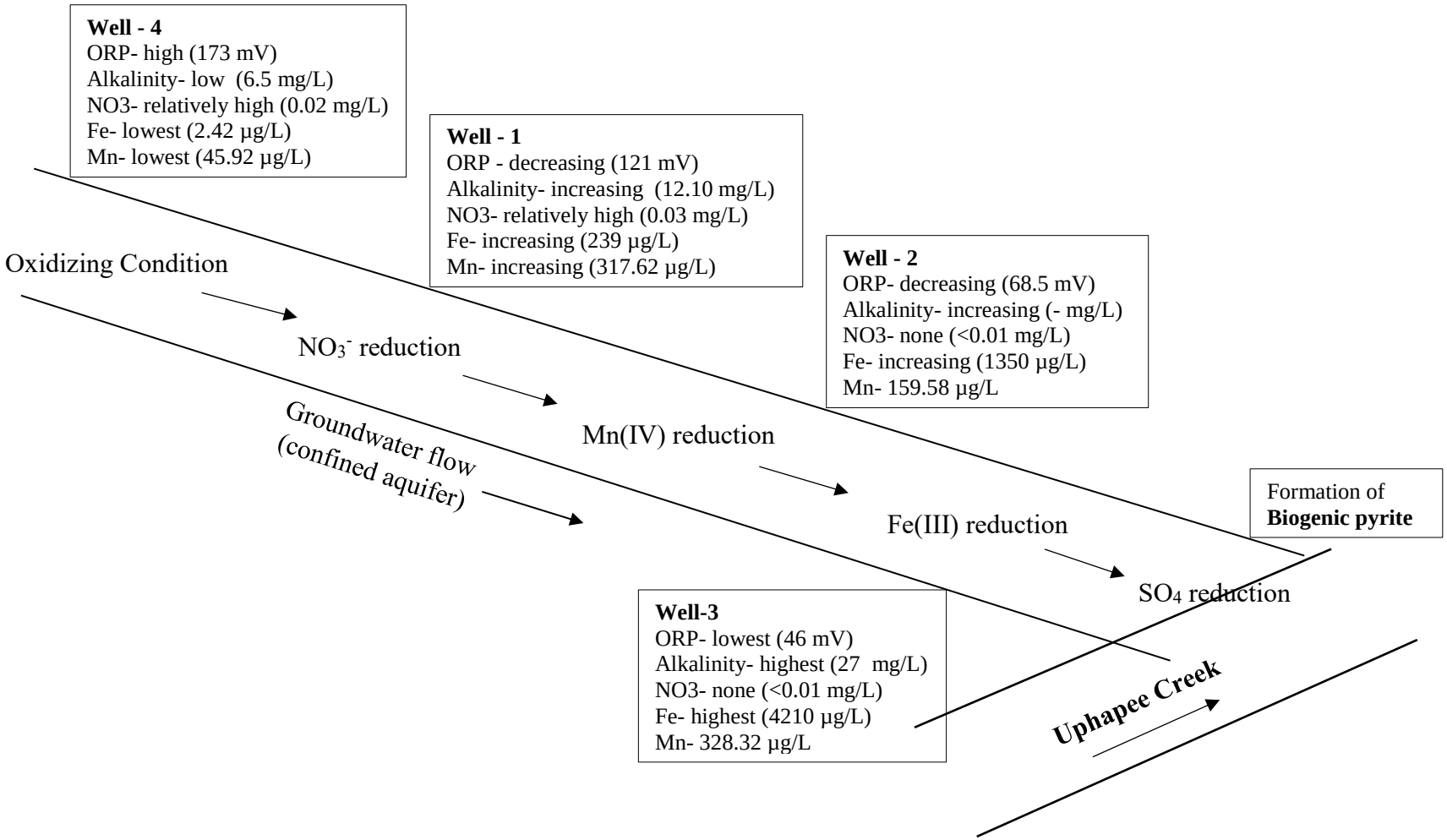

Figure 15. Oxidation-reduction sequences in the Uphapee Creeck fluvial groundwater flow system.

In the study area authigenic pyrite, occurring as coarse-grained crystals, replaced lignitic wood fragments near the base of the alluvial aquifer (Figure 16A) (Saunders et al. 1997). Pyrite most commonly precipitates in zones of natural permeability and porosity in the wood and also fills secondary fractures. In the pyrite crystals there is no signs of visible organic matter other than remnant wood cellular textures (Figure 16B). Pyrite also forms concretions up to a few centimeters in diameter that may have only a small core of replaced wood. The concretions show that most pyrite crystal has euhedral forms (i.e. cubes, octahedrons).

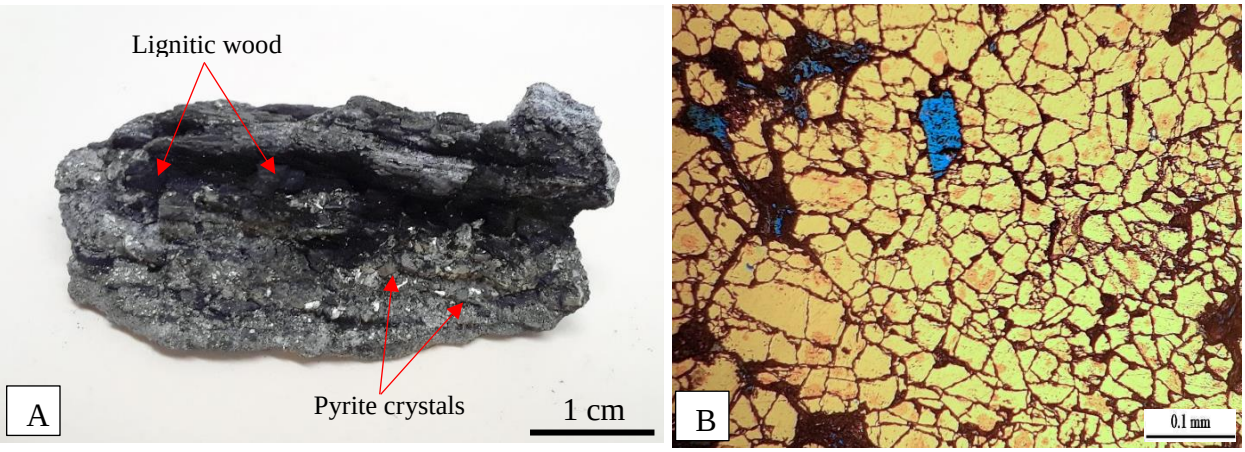

Figure 16. (A) Naturally occurring biogenic pyrite associated with lignitic wood material from the Uphapee Creek, (B) Photomicrograph of pyrite grains under reflected light showing cellular texture.

The samples of lignitic wood layer and associated fluvial sediments (from the wells) were studied under microscope (Figure 17). Individual wood/ black pieces of solids (Figure 18) were separated from the associated sediments and then analyzed to get better results.

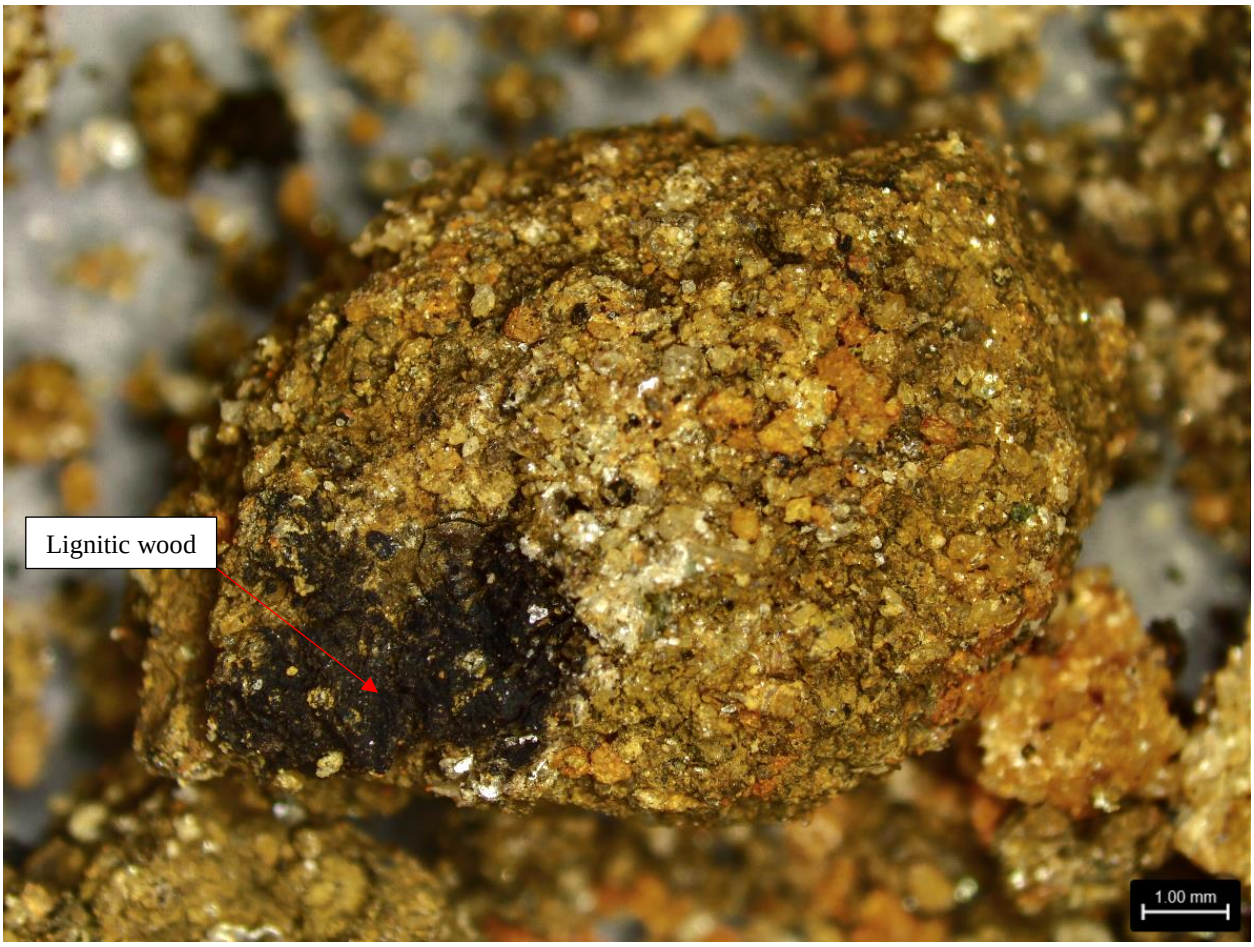

Figure 17. Lignitiic wood materials (from the wells) with associated sediments under microscope.

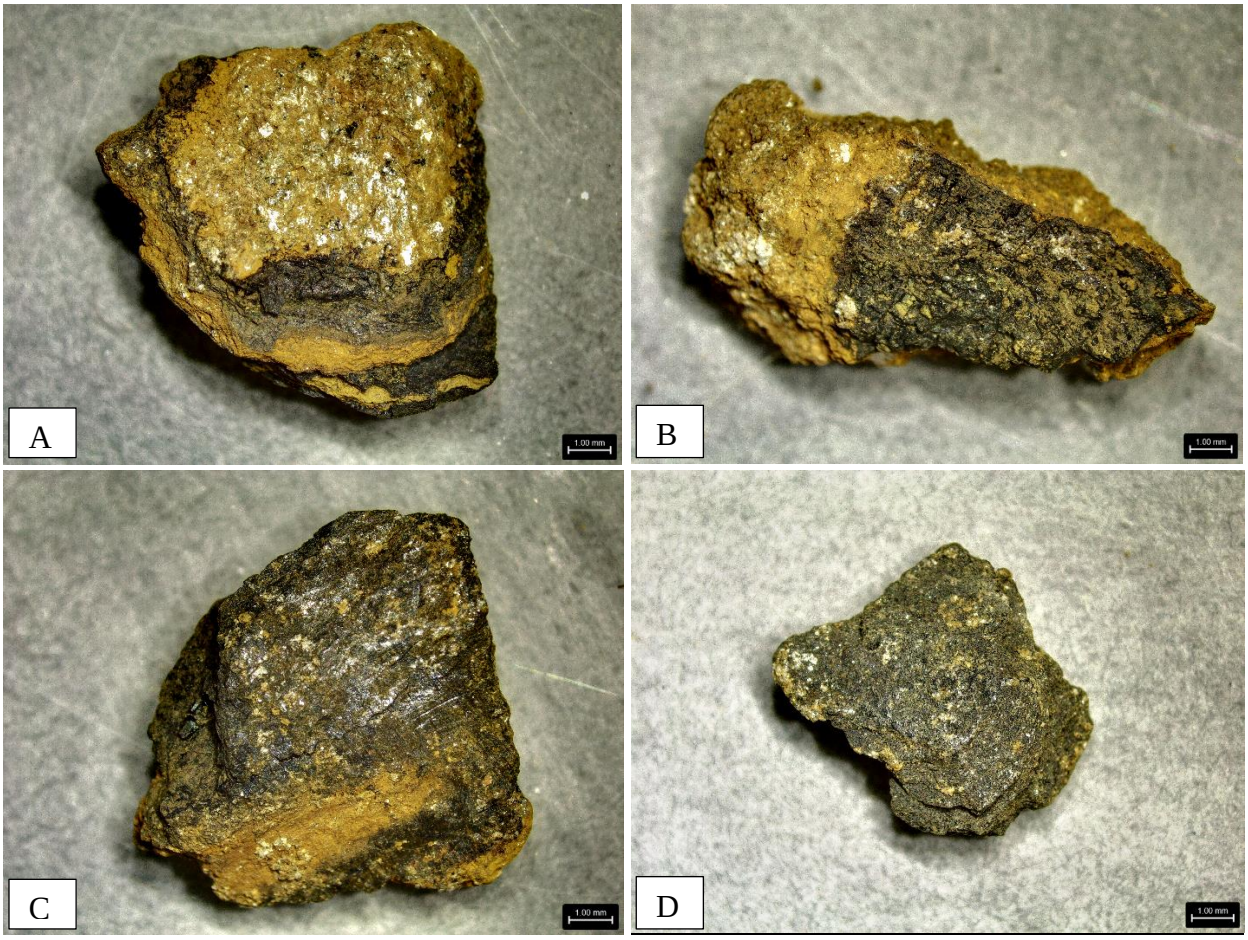

Figure 18. Individual pieces of lignitic wood materials collected from the wells during drilling.

X-ray Fluorescence Analysis

X-ray fluorescence (XRF) analysis was conducted for individual pieces of lignitic wood (from wells) material to assess the overall chemical composition including the trace elements. The XRF spectrum showed peaks for iron, sulfur and arsenic (Figure 19). XRF analysis of the lignitic wood material that was associated with pyrite grains showed similar spectrum for iron, sulfur and arsenic (Figure 20); where sulfur and arsenic peaks were much stronger than the wood material recovered from wells. In the spectrum another element germanium showed a strong peak. Presence of germanium was not reported in previous literatures. Germanium has little or no health impact. It usually occurs only as a trace element in ores, carbonaceous materials or a mineral called Argyrodite (Ag_8GeS_6) (Wikipedia). The significance of presence of germanium in the fluvial sediment was not understood and documented. XRF spectrum for the pyrite grains showed strong peaks iron, sulfur and arsenic (Figure 17).

X-ray Diffraction Analysis

The XRD spectrum of the pyrite from the creek and lignitic wood associated with pyrite showed presence of pure pyrite (COD 5000115), (COD 9013069) and arsenian-pyrite (COD 9013070). The chemical formula for this arsenian-pyrite is $As_{0.026}FeS_{1.974}$ (Reider et al. 2007). The peak positions of arsenian-pyrite (COD 9013070) and pyrite (COD 9013069), (COD 5000115) in and closely match arsenian-pyrite spectrum at 2theta = 28.5°, 33.0°, 37.0°, 40.7°, 47.3°, and 56.2° (Figures 22, 23).

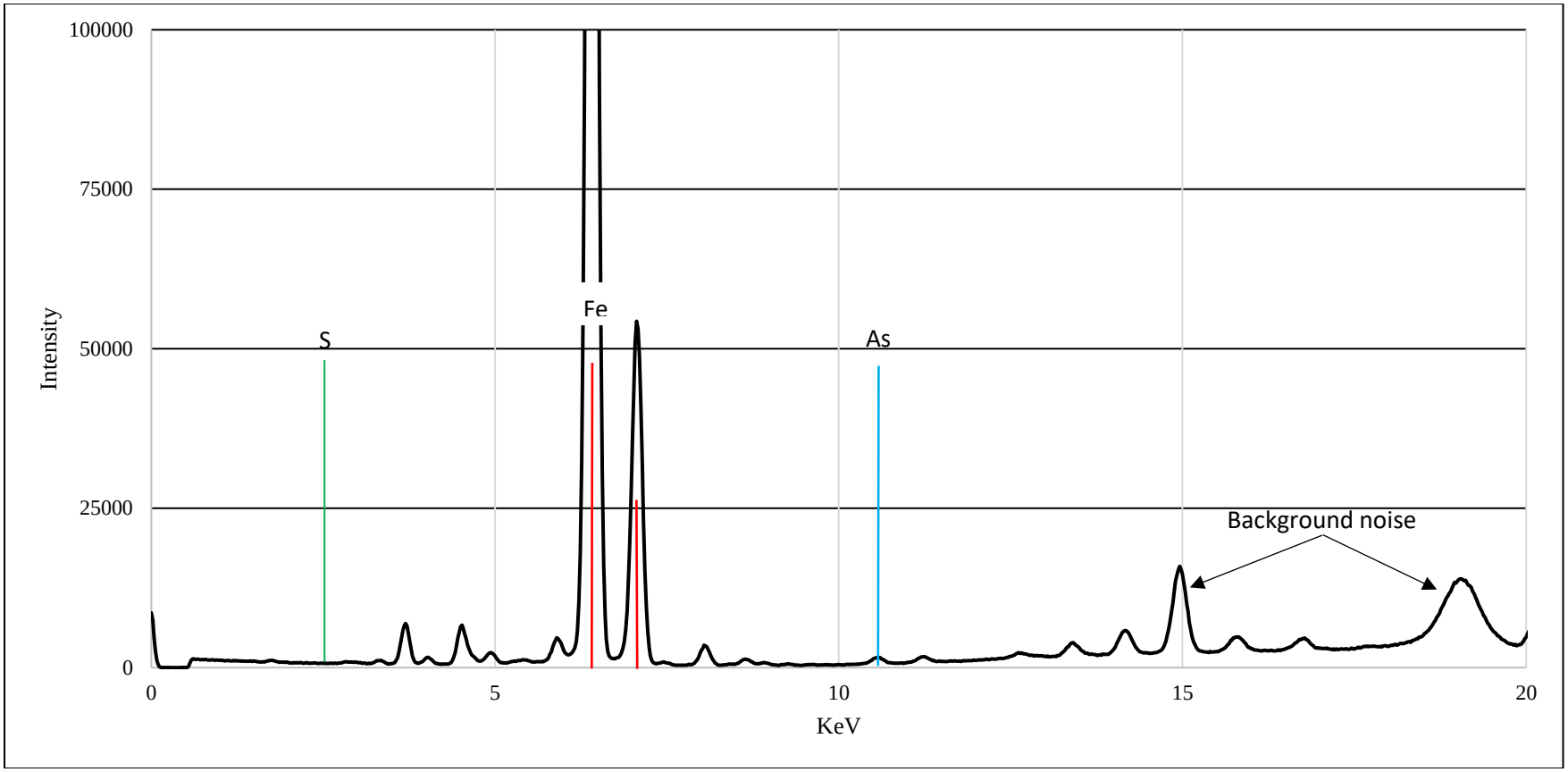

Figure 19. XRF spectrum showing Fe, S, and As peaks for the lignitized wood or black material collected from well-3.

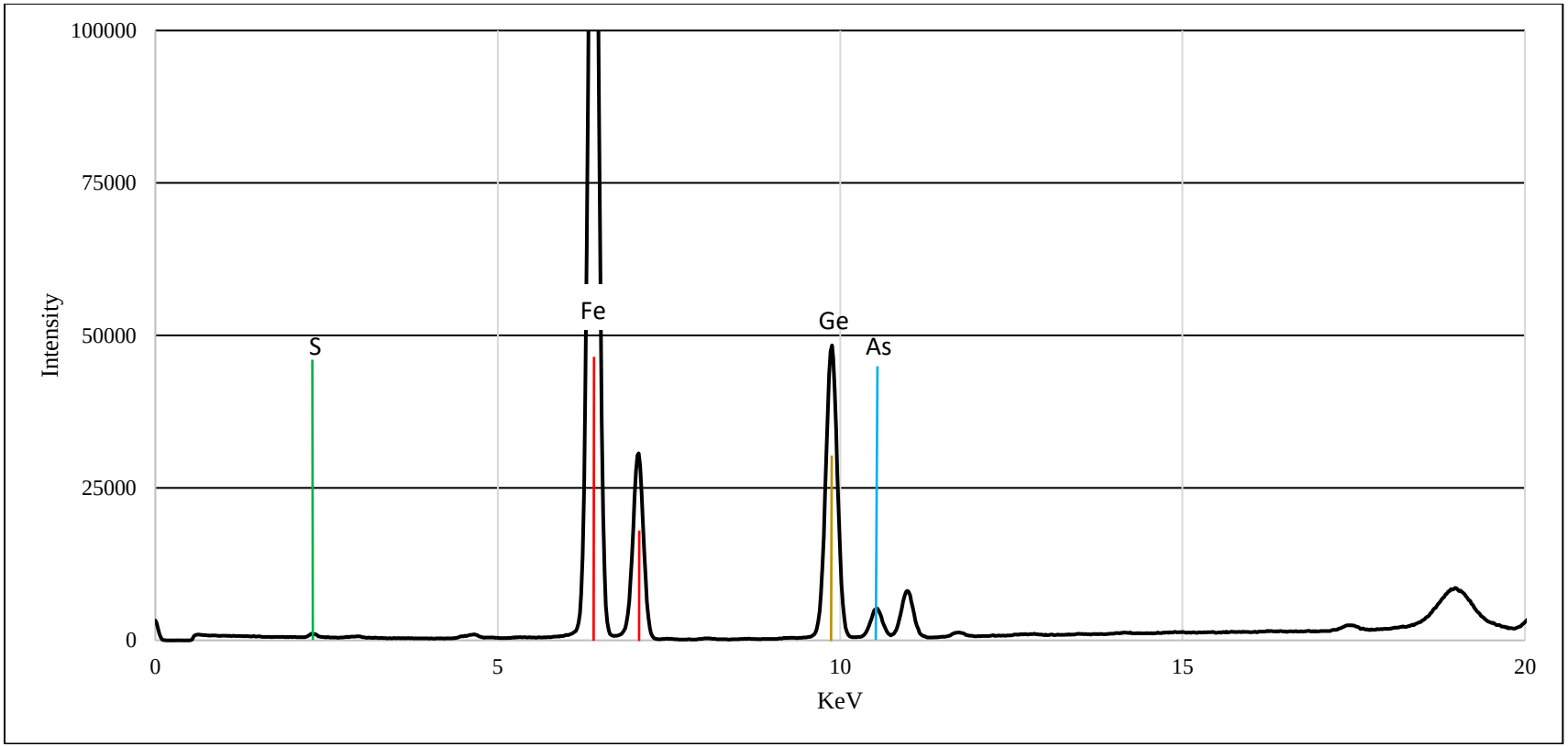

Figure 20. XRF spectrum showing Fe, As, S, Ge peaks for the lignitized wood or black material associated with pyrite grains collected from the creek outcrops.

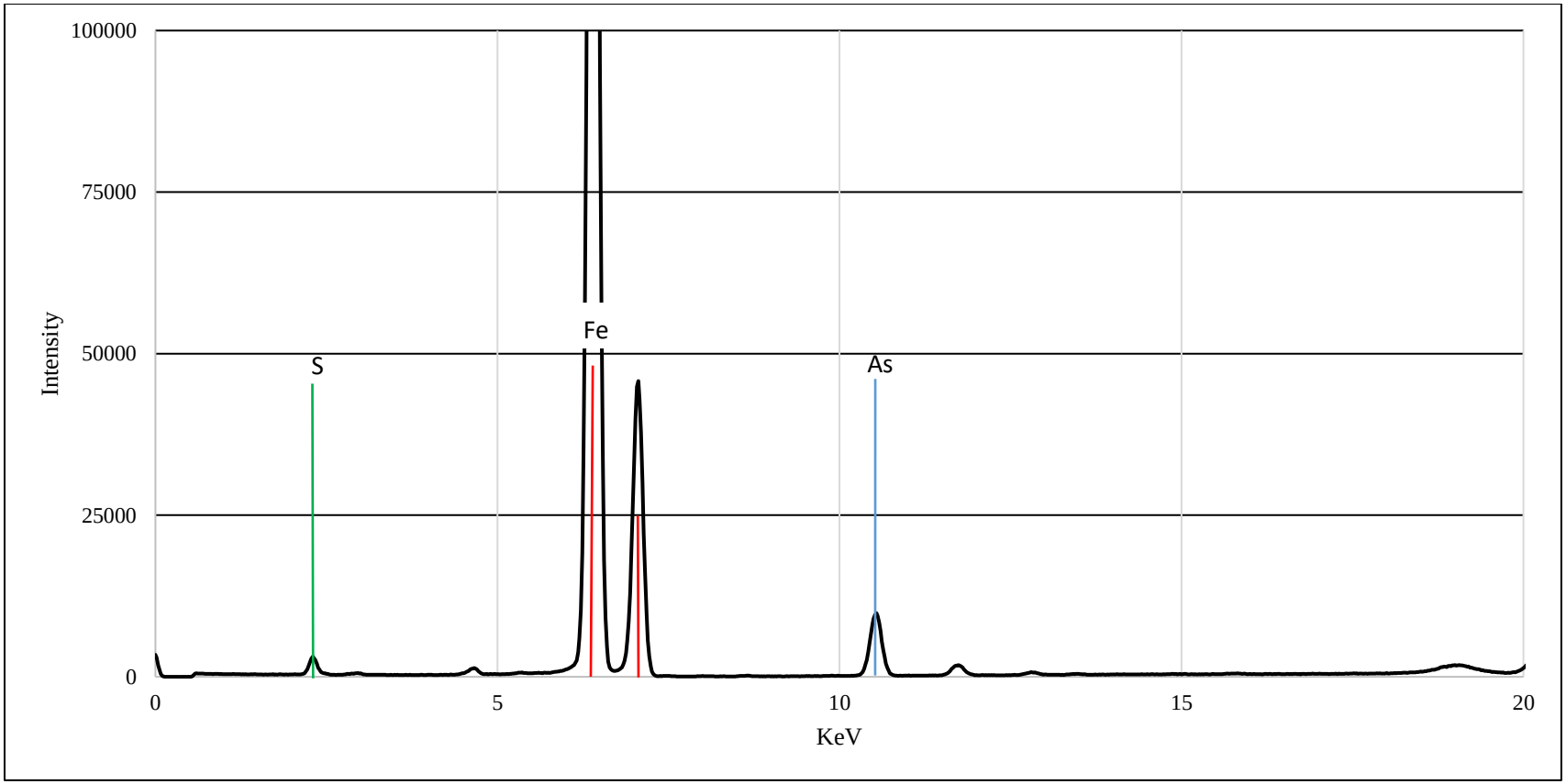

Figure 21. XRF spectrum showing Fe, As, S peaks for pyrite grains, collected from the creek.

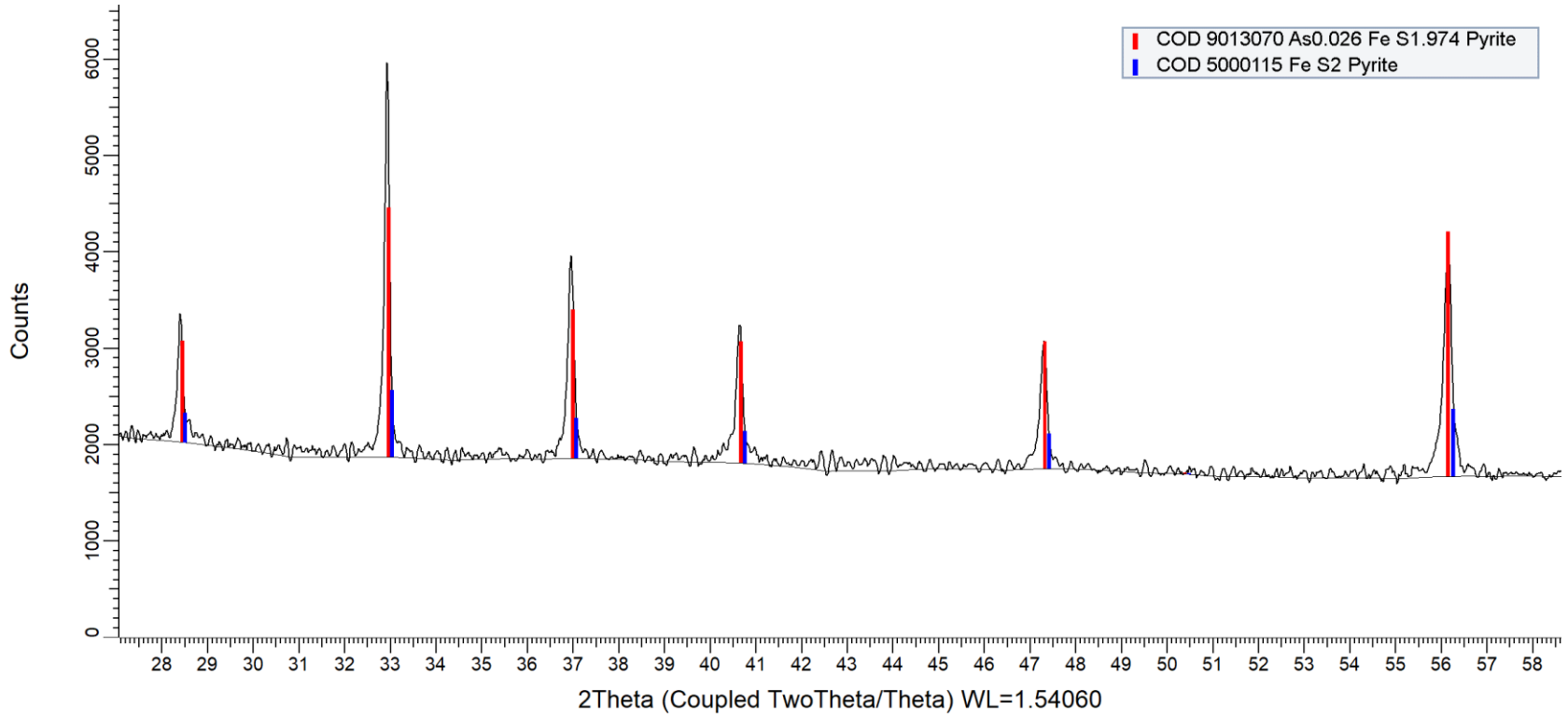

Figure 22. XRD spectra showing representative pyrite and arsenian-pyrite peaks in the lignitic wood material recovered from the creek outcrops. The blue and red vertical lines serve as indicators for pure pyrite and arsenian-pyrite, respectively.

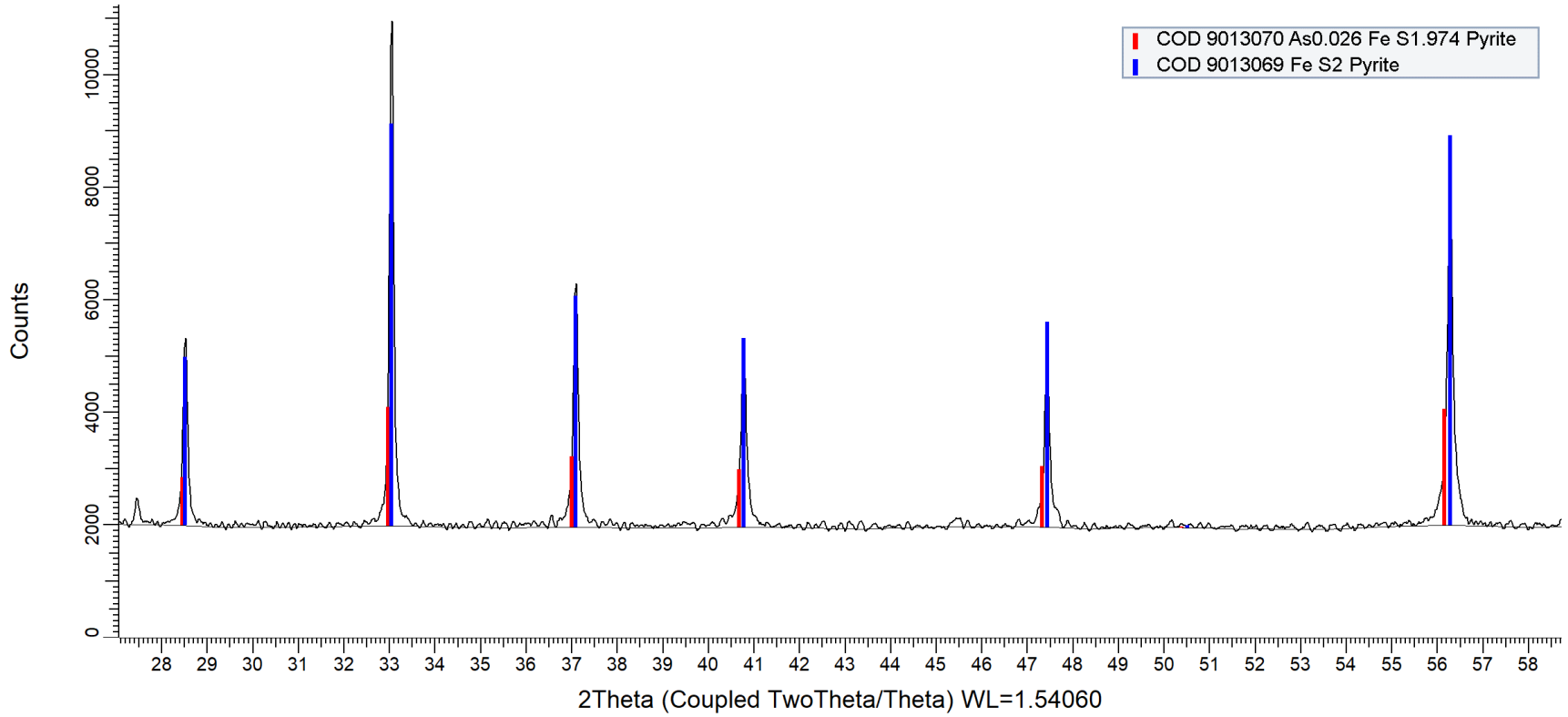

Figure 23. XRD spectra showing representative pyrite and arsenian-pyrite peaks in pyrites grains recovered from the creek outcrops. The blue and red vertical lines serve as indicators for pure pyrite and arsenian-pyrite, respectively.

Scanning Electron Microscope Analysis

The Scanning Electron Microscope (SEM) connected with an Energy Dispersive Spectroscopy (EDS) provided a quantitative elemental composition of the pyrite grains. The elements were identified from the peaks in the spectrum. The spectrum showed the presence of various elements including iron, sulfur, arsenic, cobalt, and nickel (Figures 24A, 24B). The results show that the pyrite grains contain trace elements 0.17 wt.% of As, 0.19 wt.% of Co, 0.15 wt.% of Ni, 0.18 wt.% of Al in oxide forms (Table 4). The concurrent SEM-EDS peaks of Fe, S, and As and XRD results confirm that the solids are arsenian pyrite rather than pure pyrite. In additional arsenic, other trace elements such as Co and Ni are also sequestered into biogenic pyrite. The arsenic concentration of biogenic pyrite observed in the SEM analysis is consistent with the result from the EMP analysis (see next section), suggesting its excellent sorbing capability. The ICP-MS analysis of the groundwater showed that measurable amounts of As, Co, and Ni are present in the groundwater (Tables 1 and 2). The results are also compatible with the previous study by Saunders et al. (1997).

Table 4. Elemental composition of the pyrite grains in this study

Element	Weight%	Atomic%	Comp%	Formula
Al	0.18	0.15	0.34	Al_2O_3
Si	0.21	0.17	0.45	SiO_2
S	26.71	19.48	66.69	SO_3
Fe	24.96	10.45	32.11	FeO
Ni	0.15	0.06	0.18	NiO
As	0.17	0.05	0.23	As_2O_3
Co	0.19	0.08	0.25	CoO
O	47.62	69.62		
Total	100.00			

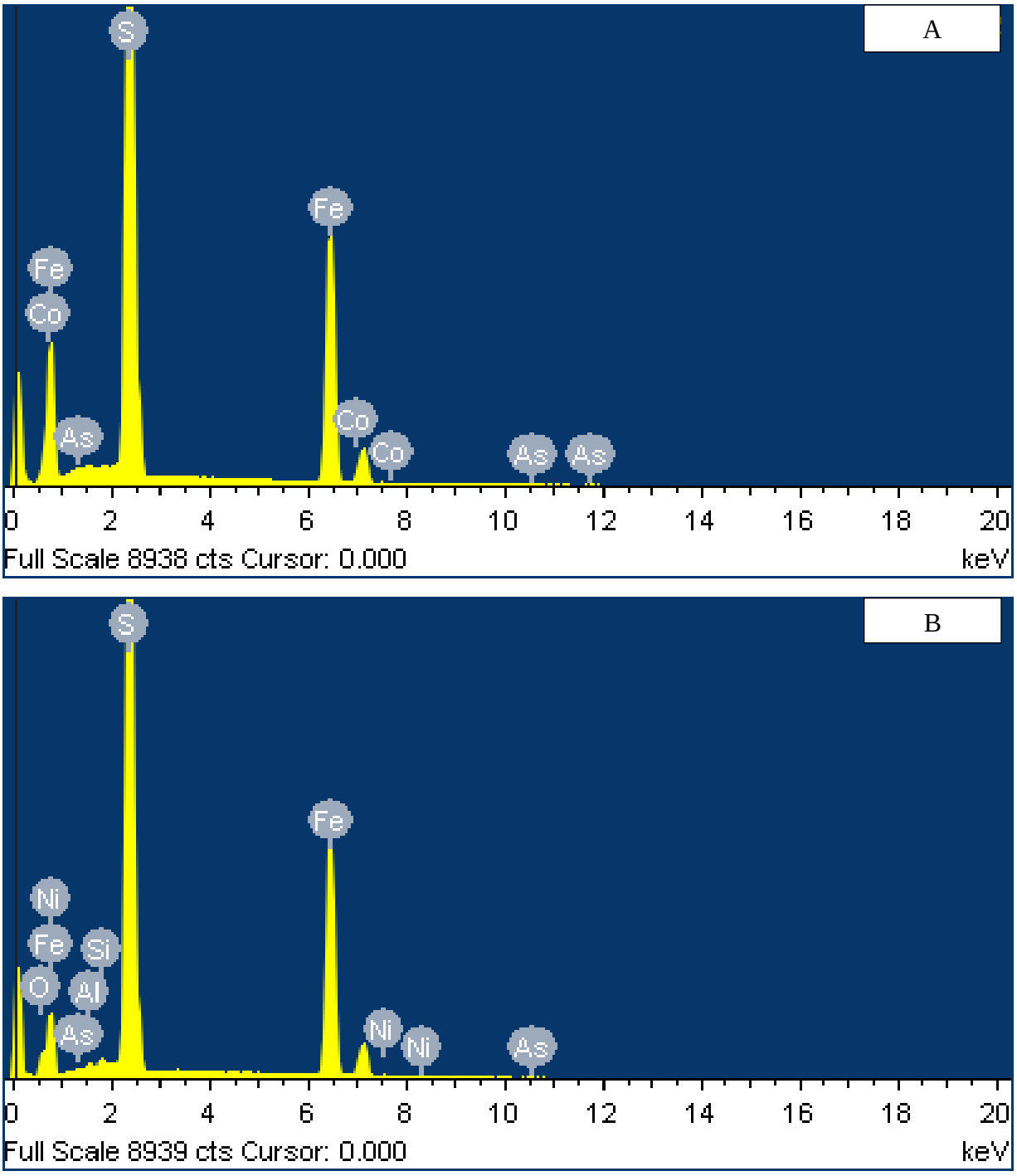

Figure 24. Energy Dispersive Spectroscopy (EDS) spectrum showing the chemical composition of the pyrite grains with different peaks for respective elements.

The scanning electron microscope imaging analysis provided more detail about the morphologies (shape and size) of the pyrite crystals. The analysis showed that most of the pyrite grains are euhedral (i.e. cubes, truncated octahedrons) shaped large crystals (20µm- 200 µm), and formed as individual grains (Figures 25, 26). Relatively smaller (20 µm -30 µm) pyrite grains were also observed which formed as non-framboid aggregates (Figures 27, 28) and have the same morphology as large crystals. Individual pyrite crystals were reported as big as 1.50 cm by Saunders et al. (1997). Microcrystalline spherical aggregates or pyrite framboids were not found in the samples from Macon County site formed quickly (in days) by biostimulation. Though the age of the pyrite grains was not studied, from the size of grains and lack of framboids it was assumed that it took a long time to develop the large crystals at a natural fluvial setting.

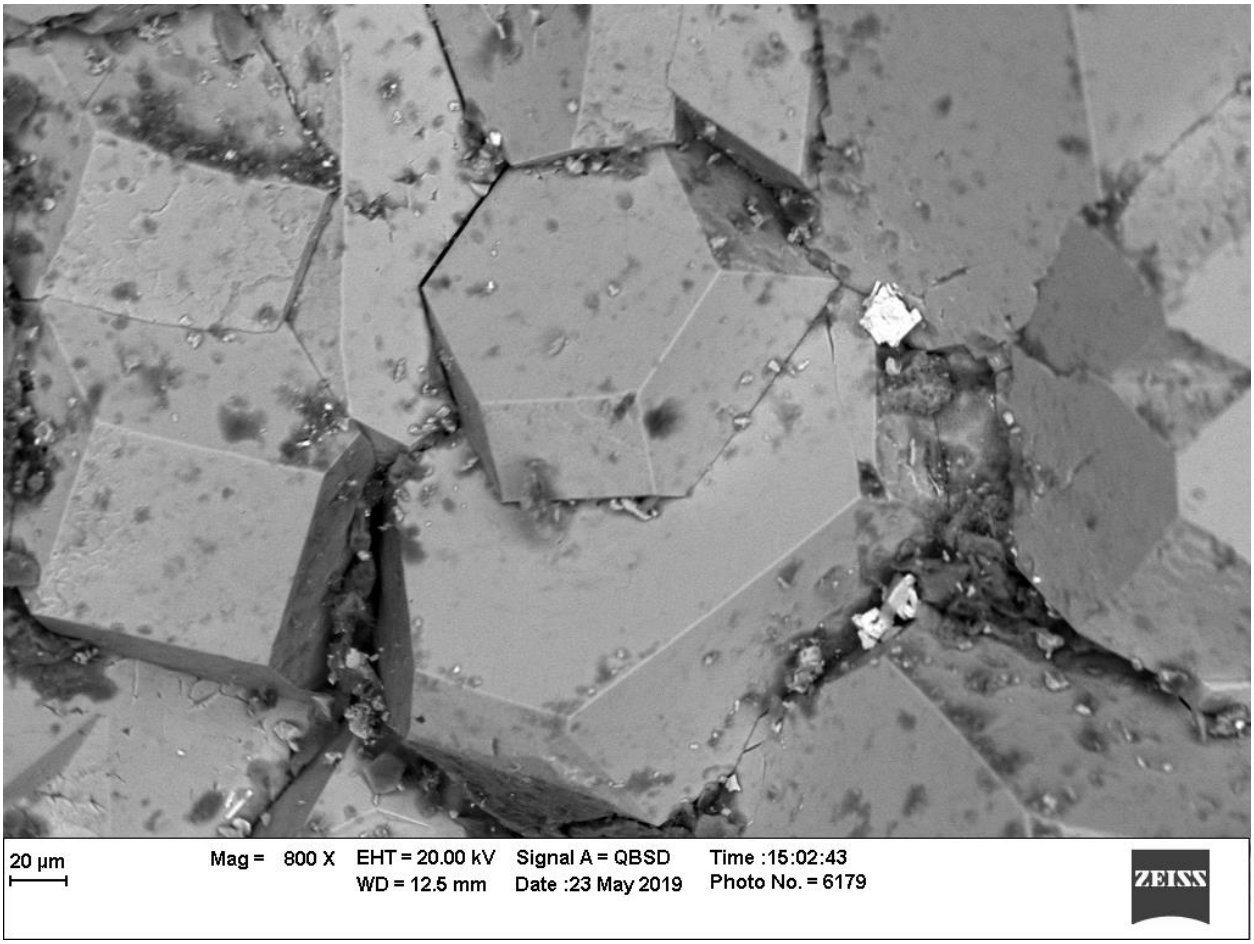

Figure 25. Scanning electron microscope (SEM) backscatter image of crystalline euhedral shape of pyrite grains at eight hundred times magnification from sample MC-1.

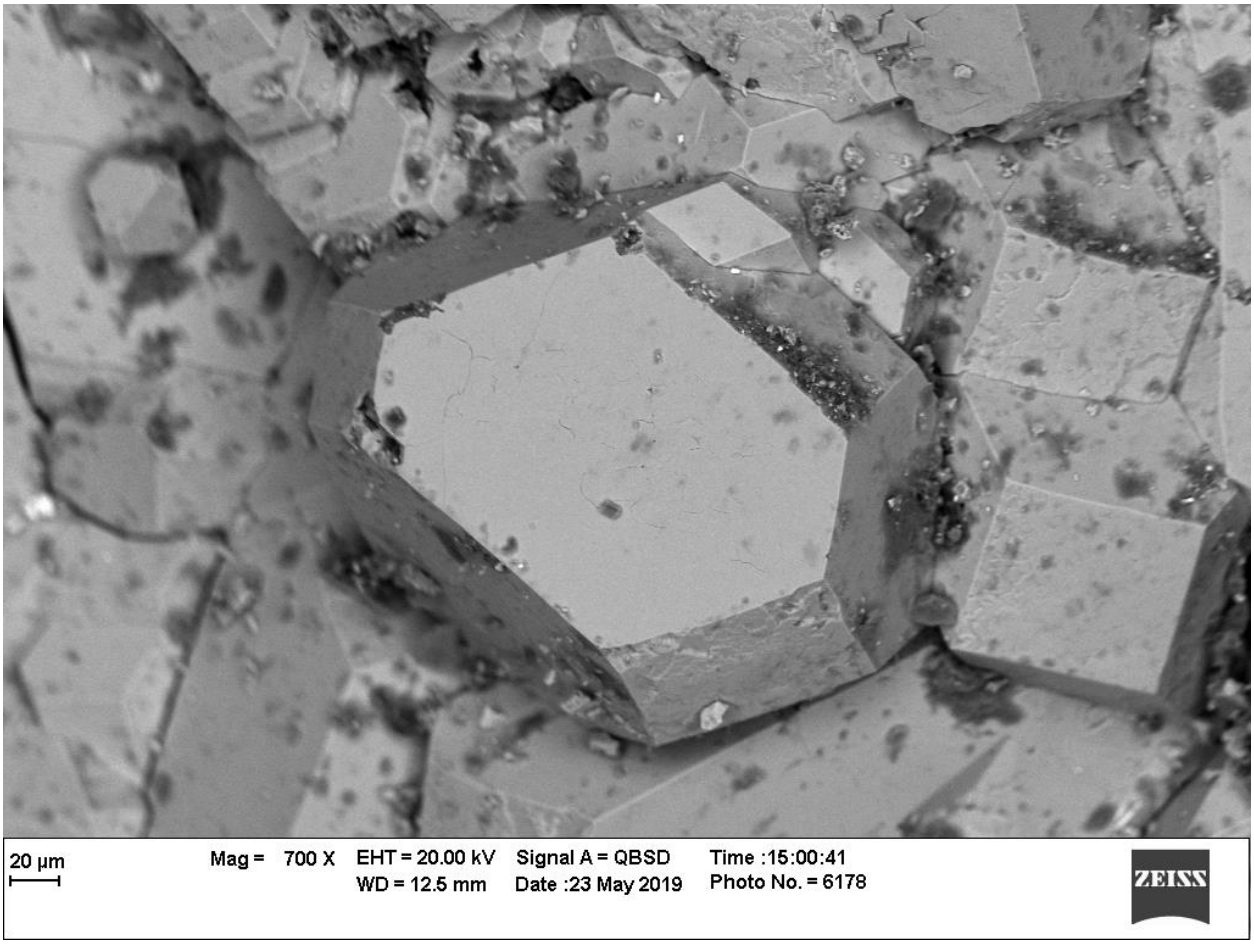

Figure 26. Scanning electron microscope (SEM) backscatter image of crystalline euhedral shape of pyrite grains at seven hundred times magnification from sample MC-1.

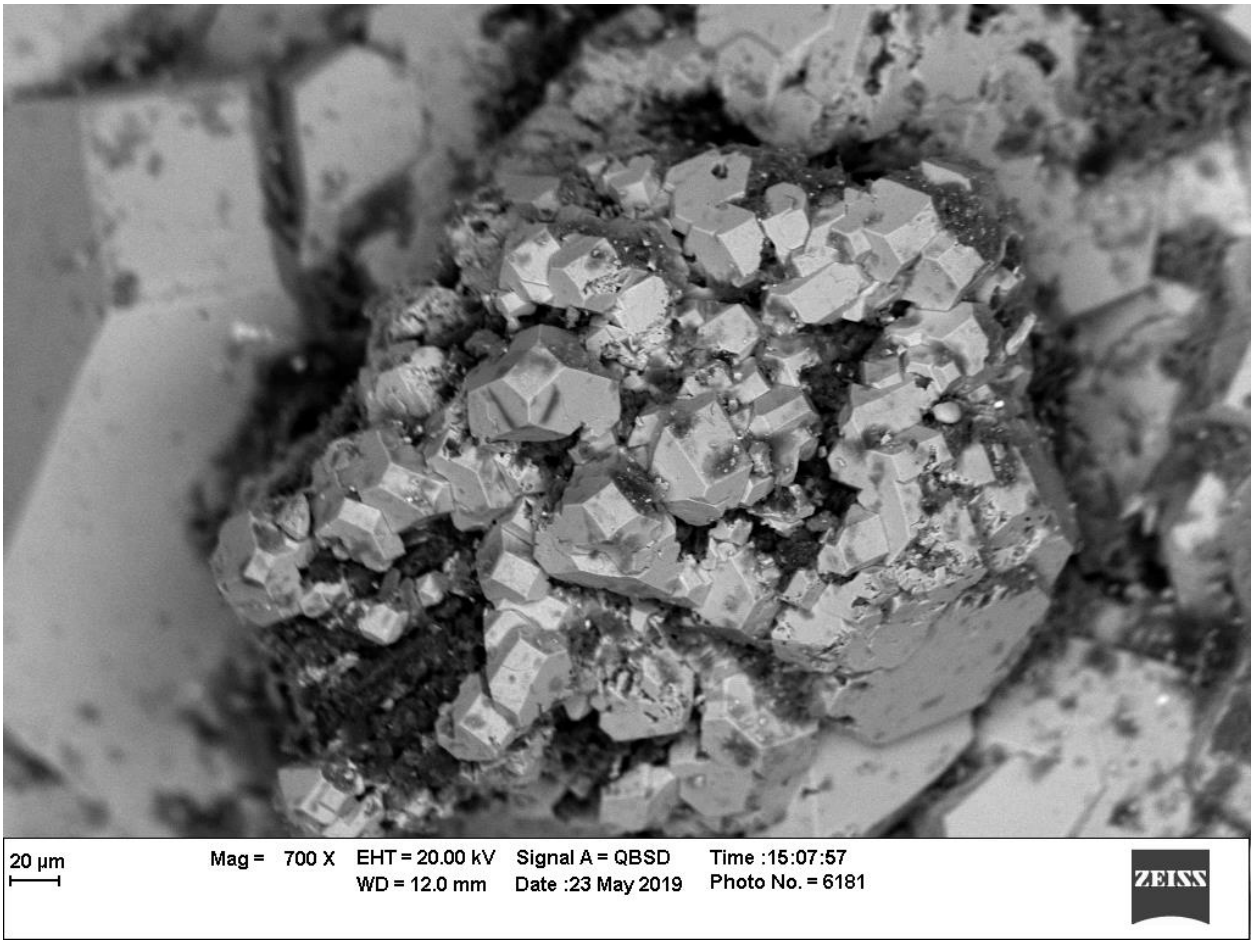

Figure 27. Scanning electron microscope (SEM) backscatter image of aggregates of crystalline euhedral shape of pyrite grains at seven hundred times magnification from sample MC-1.

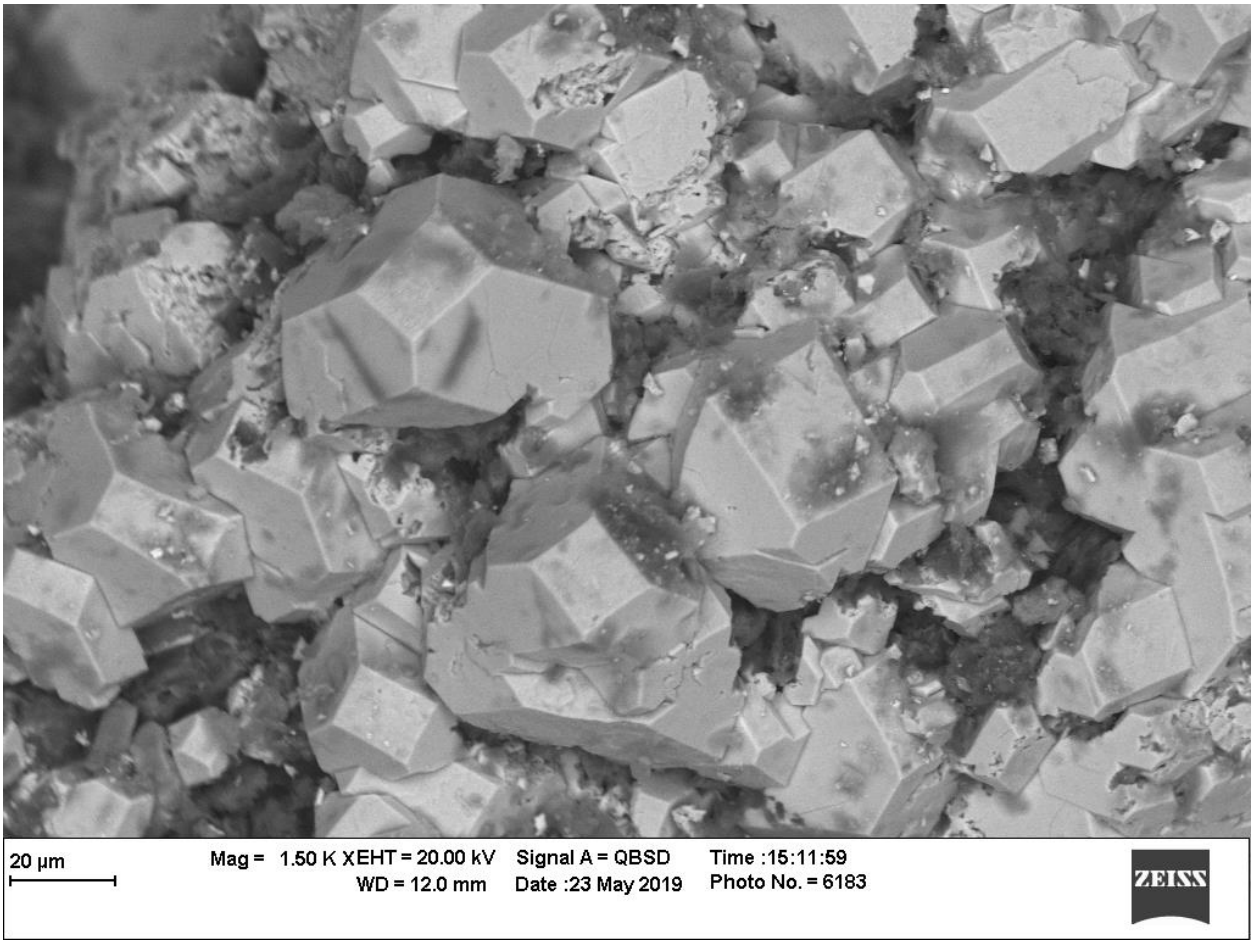

Figure 28. Scanning electron microscope (SEM) backscatter image of aggregates of crystalline euhedral shape of pyrite grain aggregate at fifteen hundred times magnification from sample MC-1.

Electron Microprobe Analysis

Electron Microprobe (EMP) analysis of three polished thin sections was conducted to obtain quantitative contents of individual elements. In this study arsenic was the main element of interest. The standard samples used allow quantification for As, Fe, S and Si. The results showed that most of the pyrite grains contain 0.20-0.92 wt% of arsenic. The results were consistent for each thin section and consistent with SEM-EDX results. The standard does not allow quantification of other trace elements such as Co, and Ni.

Backscatter images (BEI) were taken for different pyrite grains (Figures 29, 32 and 35). Elemental maps for As, Fe, S, and Si were also taken to visualize the compositional variation across the grains. The elemental maps showed that silicon is rarely present; where sulfur and iron is present in great amount and equally distributed all over the grains (Figures 30, 31, 33, 34, 36 and 37).

Arsenic maps showed that in some of the grains, arsenic is equally distributed all over the grain (Figure 36). On the other hand, in some grains arsenic is distributed in different patterns such as zoning (Figures 30, 33).

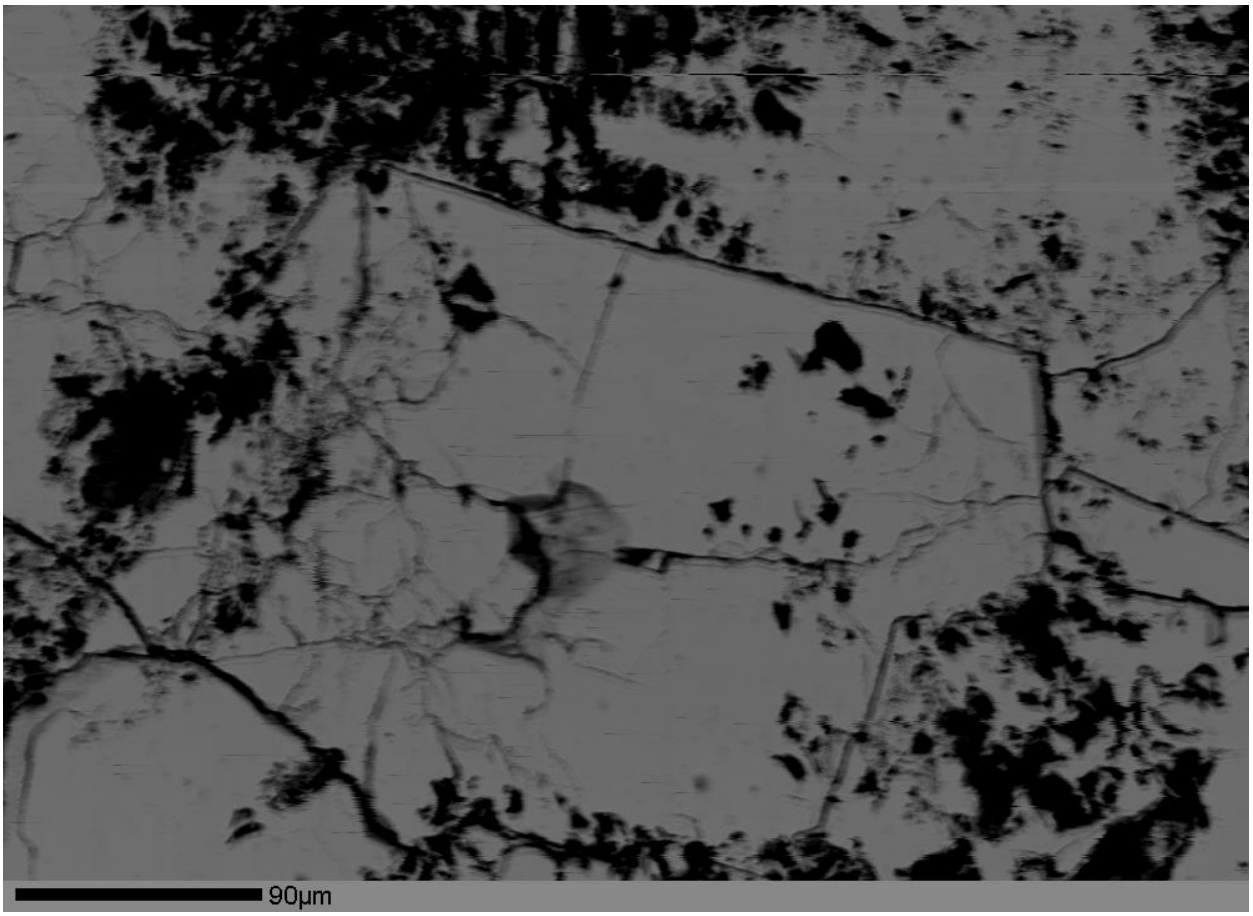

Figure 29. Stage raster photomicrograph (BSE image) of a pyrite grain-1 in sample MC-3. The grain contains 0.92 wt% of arsenic. This image was taken at magnification 250, pixel size 0.227 µm, number of pixel/line 1000 using an instrument setup of voltage 15 KV, current 50nA.

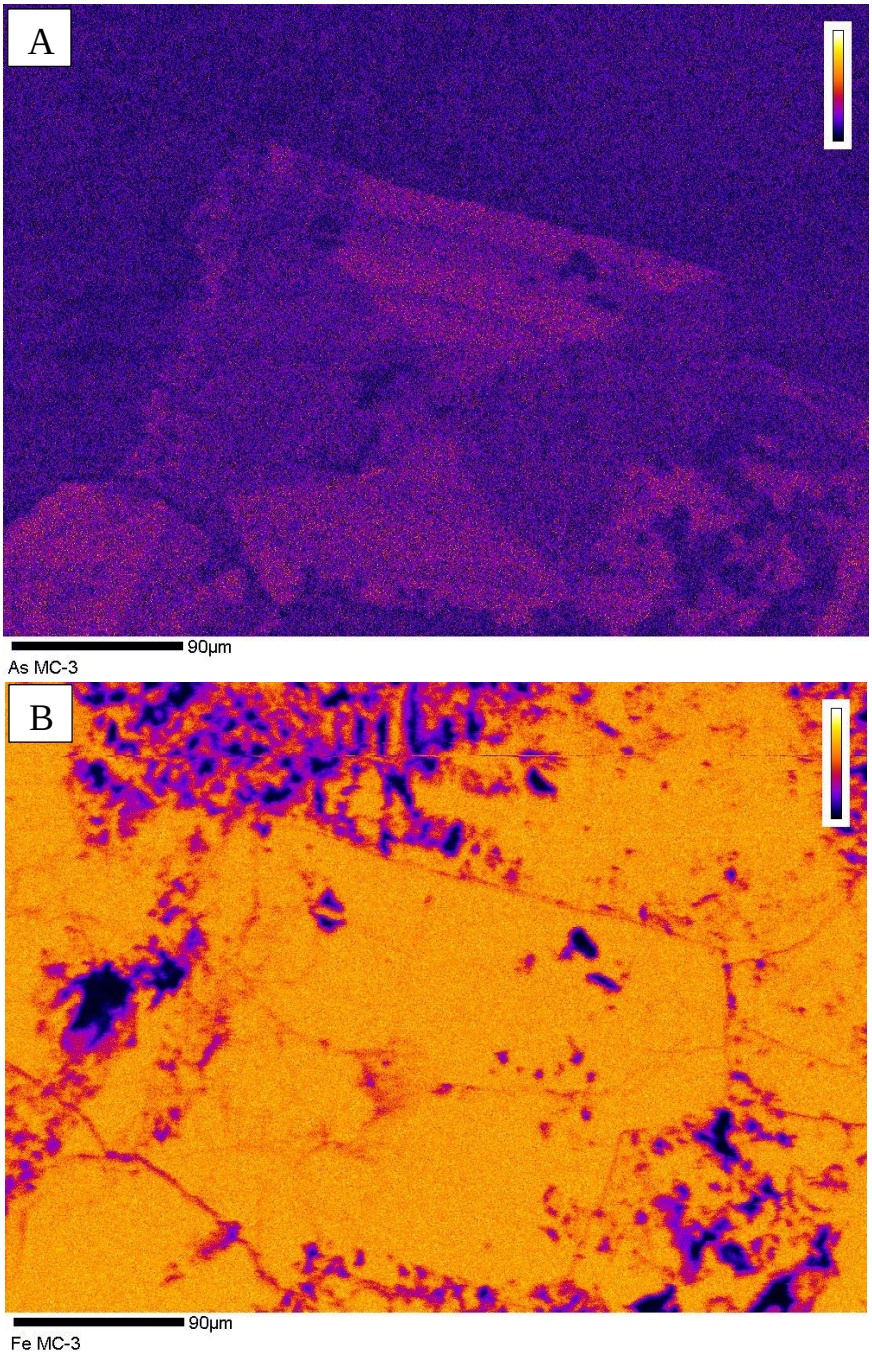

Figure 30. Stage raster photomicrograph (BSE image) showing elemental map of (A) arsenic and (B) iron of a pyrite grain-1 in sample MC-3. The grain contains 0.92 wt% of arsenic. This image was taken at magnification 250, pixel size 0.227 µm, number of pixel/line 1000 using an instrument setup of voltage 15 KV, current 50nA.

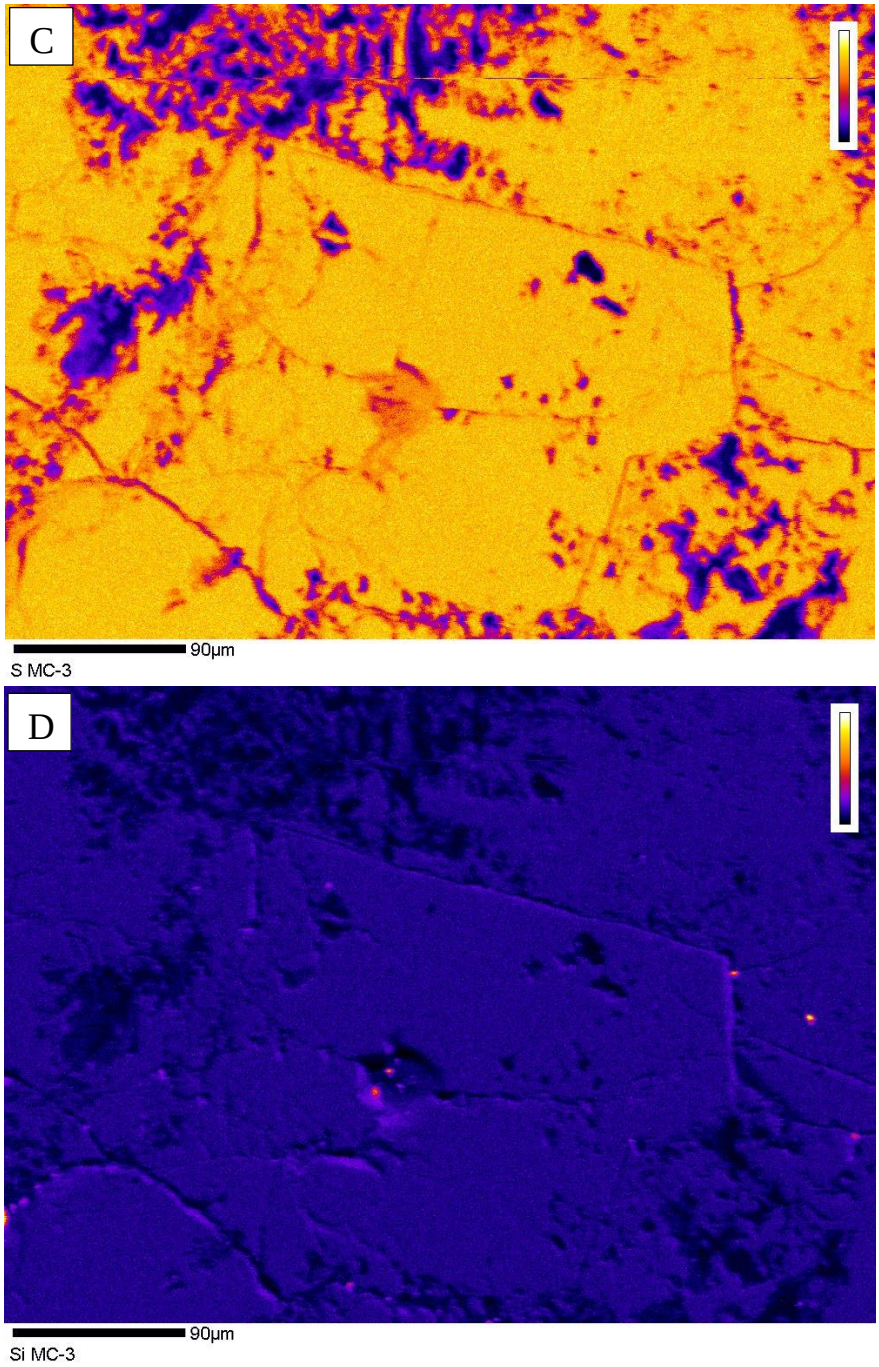

Figure 31. Stage raster photomicrograph (BSE image) showing elemental map of (C) Sulfur AND (D) Silicon of a pyrite grain-1 in sample MC-3. This image was taken at magnification 250, pixel size 0.227 µm, number of pixel/line 1000 using an instrument setup of voltage 15KV, current 50nA.

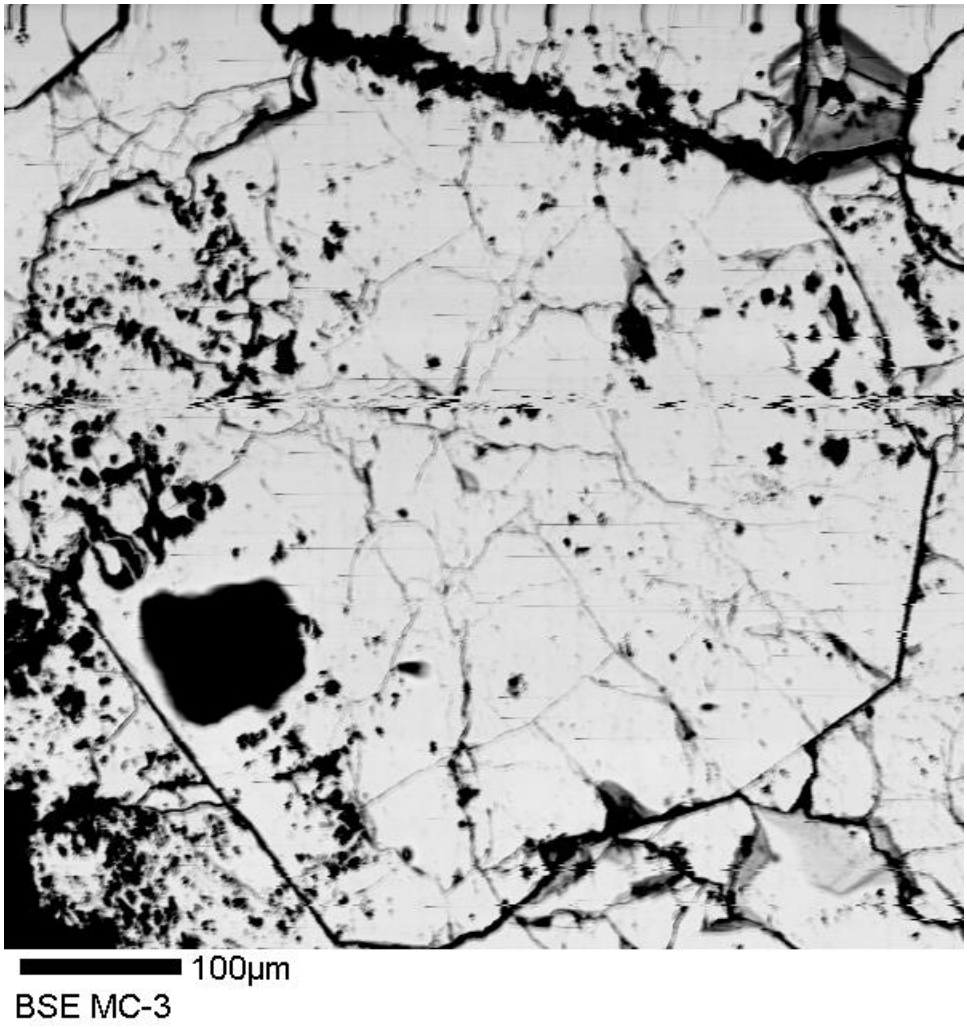

Figure 32. Beam raster photomicrograph (BSE image) of a pyrite grain-2 in sample MC-3. The grain contains 0.31 wt% of arsenic. This image was taken at magnification 150, pixel size 0.255 µm, number of pixel/line 600, voltage 15 KV, current 50nA.

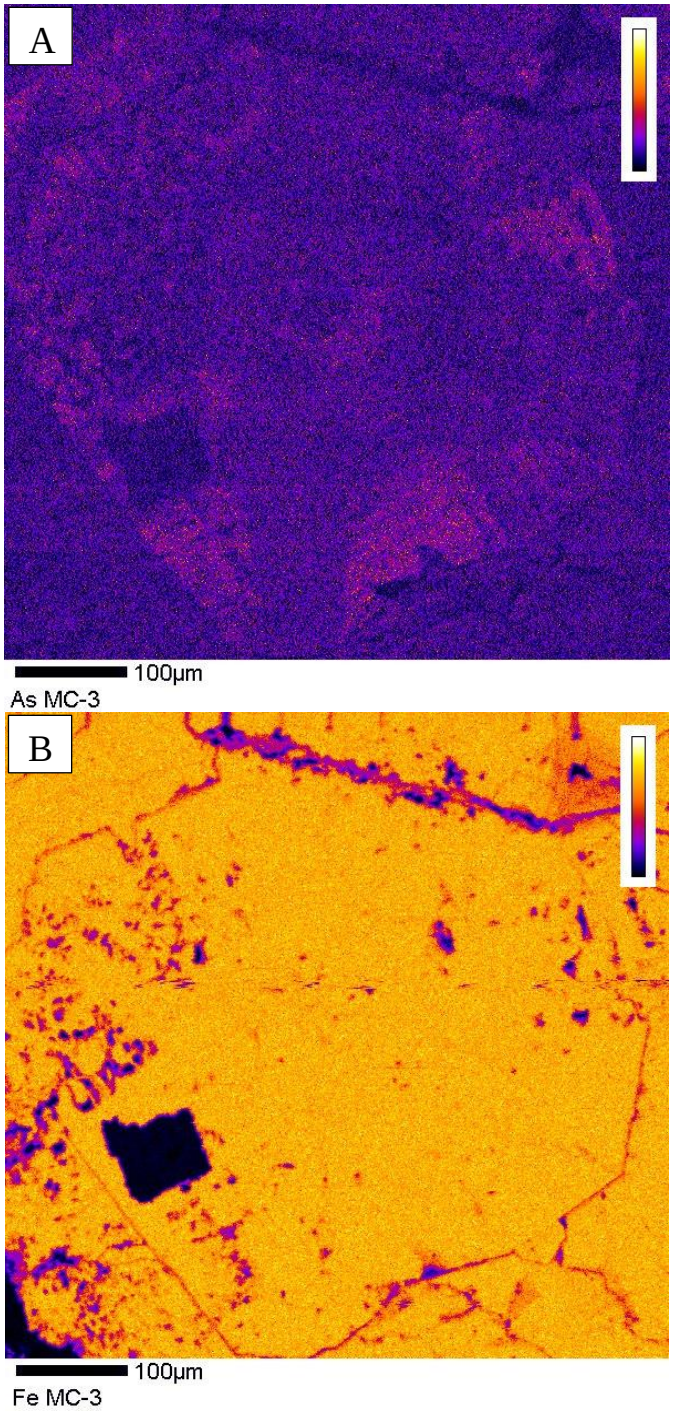

Figure 33. Stage raster photomicrograph (BSE image) showing elemental map of (A) arsenic & (B) iron of a pyrite grain-2 in sample MC-3. The grain contains 0.31 wt% of arsenic. Magnification 150, pixel size 0.255 µm, number of pixel/line 600, voltage 15 KV, current 50nA.

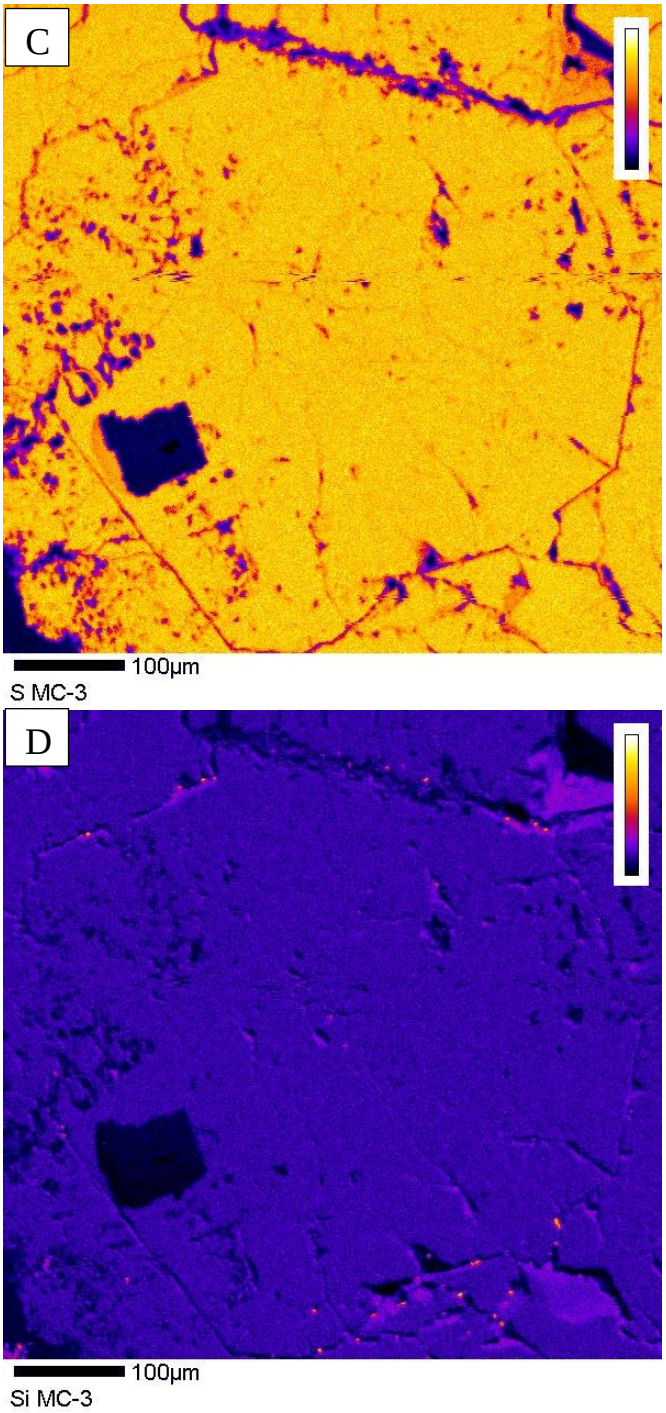

Figure 34. Stage raster photomicrograph (BSE image) showing elemental map of (C) sulfur and (D) silicon of a pyrite grain-2 in sample MC-3. Magnification 150, pixel size 0.255 µm, number of pixel/line 600, voltage 15 KV, current 50nA.

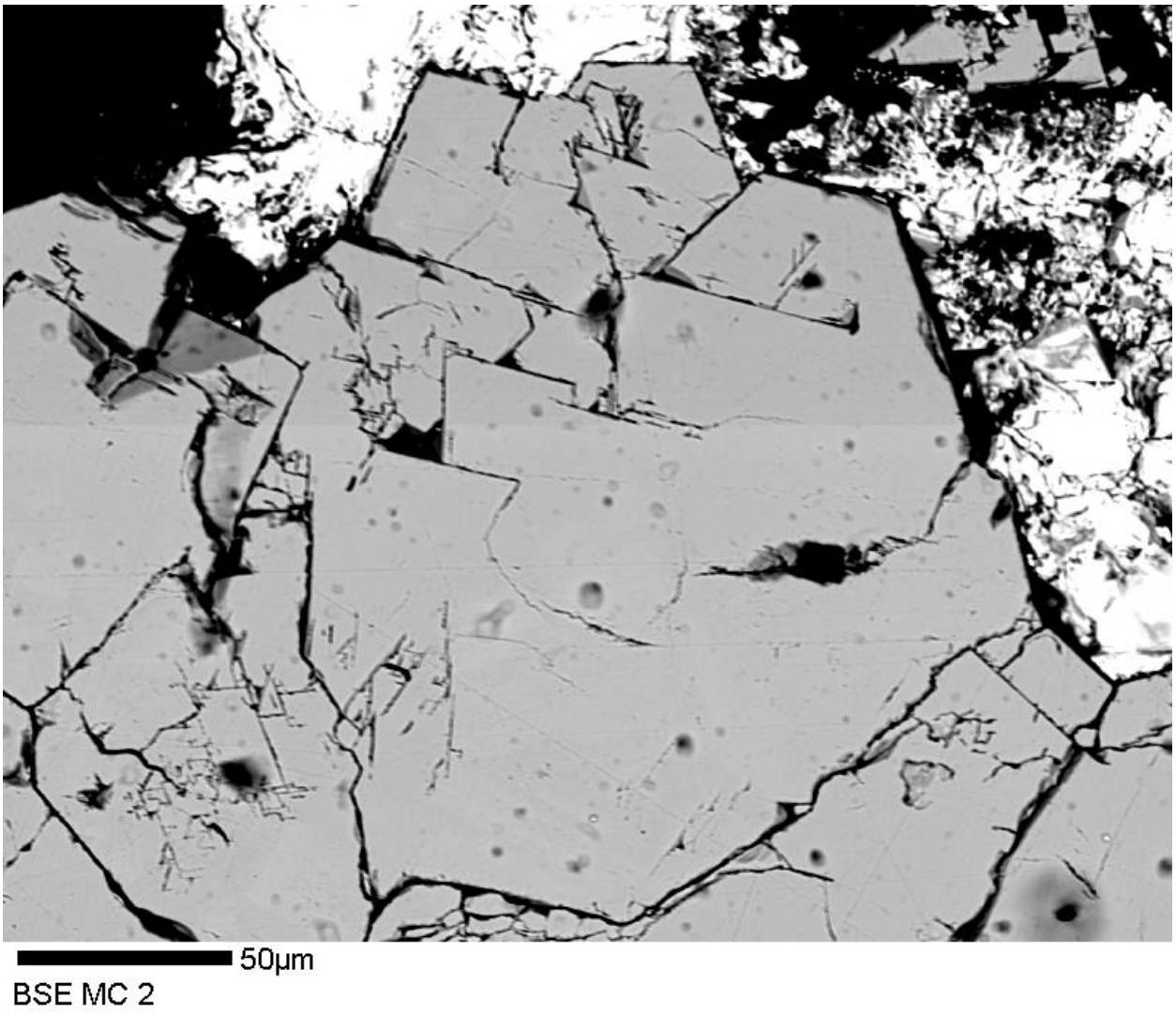

Figure 35. Beam raster photomicrograph (BSE image) of a pyrite grain-3 in sample MC-2. The grain contains 0.28 wt% of arsenic. This image was taken at magnification 150, pixel size 0.88 µm, number of pixel/line 600, voltage 15 KV, current 50nA.

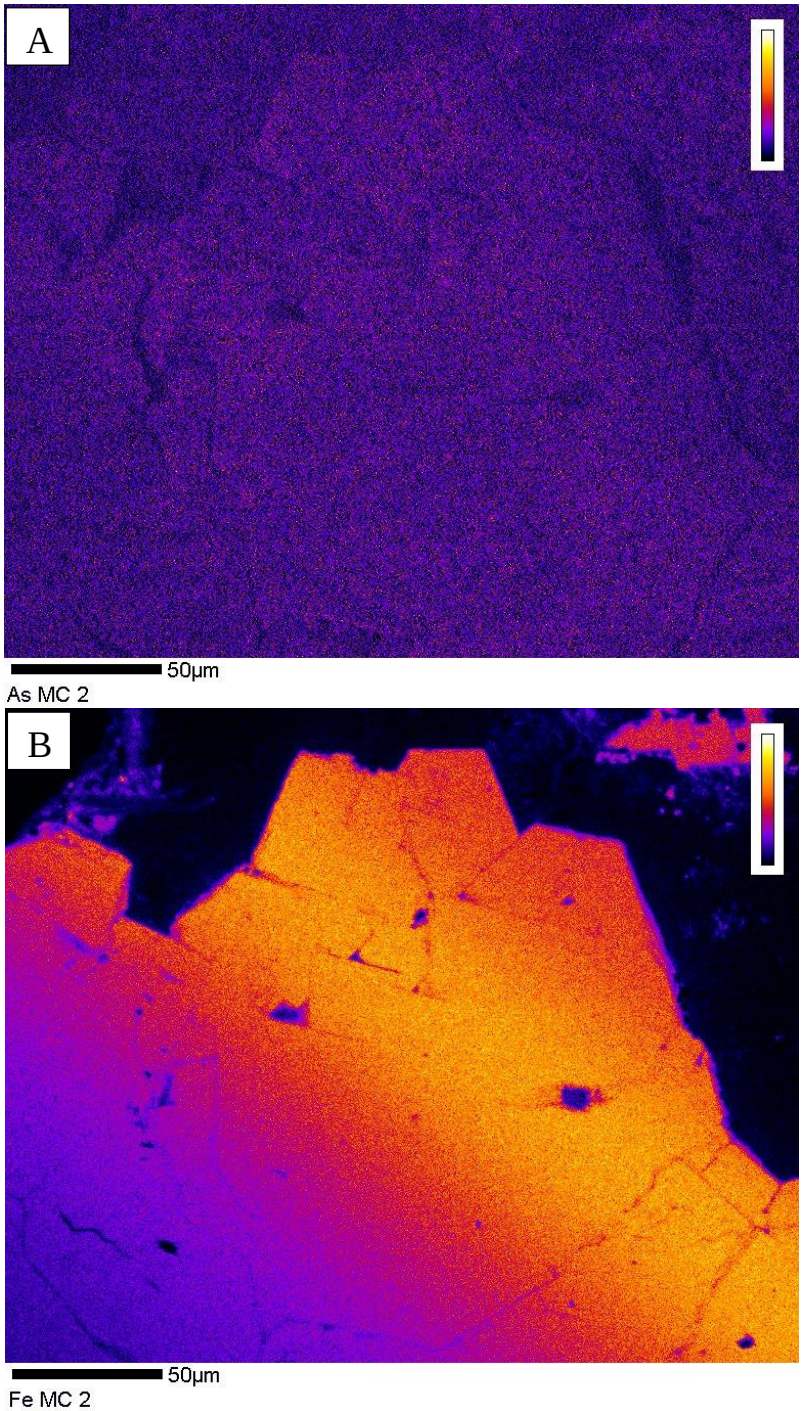

Figure 36. Stage raster photomicrograph (BSE image) showing elemental map of (A) arsenic & (B) iron of a pyrite grain-3 in sample MC-2. Magnification 150, pixel size 0.88 µm, number of pixel/line 600, voltage 15 KV, current 50nA.

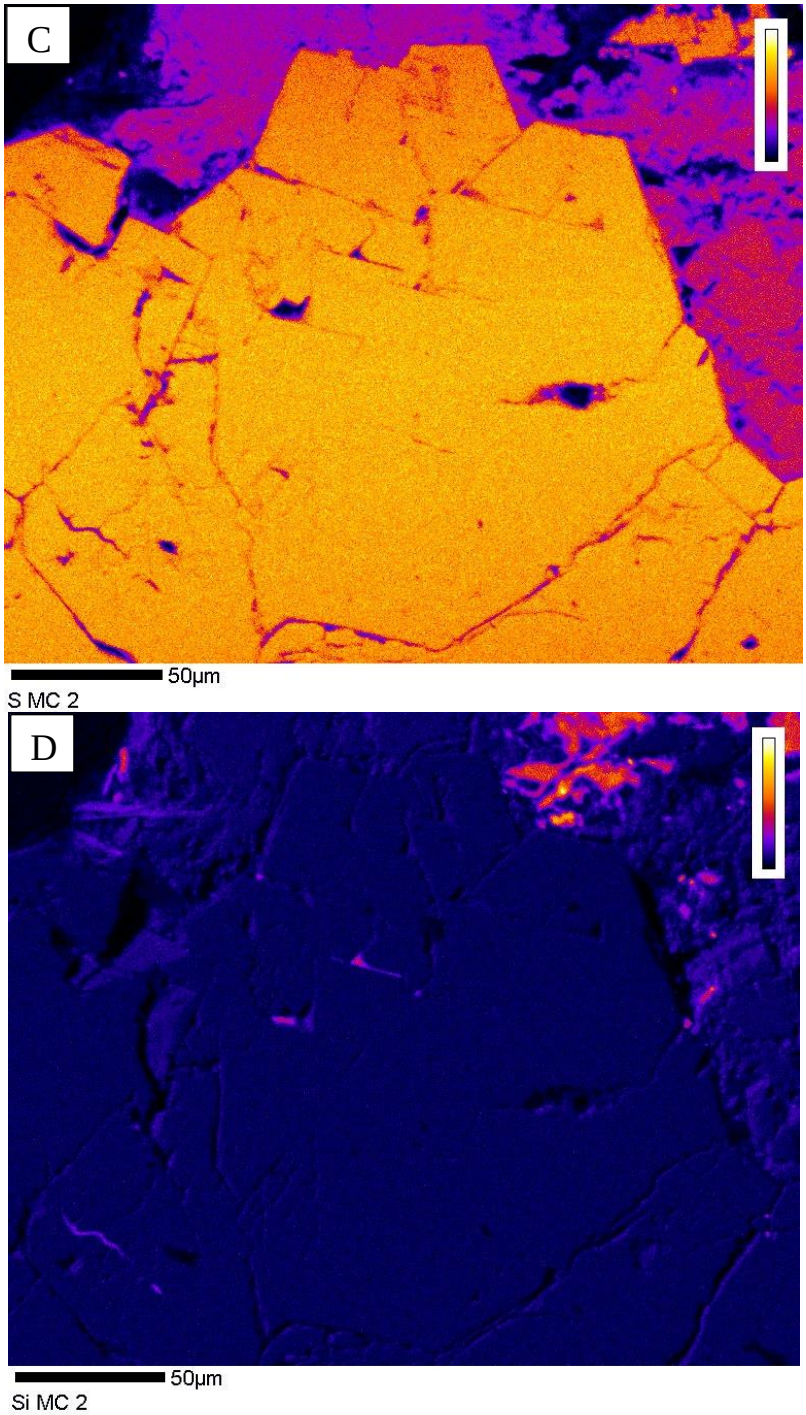

Figure 37. Stage raster photomicrograph (BSE image) showing elemental map of (C) sulfur and (D) Silicon of a pyrite grain-3 in sample MC-2. Magnification 150, pixel size 0.88 µm, number of pixel/line 600, voltage 15 KV, current 50nA.

Biogenic Pyrite Formed at Industrial Site in Florida

This study also compared the size and morphology of biogenic pyrite formed naturally in fluvial sediments and those grow via biostimulation at an industrial site in Florida. The hydrogeology and geochemistry of the industrial site was described by Starnes (2015). The research presented data of groundwater and sediment samples from a total of 22 monitoring wells located at the Lynn Haven site. Groundwater in the surficial aquifer was near-neutral to slightly acidic, with a mean pH value of 5.72. The highest ORP was recorded 130.4mV and lowest -77mV with an average of 46.72 mV; conductivity ranged from 62 μS/cm to 299 μS/cm. The groundwater was relatively low in DOC. Lab analysis confirmed an elevated level of arsenic contamination in groundwater; arsenic ranges from 0.0002 to 0.577 ppm.

Starnes (2015) concluded that groundwater is enriched in Ca, Mg, and HCO_3^- relative to the conservative mixing line of seawater. The major hydrochemical facies of groundwater in the surficial aquifer is Ca-HCO_3-Na-Cl type. The study suggested a high degree of mixing of meteoric and carbonate groundwater in the surficial aquifer. The groundwater in the site was sulfate-limited (sulfate concentration < 9 mg/L). Groundwater geochemistry data indicated that reduced ferrous iron (Fe^{2+}) and arsenite ($As(OH)_3$) are the dominated species under moderately reducing conditions. Geochemical modeling utilizing reaction path models and Eh-pH diagrams predict that a further drop in current redox conditions will lead to the precipitation of Fe-sulfides (i.e. pyrite) and arsenic sequestration.

An in-situ bioremediation experiment was conducted at field scale in the contaminated site stimulating sulfate-reducing bacteria and the changes were monitored by Ghandehari (2016), Levitt (2017) and Wilson (2018). These studies demonstrated that sulfate-reduction conditions developed after one week of injection. The artificial introduction of sulfate-reducing conditions and caused the co-precipitation and adsorption of the dissolved arsenic in biogenic pyrite. The bacterial sulfate-reduction consumes the sulfate and create H_2S. Ferrous iron reacts with the dissolved sulfide in the groundwater and produces iron sulfide minerals which adsorb and co-precipitate As. Formation' precipitation of pyrite was reported just one week after the injection. To characterize pyrite and As-bearing sulfide minerals all these studies used X-ray diffraction, X-ray fluorescence analysis. Levitt (2017) and Wilson (2018) did additional SEM and EMP analysis to determine the morphology and quantitative content of the sequestered trace elements. The pyrite formed either as well-defined euhedral nano-crystals or as spherical aggregates (framboids) of 1-50 μm in diameter (Figure 38, 39). The EMP analysis determined that the pyrite contained between 0.05-0.40 wt % of arsenic. This study also demonstrated that the iron sulfide biominerals remain stable in the aquifer even after organic carbon from the injection is exhausted. The groundwater arsenic concentration decreased to less than 50ppb from an initial concentration.

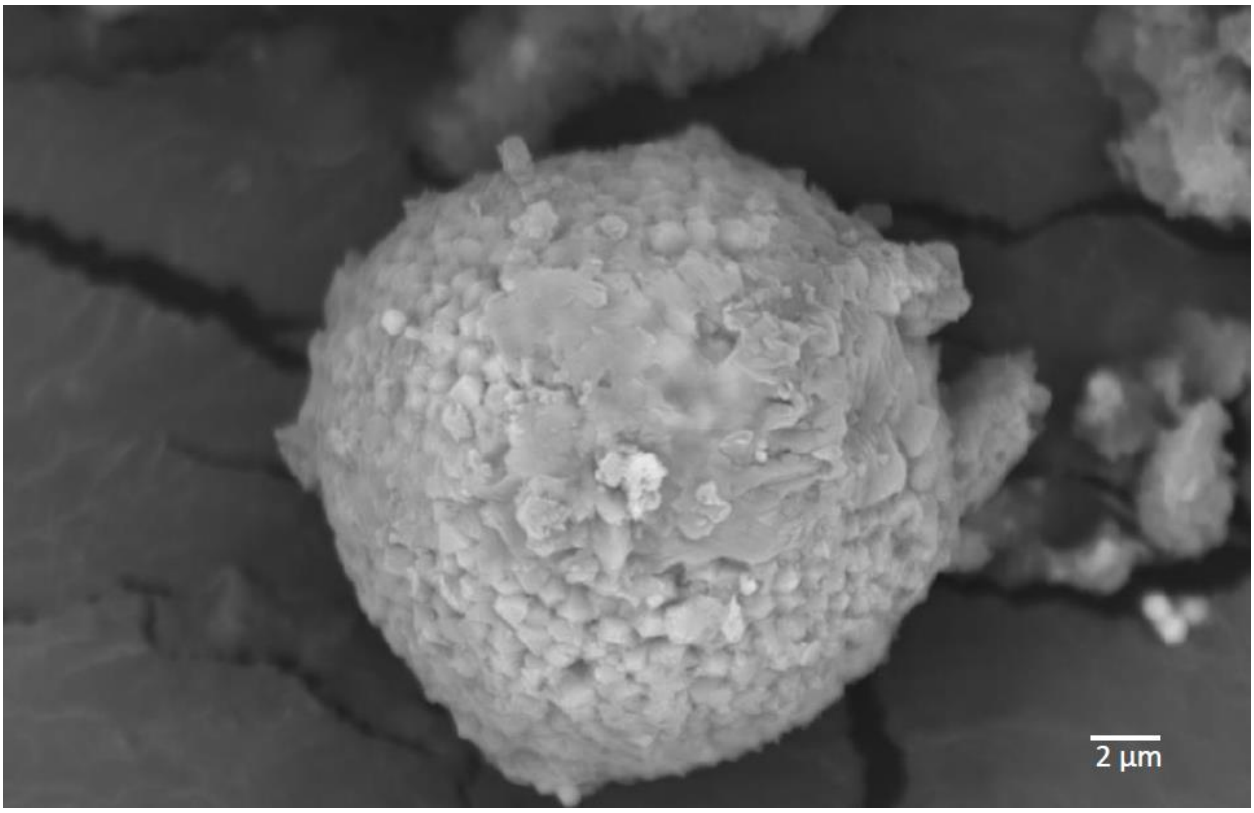

Figure 38. SEM backscatter image of a pyrite framboid at ten thousand times magnification. The precipitated sample was collected from monitoring well (M-2) (Wilson, 2018).

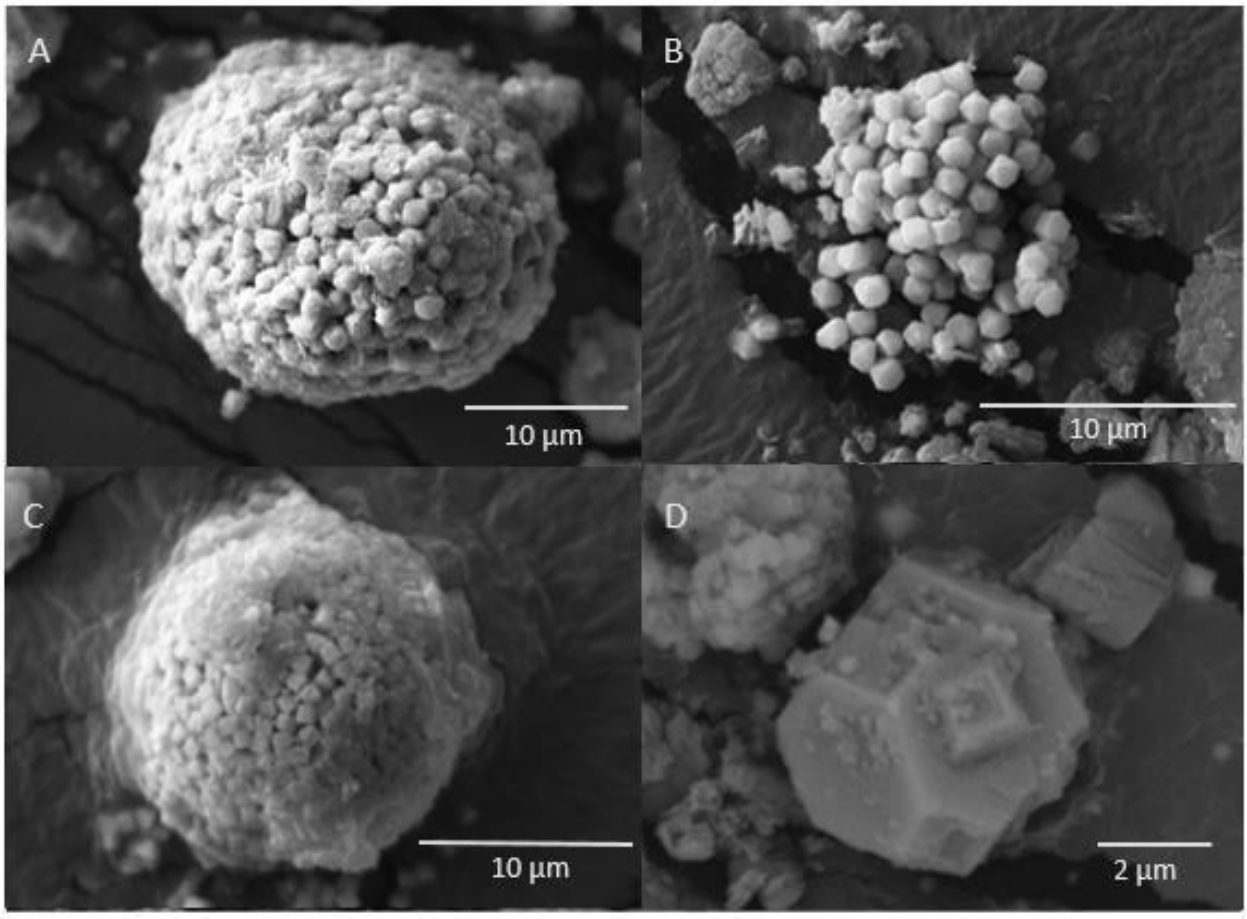

Figure 39. SEM image showing presence of pyrite grains in two different time of the experiment and a comparison of the morphology (Wilson, 2018).

Discussions

Biogenic iron sulfide mineral formation has been well documented in shallow and deep groundwater systems, in contrast, much less is known about its capacity to adsorb or co-precipitate in different environments (Saunders et al., 1997). Trace elements can be incorporated into sulfide minerals such as pyrite or form separate metal sulfide phases when reacting with biogenic H_2S at low temperature under sulfate reduction conditions. Under oxidized conditions, Saunders et al. (1997) proposed that ferromanganese coatings precipitate on stream sediments mediated by Mn- and Fe-oxidizing bacteria. A number of trace elements dissolved in stream waters either are adsorbed by ferromanganese coatings or are coprecipitated. Ferromanganese-coated sediments and plant debris are deposited in floodplain alluvium. Bacterially mediated reduction and dissolution of ferromanganese coatings below the water table in the alluvial aquifer may release Fe, Mn, and trace elements to the solution. On the other hand, where sulfate reducers got favorable environment they produced coarse-grained pyrite in and around decaying wood fragments.

Saunder et al. (1997) documented the occurrence As-, Co-, and Ni-bearing authigenic pyrite large crystals in a shallow alluvial aquifer in the Uphapee watershed. Similar trace element contents (such as As, Co, Ni) in the groundwater and the pyrite grains indicates a close relation. Arsenic is less abundant in groundwater than cobalt or nickel. Arsenic content in groundwater is as low as <2 ppb. Arsenic is more abundant in pyrite grains than other trace elements. Electron microprobe and SEM-EDS analyses indicate that arsenic content in pyrite grains is 0.20-0.92 wt.% which is consistent with the study of Saunders et al. (1997) that found 0.6 wt% (6000 ppm)

As. It is evident that not only As but also other trace elements (i.e. Co, and Ni) were co-precipitated in pyrite.

Pyrite formed within or close proximity to the lignitic wood fragments. This suggests that among others wood was one of the major sources of organic carbon required by the sulfate-reducing bacteria. Though pyrite framboid is one of the most abundant mineral textures in the natural environment, it was lacking in the studied pyrite. Pyrite framboids on average take few hours to 5 days to form (Rickard, 2019). The general coarse-grained euhedral pyrite crystals and the lack of framboidal pyrite suggested that pyrite formation was a relatively slow process.

Discrete zones of high-iron and high-manganese groundwater occur in Holocene fluvial sediments in the Macon County study area. Postma and Jakobsen (1996) suggested that various terminal electron accepting processes (TEAP's) in separate redox zones (i.e., Mn(IV), Fe(III), sulfate reduction, methanogenesis) during the degradation of organic matter in sediments, are responsible for producing these discrete geochemical zones. Previous studies (e.g., Lee, 1985; Lovley and Chapelle, 1995) found that redox potential of groundwater usually decreases along the flow path. The consumption of free oxygen by bacterially catalyzed reactions is followed by reduction of NO_3^-, reduction of MnO_2, and then reduction of iron oxides.

Well MC-4 is under oxidized condition (ORP = 173 mV) where natural organic matter is decomposed and oxygen is the dominant TEAP. Dissolved Fe and Mn concentrations are very low in MC-4 under the oxidized conditions. Well MC-1 down-gradient has relatively lower ORP (121 mV) but significantly higher Mn concentration (317 µg/L) and relatively high alkalinity

(12.10 mg/L). Mn may be released into the solution by the following Mn (IV) reduction reaction:

$$CH_2O + 3CO_2 + H_2O + 2MnO_2 \rightarrow Mn^{2+} + 4HCO_3^-$$

This reaction would increase the alkalinity (in the form of HCO_3^-) in groundwater. Further down-gradient, high iron groundwater in wells MC-2 (ORP = 68 mV) and MC-3 (ORP = 46) shifts into Fe(III) reduction conditions where Fe(III) oxyhdroxides are reduced and ferrous iron is released into groundwater by bacterial iron reduction:

$$CH_2O + 7CO_2 + 4Fe(OH)_3 \rightarrow 4Fe^{2+} + 8HCO_3^- + 3H_2O$$

This reaction will also elevate alkalinity and release arsenic sorbed by Fe(III) oxyhydroxides. This mobilization process leads to widespread groundwater arsenic contamination in Holocene fluvial aquifer worldwide. Dissolved arsenic level in the Macon County study area (< 2 µg/L), however, is significantly lower than those in Bangladesh (typically hundreds of µg/L). We propose that, with long time of flushing, only small amount of As is left on the absorbing surface of Fe (III) oxyhydroxides in the study area. This and strong hydrologic gradient (transport dominated system) would lead to a slug of plume with low arsenic level. Further study of arsenic level on the surface of Fe (III) oxyhydroxides is needed.

High iron concentration (> 0.3 mg/L) is a common water quality problem in many coastal plain aquifers (Chappelle and Lovley 1992; Penny et al., 2003). The observed close association between dissolved iron and dissolved inorganic carbon (alkalinity) as well as the lack of sulfate consumption indicates that sulfate-reducing bacteria are much less active than Fe(III)-reducing bacteria in this high-iron zone. High iron concentration in groundwater develops only when there

is little or no sulfate reduction in the aquifer. Further downgradient from the iron-rich zone, ferrous iron reacts with H_2S generated by bacterial sulfate reduction to form pyrite under sulfate reduction zone.

The bioremediation experiment monitoring data in the industrial site demonstrated that sulfate-reducing conditions were quickly established by biostimulation one week after the injection. The redox and geochemical changes were evident from the decreased ORP and increased H_2S level. The sulfate-reducing conditions led to the formation of arsenian-pyrite and to decrease groundwater arsenic concentration to less than 50 ppb from the initial concentration. Electron microprobe analyses confirmed the amount of sequestered arsenic into arsenian-pyrite ranged between 0.05 to 0.40 wt. %., compared to those of biogenic pyrite naturally formed in fluvial sediments. Biostimulation process allows rapid formation of well-formed euhedral crystals (1-10 μm diameter) or spherical framboid aggregates (10-50 μm diameter). By contrast, slow bacterial sulfate reduction in fluvial sediments produced larger euhedral crystals (tens of m in diameter) in cubic or truncated octahedral forms. The biogenic pyrite formed in fluvial sediments adsorbed not only arsenic, but also other trace elements (e.g., Co and Ni) present in the natural environments. Though solid phase of pyrite crystals was stable during the one-year monitoring period, more study is needed to assess the long-term stability of biogenic pyrite under redox conditions.

Thus active involvement of sulfate-reducing bacteria is evident from both sites. Geochemical analyses indicate that biogenic pyrite removed not only arsenic but also other trace elements such as cobalt, nickel by co-precipitation and sorption. These studies provide the basis for using biogenic pyrite in sequestering As, Co, Ni and perhaps other trace elements in contaminated groundwater under sulfate reducing condition.

Conclusions

The thesis represents a detail study of aquifer redox zonation as well as the morphology (size, shape) of biogenic pyrite and its capability of sequestering As and other trace elements in Holocene fluvial sediments at the Uphapee watershed in Macon County, Alabama. This work also presents a comparison of groundwater geochemistry and the morphology of biogenic pyrite that formed naturally in fluvial sediments (in Alabama and Bangladesh) and through a field biostimulation process at an industrial site in Florida.

- The groundwater at Macon County, AL fluvial site is slightly oxidizing to moderately reducing (Eh= 46 to173 mV), and nearly neutral to slightly acidic (pH= 5.53 to 6.51). Groundwater is not sulfate limited and the water is found to be mainly a Ca-SO_4 type. Arsenic concentration in groundwater is very low (<2ppb). Other trace elements such as Co (0.55 to 2.12ppb), Ni (0.066 to 3.97 ppb) are also present.
- Groundwater geochemistry data indicate a redox sequence of oxidation, Mn(IV) reduction, Fe(III) reduction, and sulfate reduction along the flow path in fluvial aquifers. The down-gradient increases in dissolved Mn and then Fe concentrations reflect increased Mn (II) and Fe (II) production via microbial competition as the aquifer becomes progressively more reduced. Bacterial sulfate reduction seems to dominate near the end of groundwater flow path as the availability of Mn- and Fe-oxyhydroxides becomes limited, where increased sulfate-reducing activities leading to the formation of biogenic pyrite. Such microbial-mediated zonation is of fundamental importance to influence groundwater geochemistry of many similar

fluvial aquifers (e.g., Middendorf aquifer in South Caroline, Potomac Group in New Jersey) worldwide.

- Fe- and Mn- reducing bacteria reduced and dissolved Fe- and Mn-coated sediments in the stream, releasing Fe, As, Co, and Ni. Sulfate-reducing bacteria use organic products from bacterial degradation of wood fragments to reduce dissolved sulfate to H_2S and form pyrite around the lignitic wood. During formation of pyrite dissolved As, Co, and Ni co-precipitate and become sequestered in pyrite.
- The naturally occurring biogenic pyrite formed large crystals (20-200 μm) and the lack of small crystals of pyrite framboids indicates that pyrite formation was a relatively slow process. The crystals show euhedral (cubes, truncated octahedron) shapes with sharp edges. The pyrite grains contain 0.2-92 wt.% of arsenic, 0.19wt.% of Co, 0.15 wt.% of Ni indicating its excellent capacity to sequester not only arsenic but also other trace elements.
- At the industrial site, Florida groundwater was Ca-HCO_3-Na-Cl type and had a limited amount of SO_4. Artificial introduction of sulfate reducing condition led to the formation of biogenic arsenian-pyrite and a significant decrease in the arsenic concentration in the groundwater. Pyrite formed by this biostimulation process also has high arsenic content (up to 0.40 wt%) and has a distinctive euhedral crystals (1-10 μm diameter) or spherical aggregates/ framboids (10-50 μm diameter).

The evidences from both natural and industrial site indicate that formation of biogenic pyrite and sequestration of trace elements such as As, Co, Ni etc. is possible if sulfate reducing condition is maintained.

References

Ahmed, K. M., Bhattacharya,P., Hasan. M. A., Akhter, S. H., Alam, S.M.M., Bhuyian,M.A.H.,Imam, M. B., Khan, A.A., Sracek, O. (2004) Arsenic enrichment in groundwater of the alluvial aquifers in Bangladesh: an overview: Applied Geochemistry 19 (2004) 181–200

Ahmed, K.M., Imam, M.B. Akhter, S.H., Hasan, M.A., Khan, A.A., 2001. Sedimentology and mineralogy of arsenic contaminated aquifers in the Bengal Delta of Bangladesh. In: Jacks, G., Bhattacharya, P. and Khan, A.A. (Eds.), Groundwater Arsenic Contamination in the Bengal Delta Plain of Bangladesh. Proc. KTH-Dhaka University Seminar. KTHSpecial Publication, TRITA-AMI Report 3084, pp. 97–108.

Ahmed, K.M., Imam, M.B. Akhter, S.H., Hasan, M.A., Alam, M.M., Chowdhury,S.Q., Burgess, W.G., Nickson, R., McArthur, J.M., Hasan, M.K., Ravenscroft P. and Rahman, M.M., 1998b. Mechanism of arsenic release to groundwater: geochemical and mineralogical evidence. Internat. Conf. on Arsenic Pollution of Groundwater in Bangladesh: Causes, Effects and Remedies. Dhaka, February 1998, pp. 125–126.

Akai, J., Izumi, K., Fukuhara, H., Masuda, H., Nakano, S., Yoshimura, T., Ohfuji, H., Anawar, H., and Akai K., 2004. Mineralogical and geomicrobiological investigations on groundwater arsenic enrichment in Bangladesh: Applied Geochemistry, v. 19, p. 215-230.

Bhattacharya, P., Jacks, G., Ahmed, K.M., Khan, A.A., Routh, J., 2002b. Arsenic in groundwater of the Bengal Delta Plain aquifers in Bangladesh. Bull. Environ. Contam. Toxicol. 69, 538–545.

Bhattacharya, P., Frisbie, S.H., Smith, E., Naidu, R., Jacks, G., Sarkar, B., 2002a. Arsenic in the environment: a global perspective. In: Sarkar, B. (Ed.), Handbook of Heavy Metals in the Environment. Marcell Dekker Inc., New York, pp.147–215.

Bhattacharya, P., Chatterjee, D., Jacks, G., 1997. Occurrence of arsenic-contaminated groundwater in alluvial aquifers from delta plains, eastern India: options for safe drinking water supply. Journal Water Resources Dev. 13, 79–92.

Bish, D.L., Post, J.E., 1989. Modern Powder Diffraction. Reviews in Mineralogy. Mineralogical Society of America, v. 20, p. 220-231.

Champ, D. R., Gulens, J., Jackson, R.E., 1978. Oxidation-reduction Sequences in groundwater flow systems. Canadian Journal of Earth Sciences, Volume 16, Page 12-23

Dhakal, P., 2010, Sorption of arsenic by iron sulfide made by sulfate-reducing bacteria: implications for bioremediation. [M.S. thesis: Auburn University], 118 p.

Dowling, C., Poreda, R., Basu, A., and Peters, S., 2002. Geochemical study of arsenic release mechanisms in the Bengal Basin groundwater: Water Resources Research, v. 38, no. 9, p. 12-1 – 12-18.

Fitton, G., 1997. X-Ray fluorescence spectrometry, in Gill, R. (ed.), Modern Analytical Geochemistry: An Introduction to Quantitative Chemical Analysis for Earth, Environmental and Material Scientists. Addison Wesley Longman, UK.

Farquhar, M. L., Charnock, J. M., Livens, F. R., Vaughan, D. J., 2002. Mechanisms of Arsenic Uptake from Aqueous Solution by Interaction with Goethite, Lepidocrocite, Mackinawite, and Pyrite: An X-ray Absorption Spectroscopy Study. E*nviron. Sci. Technol.*20023681757-1762

Ghandehari, S. S., 2016. Bioremediation of an Arsenic-Contaminated Site, Using Sulfate-Reducing Bacteria, Bay County, Florida. [M.S. thesis: Auburn University], 99 p.

Harvey, C. F., Swartz, C.H., Badruzzman, B., Keon, N.E., Yu. W., Ali, A., Jay, J., Beckie, R., Niedan, V., Brabander, D, Oates, P., Ashfaque, K., Islam, S., Hemond, H.F., Ahmed, F., 2002. Arsenic mobility and groundwater extraction in Bangladesh: Science, v. 298, p. 1602- 1606

Hounslow, A.W., 1980. Groundwater Geochemistry: Arsenic in Landfills: Ground Water, v. 18, p. 331-333.

Keimowitz, A. R., Mailloux, B.J., Cole, P., Stute, M., Simpson, H.J., Chillrud, S.N., 2007. Laboratory investigations of enhanced sulfate reduction as a groundwater arsenic remediation strategy. Environ. Sci. Technol, v. 41, p. 6718–6724.

Kinniburgh, D. G., Smedley, P. L., 2001. Arsenic contamination of groundwater in Bangladesh (British Geologic Survey report). 15 p.

Korte, N.E., 1991. Naturally occurring arsenic in groundwaters of the Midwestern United States. Environ. Geol. Water Sci. v. 18, p. 137–141.

Kruger, M. C., Bertin, P. N., Heipieper, H. J., & Ars_ene-Ploetze, F., 2013. Bacterial metabolism of environmental arsenicmechanisms and biotechnological applications. Applied microbiology and biotechnology, 97 , 3827{3841.

Lee, M.-K., Saunders, J. A., Wilson, T., Levitt, E., Ghandehari, S. S., Dhakal, P., Redwine, J., Marks, J., Billor, M. Z., Miller, B., Han, D., Wang, L. (2018) Field-scale bioremediation of arsenic-contaminated groundwater using sulfate-reducing bacteria and biogenic pyrite, Bioremediation Journal, 23:1, 1-21, DOI: 10.1080/10889868.2018.1516617

Lee, M.-K., Griffin, J., Saunders, J. A., Wang, Y., Jean, J., 2007. Reactive transport of trace elements and isotopes in Alabama coastal plain aquifers. J. Geophys. Res., v. 112, issue G2.

Lee, M.-K., Saunders, J.A., Wilkin, R.T., Shahnewaz, M., 2005. Geochemical modeling of arsenic speciation and mobilization: Implications for bioremediation. In: O'Day, Vlassopoulos, D., Meng, X., Benning, L.G. (Eds.), Advances in Arsenic Research: Integration of Experimental and Observational Studies and Implications for Mitigation. Am. Chem. Soc. Symp. Series, v. 915, p. 398–423.

Liu, C.-W., Wang, S.-W., Jang, C.-S., and Lin, K.-H., 2006. Occurrence of arsenic in groundwater in the Choushui river alluvial fan, Taiwan. Journal of Environ. Quality. 35, 68-75.

Levitt, E. J., 2017. Bioremediation of Arsenic Contaminated Groundwater in Northwest Florida: Mineralogy, Geochemistry, and Microbiology Changes. [M.S. thesis: Auburn University], 122 p.

Mallik, S., Rajagopal, N., 1996. R, Groundwater development in the arsenic-affected alluvial belt of West Bengal— Some questions. Curr. Sci. 70, 956–958.

Mandal, B. K., Suzuki, K. T., 2002. Arsenic round the world: a review. Talanta, v. 58, p. 201- 235.

Markewich, H. W., and Christopher, T. H. 1982 Pleistocene(?) and Holocene Fluvial History of Uphapee Creek, Macon County, Alabama. Geological Survey bulletin ; 1522

McArthur, J.M., Ravencroft, P., Safiullah, S., Thirlwall, M.F., 2001. Arsenic in groundwater: testing pollution mechanism for sedimentary aquifers in Bangladesh. Water Resour. Res. 37, 109–117.

Meng, X.; Wang, W. Speciation of arsenic by disposable cartridges, Third International Conference on Arsenic Exposure and Health Effects, San Diego, CA, July 12-15, 1998.

Mondal, P., Bhowmick, S., Chatterjee, D., Figoli, A., & Van der Bruggen, B. (2013). Remediation of inorganic arsenic in groundwater for safe water supply: a critical assessment of technological solutions. Chemosphere, 92 , 157-170.

Mukherjee, A.B., Bhattacharya, P., 2001. Arsenic in groundwater in the Bengal Delta Plain: slow poisoning in Bangladesh.Environ. Rev. 9, 189–220.

Nickson, R.T., McArthur, J.M., Shrestha, B., Kyaw-Myint, T.O., Lowry, D., 2005. Arsenic and other drinking water quality issues, Muzaffargarh District, Pakistan. Applied Geochemistry. 20, 55–68.

Nickson, R.T., McArthur, J.M., Ravenscroft, P., Burgess, W.G., Ahmed, K.M., 2000. Mechanism of arsenic release to groundwater, Bangladesh and West Bengal. Appl. Geochem. 15, 403–413.

Nickson, R., McArthur, J., Burgess, W., Ahmed, K.M., Ravenscroft, P., Rahman, M., 1998. Arsenic poisoning of Bangladesh groundwater. Nature 395, 338.

Nordstrom, D. K., 2002. Worldwide occurrences of arsenic in groundwater. Science, v. 296, p. 2143- 2145.

Penny, E., Lee, M.-K., Morton, C., 2003. Groundwater and microbial processes of the Alabama coastal plain aquifers. Water Resour. Res., v. 39, p.1320.

Postma D. and Jakobsen R., Redox zonation: Equilibrium constraints on the Fe(III)/SO4reduction interface. Geochim. et Cosmochim. 60, 3169-3175.

Rahman, M. M., Hasan, M. A., Ahmed, K. M., 2018. Alternative Options for Safe Drinking Water in Arsenic and Salinity Affected, Narail District, Bangladesh. Geological Society of America *Abstracts with Programs.* Vol. 50, No. 3 doi: 10.1130/abs/2018SE-312995

Rahman, M. M., 2015. Alternative Options for Safe Drinking Water in Arsenic and Salinity Affected Bornal-Iliasabad Union of Kalia Upzilla, Narail District. [M.S. thesis: Department of Geology, University of Dhaka], 80 p

Ravenscroft, P., Burgess, W.G., Ahmed, K.M., Burren, M., Perrin, Jerome, 2005. Arsenic in groundwater of the Bengal Basin, Bangladesh: distribution, field relations, and hydrogeological setting. Hydrogeology Journal. 13, 727-751.

Reed, S. J. B., 2005. Electron Microprobe Analysis and Scanning Electron Microscopy in Geology (2nd Ed.), Cambridge University Press.

Rickard, D., 2019. How long does it take a pyrite framboid to form? Earth and Planetary Science Letters, Volume 513, 1 May 2019, Pages 64-68

Rieder M., Crelling J.C., Šustai O., Drábek M., Weiss Z., Klementová, M., 2007. Arsenic in iron disulfides in a brown coal from the North Bohemian Basin, Czech Republic.International: Journal of Coal Geology, 71, 115-121.

Routh, J., Bhattacharya, P., Jacks, G., Ahmed, K.M., Khan, A.A., Rahman, M.M., 2000. Arsenic geochemistry of Tala groundwater and sediments from Satkhira District, Bangladesh. Eos Trans Am. Geophys. Union 81, 550.

Saunders, J. A., Dhakal, P., Ghandehari S., Wilson T., Billor Z., and Uddin, A., (2018). Bioremediation of arsenic contaminated groundwater by sequestrating of arsenic in biogenic pyrite. Applied Geochemistry, v. 96, p. 233-243.

Saunders, J. A., Lee, M.-K., Shamsudduha, M., Dhakal, P., Uddin, A., Chowdury, M., Ahmed, K., 2008. Geochemistry and mineralogy of arsenic in (natural) anaerobic groundwaters: Applied Geochemistry, v. 23, p. 3205–3214.

Saunders, J. A., Lee, M.-K., Uddin, A., Mohammad, S., Wilkin, R., Fayek, M., Korte N., 2005a. Natural arsenic contamination of Holocene alluvial aquifers by linked tectonic, weathering, and microbial processes. Geochemistry, Geophysics, Geosystems, v. 6**,** p. 66-81.

Saunders, J.A., Pritchett, M.A., Cook, R.B., 1997. Geochemistry of biogenic pyrite and ferromanganese stream coatings: a bacterial connection? Geomicrobiol. J., v. 14, p. 203–217.

Schmidt, W. and Clark, M.W. 1980. Geology of Bay County, Florida: Florida Geological Survey Bulletin 57, 96 p.

Shamsudduha et al., 2008, Spatial relationship of groundwater arsenic distribution with regional topography and water-table fluctuations in the shallow aquifers in Bangladesh. Environmental Geology, DOI 10.1007/s00254-008-1429-3.

Shamsudduha M., 2007. Mineralogical and geochemical profiling of arsenic contaminated alluvial aquifers in the Ganges-Brahmaputra floodplain, Manikganj, Bangladesh. [M.S. thesis: Auburn University], 183 p.

Smedley, P.L., and Kinniburgh, D.G., 2002, A review of the source, behavior and distribution of arsenic in natural waters. Applied Geochemistry, v. 17, p. 517-568.

Starnes, P.H., 2015. Hydrogeology and geochemistry of arsenic contaminated shallow alluvial aquifers in Florida and Alabama. [M.S. thesis: Auburn University], 129 p.

Turner, J. P., 2006. Groundwater geochemistry, Geology and Microbiology of arsenic contaminated holocene alluvial aquifers, Manikganj, Bangladesh. [M.S. thesis: Auburn University], 76 p.

USEPA, 2002. Proven Alternatives of Aboveground Treatment of Arsenic in Groundwater: Washington DC, Office of Solid Waste and Emergency Response, U.S. Environmental Protection Agency, EPA-542-S-02-002, 68 p.

USEPA, 1997. Technology alternatives for the remediation of soils contaminated with As, Cd, Cr, Hg, and Pb, Washington DC: Office of Emergency and Remedial Response, U.S. Environmental Protection Agency. EPA-540-S-97-500, 45 p.

van Geen, A., Zheng, Y., Versteeg, R., Stute, M., Horneman, A., Dhar, R., Steckler, M., Gelman, A., Small, C., Ahsan, H., Graziano, J., Hussain, I., and Ahmed, K.M., 2003. Spatial variability of arsenic in 6000 contiguous tubewells of Araihazar, Bangladesh: Water Resources Research, v. 39, p.1140.

Welch, A.H., Westjohn, D.B., Helsel, D.R., and Wanty, R.B., 2000. Arsenic in ground water of the United States; occurrence and geochemistry: Ground Water, v. 38, p. 589-604.

Wilson, T. J., 2018. Pyrite Biomineralization and Arsenic Sequestration at a Florida Industrial Site: Imaging and Geochemical Analysis. [M.S. thesis: Auburn University], 66 p.

Wolthers, M., Charlet, L., Van Der Linde, P. and Rickard. D., 2005. Arsenic mobility in the ambient sulfidic environment: Sorption of arsenic (V) and arsenic (III) onto disrordered mackinawite. Geochimica et Cosmochimica Acta 69(14):3483-3492

Zheng, Y., Stute, M., van Geen, A., Gavrieli, I., Dhar, R., Simpson, J., Ahmed, K. M., 2004. Redox control of arsenic mobilization in Bangladesh groundwater. Applied Geochemistry. 19, 201–214.

Appendix

Element weight percentage obtained by EMP analysis for the thin section MC-2

	Element Weight Percent:					Element Weight Percent normalized to 100				
Grain #	As	Si	S	Fe	Total	As	Si	S	Fe	Total
1	0.1774	0	52.58	44.27	97.03	0.1828	0	54.19	45.63	100
2	0.2433	0	51.82	44.48	96.55	0.252	0	53.67	46.07	100
3	0.1944	0	52.55	44.09	96.84	0.2008	0	54.27	45.53	100
4	0.2241	0	51.85	43.03	95.11	0.2356	0	54.52	45.25	100
5	0.2005	0	52.4	44.22	96.82	0.2071	0	54.12	45.67	100
6	0.1403	0	51.82	42.78	94.74	0.148	0	54.7	45.16	100
7	0.3741	0	52.17	43.93	96.48	0.3877	0	54.08	45.54	100
8	0.7082	0	51.21	43.27	95.19	0.744	0	53.8	45.46	100
9	0.1897	0	51.85	43.25	95.29	0.1991	0	54.42	45.39	100
10	0.2782	0	51.11	43.4	94.79	0.2935	0	53.92	45.78	100
11	0.1638	0	52.09	42.85	95.1	0.1723	0	54.77	45.05	100
12	0.2148	0	50.51	43.31	94.03	0.2284	0	53.71	46.06	100
13	0.1286	0	50.7	43.25	94.07	0.1367	0	53.89	45.97	100
14	0.2983	0	51	43.14	94.44	0.3159	0	54	45.68	100
15	0.3905	0	51.45	43.06	94.9	0.4115	0	54.21	45.38	100
16	0.3037	0	51.68	43.19	95.18	0.3191	0	54.3	45.38	100
17	0.4085	0	51.79	43.29	95.49	0.4277	0	54.24	45.33	100
18	0.3222	0	51.84	43.77	95.93	0.3359	0	54.04	45.62	100
19	0.6255	0	51.62	43.26	95.5	0.6549	0	54.05	45.29	100
20	0.5723	0	51.24	43.41	95.22	0.601	0	53.81	45.59	100
21	0.5516	0	51.14	43.36	95.05	0.5804	0	53.8	45.62	100
22	0.1133	0	52.42	43.73	96.27	0.1177	0	54.46	45.42	100
23	0.1256	0	52.35	43.33	95.81	0.1311	0	54.64	45.23	100
24	0.1215	0	47.35	37.39	84.86	0.1432	0	55.79	44.06	100
25	0.2031	0	50.08	42.92	93.21	0.2179	0	53.73	46.05	100
26	0.3637	0	49.48	43.06	92.91	0.3915	0	53.26	46.35	100
27	0.5127	0	50.36	42.99	93.87	0.5462	0	53.66	45.8	100
28	0.2915	0	50	42.13	92.42	0.3154	0	54.1	45.59	100
29	0.3811	0	49.02	42.28	91.68	0.4156	0	53.47	46.12	100
30	0.2891	0	50.11	42.91	93.31	0.3098	0	53.7	45.99	100
31	0.7365	0	49.86	42.56	93.15	0.7907	0	53.52	45.69	100
32	0.0963	0	50.99	45.03	96.12	0.1002	0	53.05	46.85	100

	Element Weight Percent:					Element Weight Percent normalized to 100				
Grain #	As	Si	S	Fe	Total	As	Si	S	Fe	Total
33	0.1436	0	50.34	45.02	95.5	0.1504	0	52.71	47.14	100
34	0.1596	0	50.08	43.83	94.08	0.1697	0	53.24	46.59	100
35	0.1416	0	50.47	44.51	95.12	0.1489	0	53.06	46.79	100
36	0.5135	0	49.86	44.56	94.94	0.5409	0	52.52	46.94	100
37	0.2532	0	50.05	44.64	94.95	0.2667	0	52.71	47.02	100
38	0.7115	0	49.44	44.54	94.69	0.7514	0	52.21	47.04	100
39	0.6219	0	49.83	44.39	94.84	0.6558	0	52.54	46.8	100
40	0.4453	0	49.93	44.73	95.11	0.4682	0	52.5	47.03	100
41	0.561	0	49.68	44.49	94.73	0.5922	0	52.44	46.97	100
42	0.2669	0	50.61	44.98	95.86	0.2784	0	52.8	46.92	100
43	0.4941	0	50.06	44.25	94.8	0.5212	0	52.81	46.67	100
44	0.6482	0	49.99	44.01	94.65	0.6849	0	52.82	46.49	100
45	0.4879	0	49.25	45.65	95.39	0.5114	0	51.63	47.86	100
46	0.6673	0	48.99	44.81	94.47	0.7064	0	51.85	47.44	100
47	0.6712	0	49.34	45.42	95.43	0.7034	0	51.7	47.59	100
48	0.406	0	50.09	45.66	96.15	0.4222	0	52.09	47.49	100
49	0.4044	0	50	45.17	95.57	0.4231	0	52.31	47.26	100
50	0.1487	0	49.79	46.08	96.02	0.1548	0	51.85	47.99	100
51	0.4632	0	50.14	45.19	95.79	0.4835	0	52.34	47.17	100
52	0.4548	0	49.96	45.14	95.56	0.476	0	52.29	47.24	100
53	0.3695	0	49.36	44.8	94.53	0.3909	0	52.21	47.4	100
54	0.4692	0	49.46	44.82	94.74	0.4952	0	52.2	47.31	100
55	0.2703	0	49.81	45.73	95.81	0.2821	0	51.99	47.73	100
56	0.5907	0	50.62	46.08	97.29	0.6072	0	52.03	47.37	100
57	0.2642	0	49.15	44.45	93.87	0.2815	0	52.37	47.35	100
58	0.2861	0	49.78	44.93	95	0.3011	0	52.4	47.3	100
59	0.3961	0	49.65	43.67	93.72	0.4226	0	52.98	46.59	100
60	0.1531	0	49.59	44.53	94.27	0.1624	0	52.6	47.24	100
61	0.6841	0	49.85	45.08	95.61	0.7155	0	52.14	47.15	100
62	0.3924	0	50.29	44.68	95.37	0.4115	0	52.73	46.85	100
63	0.4165	0	49.92	44.65	94.99	0.4384	0	52.55	47.01	100
64	0.3217	0	50.43	45.32	96.08	0.3349	0	52.49	47.17	100
65	0.2063	0	50.78	44.9	95.88	0.2151	0	52.96	46.83	100
66	0.114	0	51.2	45.96	97.28	0.1172	0	52.64	47.25	100

Element weight percentage obtained by EMP analysis for the thin section MC-3

	Element Weight Percent:					Element Weight Percent normalized to 100				
Grain #	As	Si	S	Fe	Total	As	Si	S	Fe	Total
1	0	0	55.31	44.18	99.49	0	0	55.59	44.41	100
2	0.0948	0	54.9	46.08	101.08	0.0938	0	54.32	45.59	100
3	0.2002	0	54.97	45.33	100.5	0.1992	0	54.7	45.11	100
4	0.187	0	55.26	45.52	100.96	0.1852	0	54.73	45.08	100
5	0.0152	0	55.61	45.86	101.49	0.0149	0	54.79	45.19	100
6	0.0193	0	55.02	44.83	99.87	0.0193	0	55.09	44.89	100
7	0.0457	0	55.78	46.01	101.84	0.0449	0	54.78	45.18	100
8	0.1687	0	55.84	45.18	101.19	0.1667	0	55.18	44.65	100
9	0.1469	0	55.38	45.27	100.79	0.1458	0	54.94	44.91	100
10	0.1732	0	55.34	45.24	100.76	0.1719	0	54.93	44.9	100
11	0.1459	0	54.94	45.47	100.55	0.1451	0	54.64	45.22	100
12	0.2239	0	55.32	46.22	101.77	0.22	0	54.36	45.42	100
13	0	0	54.95	45.63	100.58	0	0	54.63	45.37	100
14	0.1721	0	54.72	45.08	99.97	0.1722	0	54.74	45.09	100
15	0.1965	0	47.3	43.37	90.87	0.2162	0	52.05	47.73	100
16	0.0441	0	55.85	45.87	101.77	0.0433	0	54.88	45.08	100
17	0	0	55.17	44.94	100.11	0	0	55.11	44.89	100
18	0.1485	0	55.31	44.87	100.32	0.148	0	55.13	44.72	100
19	0.0013	0	52.96	44	96.96	0.0014	0	54.62	45.38	100
20	0.0915	0	55.92	45.71	101.72	0.0899	0	54.97	44.94	100
21	0.1375	0	55.35	45.46	100.95	0.1362	0	54.83	45.03	100
22	0.2479	0	55.32	45.57	101.14	0.2451	0	54.7	45.06	100
23	0.1258	0	55.51	45.65	101.29	0.1242	0	54.8	45.07	100
24	0	1.444	49.82	42.28	93.54	0	1.5436	53.26	45.2	100
25	0.1232	0	55.83	45.45	101.4	0.1215	0	55.06	44.82	100
26	0.1206	0	55.71	45.77	101.6	0.1187	0	54.83	45.05	100
27	0.1002	0	56.14	46.34	102.58	0.0976	0	54.73	45.18	100
28	0.1075	0	54.96	45.24	100.31	0.1072	0	54.79	45.1	100
29	0.2436	0	55.96	45.5	101.71	0.2395	0	55.02	44.74	100
30	0.1676	0	55.06	45.39	100.61	0.1666	0	54.72	45.11	100
31	0.0722	0	55.97	46.4	102.44	0.0705	0	54.63	45.29	100
32	0	0	55.74	46.17	101.91	0	0	54.69	45.31	100
33	0.1036	0	54.96	45.93	100.99	0.1026	0	54.42	45.48	100
34	0.093	0	55.29	45.5	100.88	0.0922	0	54.8	45.1	100

	Element Weight Percent:					Element Weight Percent normalized to 100				
Grain #	As	Si	S	Fe	Total	As	Si	S	Fe	Total
35	0.1275	0.0306	51.89	45.15	97.2	0.1311	0.0315	53.38	46.45	100
36	0.0614	0	55.43	45.82	101.31	0.0606	0	54.72	45.22	100
37	0.0731	0	55.58	45.04	100.69	0.0726	0	55.2	44.73	100
38	0.1807	0	55.6	44.91	100.69	0.1795	0	55.22	44.6	100
39	0.1705	0	56.68	44.65	101.51	0.168	0	55.84	43.99	100
40	0.7638	0	56.13	43.29	100.18	0.7624	0	56.02	43.21	100
41	0.2588	0	54.96	45.44	100.66	0.2571	0	54.6	45.14	100
42	0.2907	0	54.81	45.43	100.53	0.2892	0	54.52	45.19	100
43	0.8165	0	54.86	46.29	101.97	0.8007	0	53.8	45.4	100
44	0.8611	0	54.94	45.29	101.1	0.8517	0	54.35	44.8	100
45	0.6345	0	54.17	45.13	99.93	0.6349	0	54.2	45.16	100
46	0.9285	0	53.93	45.24	100.09	0.9276	0	53.87	45.2	100
47	0.7707	0	54.91	46.13	101.81	0.757	0	53.93	45.31	100
48	0.2138	0	55.36	45.97	101.54	0.2106	0	54.52	45.27	100
49	0.2263	0	55.41	45.76	101.4	0.2231	0	54.65	45.13	100
50	0.1379	0	58.01	46.29	104.44	0.1321	0	55.54	44.33	100
51	0.2351	0	54.87	45.47	100.58	0.2337	0	54.56	45.21	100
52	0.1082	0	54.54	45.11	99.76	0.1084	0	54.67	45.22	100
53	0.2275	0	55.52	46.12	101.86	0.2233	0	54.5	45.28	100
54	0.1393	0	55.74	46.77	102.65	0.1357	0	54.3	45.56	100
55	0.1801	0	55.47	46.84	102.5	0.1757	0	54.12	45.7	100
56	0	0	55.1	46.42	101.52	0	0	54.27	45.73	100
57	0.1729	0	55.34	45.86	101.38	0.1705	0	54.59	45.24	100
58	0.1486	0	55.46	46.34	101.95	0.1457	0	54.4	45.45	100
59	0.1303	0	55.37	45.98	101.48	0.1284	0	54.56	45.31	100
60	0	0	55	46.59	101.59	0	0	54.14	45.86	100
61	0.1529	0	55.99	45.88	102.03	0.1498	0	54.88	44.97	100
62	0.1032	0	55.02	46.17	101.29	0.1018	0	54.32	45.58	100
63	0.1994	0	55.32	46.23	101.75	0.1959	0	54.37	45.43	100
64	0	0	55.05	45.44	100.49	0	0	54.78	45.22	100
65	0.1495	0	55.64	45.95	101.74	0.147	0	54.69	45.17	100
66	0.299	0	55.85	45.06	101.21	0.2955	0	55.18	44.52	100
67	0.1386	0	55.63	45.86	101.62	0.1363	0	54.74	45.13	100
68	0.2609	0	54.65	45.61	100.53	0.2595	0	54.37	45.37	100
69	0.3041	0	55.12	45.81	101.23	0.3004	0	54.45	45.25	100
70	0.3176	0	55.27	45.74	101.32	0.3135	0	54.54	45.14	100

	Element Weight Percent:					Element Weight Percent normalized to 100				
Grain #	As	Si	S	Fe	Total	As	Si	S	Fe	Total
71	0.1528	0	55.71	45.42	101.29	0.1508	0	55	44.85	100
72	0	0	54.8	45.52	100.32	0	0	54.62	45.38	100
73	0	0	55.23	45.22	100.45	0	0	54.98	45.02	100
74	0.6568	0	54.51	45.02	100.19	0.6556	0	54.4	44.94	100
75	0.1911	0	51.65	41.92	93.76	0.2038	0	55.09	44.71	100
76	0.2431	0	52.24	41.64	94.12	0.2583	0	55.5	44.24	100
77	0.3447	0	52.22	40.73	93.3	0.3694	0	55.97	43.66	100
78	0.2179	0	52.48	41.66	94.36	0.2309	0	55.62	44.15	100
79	0.1412	0	52.18	41.34	93.66	0.1507	0	55.71	44.14	100
80	0.2419	0	51.62	41.71	93.56	0.2585	0	55.17	44.58	100
81	0.204	0	55.13	44.62	99.95	0.2041	0	55.15	44.64	100
82	0.2199	0	55.52	45.21	100.95	0.2178	0	55	44.78	100
83	0.3028	0	55.51	45.32	101.14	0.2994	0	54.89	44.81	100
84	0.3681	0	52.55	43.69	96.61	0.3811	0	54.39	45.22	100
85	0	0	55.12	45.8	100.92	0	0	54.62	45.38	100
86	0.2533	0	54.48	45.4	100.13	0.2529	0	54.41	45.34	100
87	0.1824	0	55.16	45.69	101.02	0.1806	0	54.6	45.22	100
88	0.3681	0	52.66	44.7	97.72	0.3766	0	53.88	45.74	100
89	0.1151	0	55.47	46.13	101.72	0.1131	0	54.53	45.36	100
90	0.2293	0	55.54	46.48	102.25	0.2242	0	54.32	45.45	100
91	0.0947	0	53.98	46.24	100.31	0.0944	0	53.81	46.1	100
92	0.1298	0	53.49	45.7	99.33	0.1307	0	53.86	46.01	100
93	0.2381	0	54.44	46.31	100.99	0.2357	0	53.91	45.85	100

Element weight percentage obtained by EMP analysis for the thin section MC-1

	Element Weight Percent:					Element Weight Percent normalized to 100				
Grain #	As	Si	S	Fe	Total	As	Si	S	Fe	Total
1	0.3912	0	52.1	43.62	96.11	0.407	0	54.2	45.39	100
2	0.4401	0	52.15	43.23	95.82	0.4593	0	54.42	45.12	100
3	0.3001	0	52.3	42.75	95.35	0.3148	0	54.85	44.83	100
4	0.3201	0	51.73	42.93	94.98	0.337	0	54.46	45.2	100
5	0.4009	0	51.91	42.45	94.75	0.4231	0	54.78	44.8	100
6	0.4118	0	52.84	43.33	96.58	0.4263	0	54.71	44.86	100
7	0.3321	0	51.86	42.95	95.14	0.3491	0	54.51	45.14	100
8	0.3216	0	52.12	42.89	95.33	0.3373	0	54.67	44.99	100
9	0.2763	0	52.25	42.83	95.36	0.2897	0	54.8	44.91	100
10	0.3608	0	52.02	42.47	94.85	0.3804	0	54.85	44.77	100
11	0.3388	0	52.41	42.55	95.3	0.3555	0	54.99	44.65	100
12	0.1895	0	52.1	42.58	94.87	0.1998	0	54.91	44.89	100
13	0.1964	0	52.24	42.41	94.84	0.2071	0	55.08	44.72	100
14	0.221	0	52.36	42.73	95.31	0.2319	0	54.93	44.84	100
15	0.1693	0	52.18	43.05	95.4	0.1775	0	54.7	45.13	100
16	0.1413	0	52.13	43.21	95.48	0.148	0	54.6	45.25	100
17	0.1144	0	51.98	42.58	94.67	0.1208	0	54.9	44.97	100
18	0.1221	0	52.12	42.84	95.08	0.1284	0	54.81	45.06	100
19	0.1512	0	52.15	42.56	94.86	0.1594	0	54.98	44.87	100
20	0.1349	0	52.72	43.13	95.98	0.1406	0	54.92	44.94	100
21	0.1983	0	52.32	43.07	95.58	0.2074	0	54.74	45.06	100
22	0.1688	0	51.29	41.81	93.27	0.181	0	54.99	44.83	100
23	0.2209	0	52.4	42.97	95.59	0.2311	0	54.81	44.96	100
24	0.188	0	50.16	42.98	93.33	0.2015	0	53.75	46.05	100
25	0.1146	0	52.11	43.45	95.67	0.1198	0	54.47	45.41	100
26	0.1359	0	51.91	42.69	94.74	0.1435	0	54.79	45.06	100
27	0.1181	0	52.65	42.95	95.72	0.1233	0	55.01	44.87	100
28	0.1249	0	51.91	43.56	95.6	0.1306	0	54.3	45.57	100
29	0.2215	0	35.79	28.83	64.83	0.3416	0	55.2	44.46	100
30	0.1264	0	53.63	43.43	97.18	0.1301	0	55.18	44.69	100
31	0.4712	0	53.84	43.7	98.02	0.4807	0	54.93	44.59	100
32	0.3748	0	53.56	43.45	97.38	0.3849	0	55	44.62	100
33	0.3415	0	53.83	43.74	97.91	0.3488	0	54.98	44.67	100
34	0.3482	0	53.78	43.47	97.6	0.3568	0	55.11	44.54	100

	Element Weight Percent:					Element Weight Percent normalized to 100				
Grain #	As	Si	S	Fe	Total	As	Si	S	Fe	Total
35	0.4323	0	54.77	43.93	99.13	0.436	0	55.25	44.31	100
36	0.5477	0	54.27	43.66	98.48	0.5561	0	55.11	44.34	100
37	0.3979	0	54.37	43.96	98.73	0.4031	0	55.07	44.53	100
38	0.41	0	53.65	43.84	97.9	0.4188	0	54.8	44.78	100
39	0.1279	0	54.46	43.79	98.37	0.1301	0	55.36	44.51	100
40	0.1576	0	54.1	43.96	98.22	0.1605	0	55.08	44.76	100
41	0.2664	0	54.12	42.75	97.13	0.2742	0	55.71	44.01	100
42	0.0613	0	53.72	42.66	96.44	0.0636	0	55.7	44.23	100
43	0	0	53.05	43.19	96.25	0	0	55.12	44.88	100
44	0	0.7025	52.12	42.23	95.05	0	0.739	54.83	44.43	100
45	0.1791	0	54.14	43.79	98.11	0.1826	0	55.19	44.63	100
46	0.0708	0	54.01	44.17	98.25	0.0721	0	54.97	44.96	100
47	0	0	53.86	43.5	97.36	0	0	55.32	44.68	100
48	0.1989	0	53.22	43.8	97.22	0.2046	0	54.74	45.05	100
49	0.1188	0	53.48	43.53	97.14	0.1223	0	55.06	44.82	100
50	0.119	0	53.3	43.88	97.3	0.1223	0	54.78	45.09	100
51	0	0	53.31	44.31	97.62	0	0	54.61	45.39	100
52	0	0	53.8	44.15	97.96	0	0	54.92	45.08	100
53	0.0952	0	53.11	44.29	97.49	0.0976	0	54.47	45.43	100
54	0.275	0	54.34	44.14	98.75	0.2784	0	55.03	44.7	100
55	0.4494	0	54.13	44.28	98.86	0.4546	0	54.76	44.79	100
56	0.5741	0	52.87	43.9	97.34	0.5898	0	54.32	45.09	100
57	0.5579	0	53.33	43.74	97.63	0.5715	0	54.63	44.8	100
58	0.4633	0	53.75	43.52	97.73	0.474	0	54.99	44.53	100
59	0.4747	0	53.83	44.34	98.64	0.4812	0	54.57	44.95	100
60	0.312	0	53.75	43.99	98.05	0.3183	0	54.82	44.86	100
61	0.2692	0	53.84	44.14	98.25	0.274	0	54.8	44.93	100
62	0.4026	0	53.11	43.87	97.39	0.4134	0	54.54	45.05	100
63	0.4329	0	53.69	44.56	98.69	0.4386	0	54.41	45.15	100
64	0.4301	0	53.25	43.23	96.91	0.4439	0	54.95	44.61	100
65	0	0	54.12	43.14	97.26	0	0	55.64	44.36	100
66	0.3552	0	53.74	44.02	98.11	0.362	0	54.77	44.87	100
67	0.426	0	53.39	43.79	97.61	0.4365	0	54.7	44.87	100
68	0.3312	0	54.03	43.64	98.01	0.338	0	55.13	44.53	100
69	0.3766	0	53.23	43.85	97.46	0.3864	0	54.62	45	100
70	0.2351	0	53.34	44.72	98.29	0.2392	0	54.26	45.5	100

	Element Weight Percent:					Element Weight Percent normalized to 100				
Grain #	As	Si	S	Fe	Total	As	Si	S	Fe	Total
71	0.4007	0	53.61	44.24	98.25	0.4078	0	54.56	45.03	100
72	0.3048	0	53.01	43.42	96.74	0.315	0	54.8	44.88	100
73	0.173	0	54.19	44.1	98.46	0.1757	0	55.04	44.79	100
74	0.2447	0	52.63	43.82	96.7	0.2531	0	54.43	45.32	100
75	0.3716	0	50.79	42.42	93.58	0.3971	0	54.27	45.33	100
76	0.3194	0	53.48	42.29	96.09	0.3324	0	55.66	44.01	100
77	0.1773	0	53.01	41.85	95.04	0.1866	0	55.78	44.04	100
78	0.4566	0	53.4	43.61	97.47	0.4685	0	54.79	44.74	100